PHILOSOPHICAL TRANSACTIONS OF THE ROYAL SOCIETY A MATHEMATICAL, PHYSICAL & ENGINEERING SCIENCES

Electromagnetic Induction in Rotating Conductors

A. Herzenberg and F. J. Lowes

Phil. Trans. R. Soc. Lond. A 1957 **249**, 507-584
doi: 10.1098/rsta.1957.0006

ELECTROMAGNETIC INDUCTION IN ROTATING CONDUCTORS

By A. HERZENBERG
Physical Laboratories, University of Manchester

and F. J. LOWES *
Department of Geodesy and Geophysics, University of Cambridge

(*Communicated by P. M. S. Blackett, F.R.S.—Received* 15 *June* 1954—
Revised 14 *July* 1956)

CONTENTS

PAGE

PART A

1. Introduction 508
1·1. Basic formulae 509
1·2. Notation 512

PART B

2. Experimental investigations 513
2·1. Non-dimensional parameters 514
2·2. Design consideration 515
2·3. Description of apparatus 516
2·4. Experimental method 519
2·5. Discussion of errors 520
2·6. Experimental results and discussion 521

PART C. BASIC THEORY OF INDUCTION IN ROTATING CONDUCTORS

3. Axial symmetry 528
3·1. Field equations 528
3·2. Cylinder 530
3·3. Sphere 533
3·4. Electromagnetic couples 534
3·5. Time-dependent angular velocity 535

4. Transverse magnetic field at low angular velocity 539
4·1. Time-independent case: solution in powers of ω 539
4·2. Examples 541
4·3. Dynamo processes 542
4·4. Time-dependent angular velocity 542

5. Transverse field at high angular velocity 543
5·1. The boundary layer 544
5·2. Solution near the boundary 544
5·3. Boundary conditions for the isolated rotator as $\omega \to \infty$ 545
5·4. Boundary conditions as $\omega \to \infty$ for the rotator embedded in conducting material 546
5·5. A theorem about **h** 547
5·6. Examples 547
5·7. Time-dependent angular velocity; a particular problem 549

PART D. INDUCTION IN ROTATORS EMBEDDED IN FINITE CONDUCTING SHELLS

6. General analysis 552
6·1. A symmetry theorem 552
6·2. Plane boundary, first method 552
6·3. Plane boundary, second method 553
6·4. Spherical boundary 556
6·5. Time-dependent case, plane boundary 557
6·6. Time-dependent case, spherical boundary 560

7. The external field due to a rotator near a boundary of conducting region 562
7·1. Axial inducing field (case A) 563
7·2. Transverse inducing field (case B) 564
7·3. Transverse inducing field (case C) 565
7·4. Effect of the reflected currents 565
7·5. Charts of induced field 568
7·6. Discussion 574
7·7. Summary of the results of part D 575

PART E. THE EDDY HYPOTHESIS

8. The minimum radius of an eddy 577
8·1. Magnitude of the induced field 577
8·2. Power consumption 578

9. Summary and conclusions 581

References 584

* Now at the Physics Department, King's College, Newcastle upon Tyne.

Vol. 249. A. 970. (Price 26*s*.) 62 [Published 16 May 1957

This paper describes an experimental and theoretical investigation of induction in a rotating conductor surrounded by a rigid conductor of finite or infinite extent. The results are applied to a discussion of induction in rotating eddies in the fluid core of the earth as a possible origin of the geomagnetic non-dipole field.

Model experiments were made with rigid rotators in a steady magnetic field; the induced magnetic field was measured outside the conductors. The results confirmed the appropriate parts of the theoretical work.

In the theoretical work solutions are first obtained for a rotator embedded in a solid conductor of infinite extent; a method is then developed for extending this solution to a finite surrounding conductor. Charts are given for the induced field on the surface of the earth due to a hypothetical rotator in the earth's core. The analysis is based on integral solutions of the field equations; wherever possible the field vectors themselves are used rather than a vector potential.

The induced magnetic fields depend on the relative symmetry of the rotator, the surrounding conductor, and the applied magnetic field. For an applied field parallel to the axis of rotation, the induced field is proportional to the angular velocity; for an applied field perpendicular to the axis, the induced field reaches a limit at high angular velocities. If both the surrounding conductor and the applied magnetic field have rotational symmetry about the axis there is no induced field outside the surrounding conductor.

The conclusion of the geophysical discussion is that eddies must have radii of several hundred kilometres if they are to account for the observed magnitude of the non-dipole field. Because of the skin effect such large radii would not be tenable if the core material were effectively rigid. However, fluid motions must occur due to the electromagnetic forces, and the consequent magneto-hydrodynamic disturbances probably have decay lengths much larger than the rigid conductor skin depth; therefore arguments based on the rigid conductor skin depth are not applicable. Thus the eddy model might be satisfactory if the fluid motion does not seriously alter the basic induction mechanism.

PART A

1. Introduction

This paper is concerned with the mechanism underlying the secular variation and the non-dipole part of the earth's magnetic field. (For a brief description of these fields see § 8·1 of this paper. Fuller discussions are given by Chapman & Bartels 1940; Elsasser 1950; Inglis 1955.) It was suggested by Elsasser (1946*b*) and Bullard (1948) that the secular variation and the non-dipole field might be due to induction caused by the interaction of the earth's main magnetic field with eddies in the fluid core of the earth. We shall refer to this suggestion as the 'eddy hypothesis'. The eddy hypothesis has been discussed quantitatively by Bullard (1948) in terms of a model in which an eddy is treated as a rigid conducting sphere rotating in non-conducting surroundings and in a constant applied magnetic field. In a later paper, Bullard (1949*b*) treated induction in a spinning conducting sphere surrounded by and in electrical contact with a rigid concentric conducting shell. He found the surprising result that, for steady rotation, the induced magnetic field outside the shell is the same as if the shell were not there. Both of the models discussed by Bullard contain questionable simplifications. The first model ignores the spread of current outside an eddy surrounded by conducting material, and the second imposes a degree of symmetry which there is no reason to suppose exists.

Our aim in the work reported here was to develop the eddy hypothesis beyond the point at which Bullard has left it. We have investigated how the eddy hypothesis is affected by

(i) the spread of current out of an eddy surrounded by solid conducting material,

(ii) the degree of geometrical symmetry of the eddy, the conducting core, and the applied magnetic field, and

(iii) the shape of the eddy.

When we started, we did not believe that much progress could be made by a mathematical investigation. We therefore made an experiment with a rotating conducting cylinder surrounded by, and in electrical contact with, a stationary conductor of variable shape. The whole arrangement was placed in a magnetic field which could be oriented in various ways. The induced magnetic field was measured outside the conductor. This experiment is described in part B of this paper.

After the experimental work had been started, we found that theoretical progress was possible after all. We did this theoretical work in two stages. In the first stage, we considered a rotating conductor surrounded by a rigid conductor of infinite extent; a magnetic field with its sources outside the rotator was applied with various orientations. An account of this investigation is given in part C, where we discuss the induced magnetic field from rotators of different shapes. We believe that our approach here brings out the basic physical features in a clearer way than was possible with the previous treatments (Bullard 1949*b*; MacDonald 1934). In the second stage of the theoretical work, part D, the extent of the conductor surrounding the rotator is made finite. In particular, we work out the induced magnetic field which would be observed at the surface of the earth if there were an eddy near the surface of the earth's core.

Because of the stage the experiment had reached when the theoretical work was done, it has not been possible to correlate theory and experiment as closely as would have been possible had the theory been done first. Nevertheless, it has been possible to discuss the experimental results in the light of the theory. This is done at the end of part B; the agreement is satisfactory.

In part C we shall derive from our approach the formulae for the induced field due to a sphere spinning in a conducting medium of infinite extent, although these formulae are special cases of results given by Bullard (1949*b*). We feel that the inclusion of these results is justified, on the one hand because of the simplicity of our derivation, and on the other hand because we need these formulae in part D, so that their derivation makes the paper self-contained.

The results of the experimental and theoretical work given in parts B, C and D enable us to re-discuss the eddy hypothesis, and to answer the three questions posed above. This discussion is given in part E. The basis of the discussion is now a model in which a rigid eddy with a sharp boundary is spinning steadily in a rigid conducting core. This model is still unsatisfactory because it ignores the effect of the motion of the core material under the influence of the electromagnetic forces.

1·1. *Basic formulae*

It is convenient to write down the basic formulae at this point. We shall then have the basis of the discussion of the non-dimensional parameters which enter into the experiment described in part B, and we shall also be able to derive the physical features which will make the subdivision of the discussion of the basic induction mechanism in part C appear natural.

PHILOSOPHICAL TRANSACTIONS OF THE ROYAL SOCIETY A MATHEMATICAL, PHYSICAL & ENGINEERING SCIENCES

When all quantities are referred to an inertial frame of reference, Maxwell's equations become, in the presence of moving conducting matter,

$$\nabla \wedge \mathbf{H} = 4\pi\sigma(\mathbf{E} + \mathbf{v} \wedge \mathbf{H}), \tag{1·1}$$

$$\nabla \wedge \mathbf{E} = -\frac{\partial \mathbf{H}}{\partial t}, \tag{1·2}$$

$$\nabla . \mathbf{E} = 4\pi c^2 q, \tag{1·3}$$

$$\nabla . \mathbf{H} = 0. \tag{1·4}$$

(We use unrationalized e.m.u. A note on units and notation will be found in § 1·2.) $\mathbf{E}$, $\mathbf{H}$ are the electric and magnetic fields; q is the electric charge density; $\mathbf{v}$ is the local velocity of the matter and σ is its conductivity; c is the velocity of light *in vacuo*. We have assumed the dielectric constant and the permeability to be unity, and have neglected the displacement current, terms of order (v^2/c^2), and a convection current term $4\pi q\mathbf{v}$ on the right of (1·1).

We note that by taking the divergence of both sides in (1·1) and then using (1·3) we obtain, for constant σ,

$$q = -\frac{1}{4\pi c^2} \nabla . (\mathbf{v} \wedge \mathbf{H}). \tag{1·5}$$

Therefore a charge distribution can be maintained within moving conducting matter.

The induction process in moving conducting matter is best discussed by eliminating $\mathbf{E}$ from (1·1) to (1·4). By taking the curl of (1·1), and using (1·2) and (1·4), we obtain

$$\frac{\partial \mathbf{H}}{\partial t} = \frac{1}{4\pi\sigma} \nabla^2 \mathbf{H} + \nabla \wedge (\mathbf{v} \wedge \mathbf{H}). \tag{1·6}$$

The non-dimensional form of (1·6) is discussed in part B.

We next rewrite (1·6) in a form appropriate for a rotational motion. Let us suppose that we have a fluid of uniform conductivity σ filling all space, and let a part of this fluid be in rotational motion about a straight axis. Let us take cylindrical polar co-ordinates (ρ, λ, z) in the inertial frame in which the rotational axis is stationary. Let the unit vectors corresponding to the direction of increasing (ρ, λ, z) at any point be $(\hat{\boldsymbol{\rho}}, \hat{\boldsymbol{\lambda}}, \hat{\mathbf{z}})$ respectively. Let the angular velocity $\boldsymbol{\omega}$ be a function of ρ and z; the velocity $\mathbf{v}$ is therefore

$$\mathbf{v}(\rho, \lambda, z) = \omega(\rho, z)\, \rho \hat{\boldsymbol{\lambda}}. \tag{1·7}$$

Let us suppose that there is applied a magnetic field $\mathbf{H}_0$ whose components $H_{0\rho}$, $H_{0\lambda}$, H_{0z} contain λ only in a factor $e^{im\lambda}$. Then, owing to the axial symmetry of the velocity field, the components of the total magnetic field $\mathbf{H}$ will also contain λ only in a factor $e^{im\lambda}$.

If we now substitute for $\mathbf{v}$ from (1·7) into (1·6), and use (1·4), then we obtain

$$\frac{\partial \mathbf{H}}{\partial t} = \frac{1}{4\pi\sigma} \nabla^2 \mathbf{H} - im\omega \mathbf{H} + \hat{\boldsymbol{\lambda}} \rho \mathbf{H} . \nabla \omega. \tag{1·8}$$

This is the fundamental equation in the theory of induction in rotating conductors embedded in conducting materials. The first term on the right represents a diffusion of the field (if we put $\omega = 0$, we are left with a vector form of the equation of heat conduction). The second and third terms on the right of (1·8) represent the induction process. Their physical significance

can be seen by supposing that the diffusion term is negligible. Then we have, in a region of constant ω,

$$(H_\rho, H_\lambda, H_z) \propto e^{im(\lambda-\omega t)}, \tag{1·9}$$

i.e. the second term drags the magnetic field round with the matter, *provided that* $m \neq 0$. The third term on the right of (1·8) represents a process of stretching of lines of force so that they remain attached to the fluid particles; this term operates only in a region of changing angular velocity. (For example, if ω decreases in the direction $+\hat{\boldsymbol{\rho}}$, then a field $\mathbf{H}$ having a positive component H_ρ will develop a negative component H_λ.)

The form of equation (1·8) shows that the induction phenomena are quite different according to whether there is axial symmetry ($m = 0$) or not ($m \neq 0$). To consider these two cases, it is convenient to split $\mathbf{H}$ into two parts, i.e.

$$\mathbf{H} = \mathbf{H}_0 + \mathbf{h}, \tag{1·10}$$

where $\mathbf{H}_0$ is the applied magnetic field, and $\mathbf{h}$ is the induced magnetic field. (Throughout this paper we shall suppose that in the region of rotating matter the applied magnetic field satisfies the equations

$$\frac{\partial \mathbf{H}_0}{\partial t} = 0, \quad \boldsymbol{\nabla} \wedge \mathbf{H}_0 = 0, \quad \boldsymbol{\nabla} . \mathbf{H}_0 = 0, \tag{1·11}$$

i.e. we are supposing that $\mathbf{H}_0$ is constant and has its sources outside the rotating region.)

If we have axial symmetry, then $m = 0$ in (1·8), so that the term $-im\omega\mathbf{H}$ drops out. Moreover, as we shall show in § 3·1, we can replace $\mathbf{H}$ by $\mathbf{H}_0$ in the term $\mathbf{H} . \boldsymbol{\nabla}\omega$ because the lines of force of $\mathbf{h}$ are perpendicular to $\boldsymbol{\nabla}\omega$ on account of the symmetry. Thus (1·8) becomes

$$\frac{\partial \mathbf{h}}{\partial t} - \frac{1}{4\pi\sigma}\nabla^2\mathbf{h} = \hat{\boldsymbol{\lambda}}\rho\mathbf{H}_0 . \boldsymbol{\nabla}\omega, \tag{1·12}$$

where we have used (1·11). Equation (1·12) is the vector form of the equation of heat conduction with sources; the sources lie where the angular velocity varies and depend only on the component of $\mathbf{H}_0$ along $\boldsymbol{\nabla}\omega$. Clearly, $\mathbf{h}$ is proportional to the source strength, and therefore to $\mathbf{H}_0$ and ω. In particular, under steady conditions ($\partial\mathbf{h}/\partial t = 0$), the magnitude of $\mathbf{h}$ falls off only slowly with the distance from the sources.

This last result is in sharp contrast with what happens under steady conditions when there is no axial symmetry ($m \neq 0$). The last term in (1·8) then still acts as the source of $\mathbf{h}$, but these sources now depend on $\mathbf{h}$ as well as $\mathbf{H}_0$ because there is no longer a symmetry requirement forcing $\mathbf{h}$ to be perpendicular to $\boldsymbol{\nabla}\omega$. Thus $\mathbf{h}$ is no longer proportional to $\mathbf{H}_0$ and ω. Moreover, the term $-im\omega\mathbf{H}$ is now non-vanishing, and leads to an exponential fall-off of $\mathbf{H}$ with distance from the sources. This last result can be seen most easily by taking the point of view of an observer moving with the matter. This observer would see magnetic and electric fields $\mathbf{H}^*$ and $\mathbf{E}^*$ given by

$$\mathbf{H}^* = \mathbf{H} + \frac{\mathbf{v} \wedge \mathbf{E}}{c^2}, \quad \mathbf{E}^* = \mathbf{E} + \mathbf{v} \wedge \mathbf{H}, \tag{1·13}$$

where terms of order (v^2/c^2) have been neglected. $\mathbf{H}^*$ and $\mathbf{E}^*$ would vary harmonically in time with angular frequency $m\omega$, and would therefore penetrate only a distance of the order $d/\sqrt{m} = (2\pi\sigma\omega m)^{-\frac{1}{2}}$ from the sources. The same is true of $\mathbf{E}$ and $\mathbf{H}$ because of (1·13). In particular, within a rigid rotator, $\mathbf{E}$ and $\mathbf{H}$ are confined to a boundary layer of thickness $\sim(2\pi\sigma\omega m)^{-\frac{1}{2}}$.

PHILOSOPHICAL TRANSACTIONS OF THE ROYAL SOCIETY A MATHEMATICAL, PHYSICAL & ENGINEERING SCIENCES

It is useful to define a non-dimensional parameter

$$\alpha \equiv 2\pi\sigma\omega a^2 = (a/d)^2, \tag{1·14}$$

where a is the radius of the rotating region. In the steady case, the value of α determines the main features of the electromagnetic field in a rotator; if we have axial symmetry then $h \propto \alpha$; if we do not have axial symmetry then the electromagnetic field extends throughout the rotator when $\alpha \ll 1$, and is confined to a boundary layer near the rotator surface when $\alpha \gg 1$. The theoretical discussion therefore falls naturally into the three parts

$$m = 0, \quad (m \neq 0, \alpha \ll 1), \quad (m \neq 0, \alpha \gg 1).$$

But before we develop the theory further (part C) we shall give an account of the experimental work.

1·2. *Notation*

Throughout the paper electric and magnetic quantities are expressed in unrationalized electromagnetic units. In formulae, c.g.s. units are always used, but in the text, tables and graphs other units are occasionally used.

The symbol $\simeq$ stands for 'is approximately equal to' and $\sim$ for 'is of the order of magnitude of'. The magnitude of a vector is denoted by a light face italic symbol, e.g. $|\mathbf{H}_0| = H_0$. In integrals variables of integration are always primed.

This list gives notation which is used generally throughout the paper. Other symbols used in only one section are defined when introduced.

a	radius of rotator
c	velocity of light
d	skin depth $= (2\pi\sigma\omega)^{-\frac{1}{2}}$
e, $\mathbf{e}$	induced electric field
h, $\mathbf{h}$	induced magnetic field
i	$(-1)^{\frac{1}{2}}$
j, $\mathbf{j}$	current density
l	typical dimension of moving conductor
m	integer, order of spherical harmonic, exponent in $\mathrm{e}^{\mathrm{i}m\lambda}$
n	integer, degree of spherical harmonic
$\hat{\mathbf{n}}$	unit normal vector
q	charge density
r, $\mathbf{r}$	radius
$\hat{\mathbf{r}}$	unit vector in the direction of r increasing
s	integer
$\mathrm{d}\mathbf{s}$	line element
t	time
t_0	a typical acceleration time
u	half-length of cylindrical rotator
v, $\mathbf{v}$	velocity, peripheral velocity
x, y, z	Cartesian co-ordinates
$\hat{\mathbf{x}}, \hat{\mathbf{y}}, \hat{\mathbf{z}}$	unit vectors in the directions of x, y, z increasing
$\mathrm{d}A$	surface element
E, $\mathbf{E}$	total electric field
$H_n^{(1)}$	Hankel function of first kind
H, $\mathbf{H}$	total magnetic field
H_0, $\mathbf{H}_0$	applied magnetic field
J_n	Bessel function
M, $\mathbf{M}$	magnetic dipole moment
P_n^m	Legendre function
R	distance between field point and point of integration
R_C	radius of earth's core $= 3500$ km
R_E	radius of earth $= 6400$ km
T	duration
$\mathrm{d}V$	volume element
α	$= 2\pi\sigma\omega a^2 = 2\pi\sigma v a$, a non-dimensional parameter
γ	10^{-5} G

$\Gamma, \mathbf{\Gamma}$	torque	ν	angular frequency in $e^{i\nu t}$
Δ	small thickness	$\rho, \boldsymbol{\rho}$	radius in cylindrical polar co-ordinates
ϵ	eddy power consumption		
θ	polar angle in spherical polar co-ordinates	$\hat{\boldsymbol{\rho}}$	unit vector in the direction of ρ increasing
κ	core power consumption	σ	electrical conductivity
λ	azimuthal angle co-ordinate	τ	period
$\hat{\boldsymbol{\lambda}}$	unit azimuthal vector in the direction of λ increasing	ϕ, Φ ψ, Ψ	potential functions
μ	$= 4\pi\sigma l^2/t_0$, a non-dimensional parameter	$\omega, \boldsymbol{\omega}$	angular velocity

PART B

2. Experimental investigations

It was decided to investigate the following problems:

(i) There had been some uncertainty about the behaviour of an isolated rotator at high velocities in a traverse applied magnetic field. We wished to verify Bullard's (1949*b*) treatment of this problem.

(ii) In a transverse applied field, an isolated rotating sphere gives an induced field which approaches a limit at high velocities, the magnitude of the limiting field depending only on the radius of the sphere and the magnitude of the applied field. Bullard (1949*b*) had shown that if a stationary concentric spherical conducting shell were placed around and in electrical contact with the rotator, then the induced field outside the conductor is unchanged. We wished to know how the external induced field would be altered if the conductors were not spherically symmetrical.

(iii) An applied magnetic field parallel to the axis of an isolated rotating sphere gives no induced field. There is also no external induced field if a spherical shell is placed round the rotator (Bullard 1949*b*). However, it seemed possible that with an unsymmetrical surrounding shell there would be an external induced field which might increase without limit as the velocity was increased.

Experiments to investigate these problems would involve rotating a conductor in intimate electrical contact with stationary surrounding conductors of various shapes, the whole being in a large magnetic field parallel or transverse to the axis of rotation. The small induced fields would have to be measured outside the conductor, and in the presence of the large inducing field. This section describes the design, construction and operation of such an apparatus, and includes a discussion of the experimental errors and limitations. It concludes with a summary and discussion of the results obtained. This discussion for axial inducing field depends to a certain extent on the ideas and results of § 7; it is suggested that the reader return to this discussion after reading § 7.

The experimental work was limited to the steady-state problem. As we shall now show, scale considerations made it impossible to investigate time varying cases of geomagnetic relevance with the same apparatus.

2·1. *Non-dimensional parameters*

Before giving the details of the experiment we discuss the non-dimensional parameters which enter into the problem. We assume that the applied field $\mathbf{H}_0$ is constant, and that where the conductivity σ does not vanish it is constant; the velocity v of the rotator may vary with time.

As we saw in § 1·1, the elimination of $\mathbf{E}$ from (1·1) and (1·2) leads to

$$\nabla^2\mathbf{H}+4\pi\sigma\nabla\wedge(\mathbf{v}\wedge\mathbf{H})-4\pi\sigma\,\partial\mathbf{H}/\partial t=0. \tag{2·1}$$

To reduce this equation to non-dimensional form we introduce the quantities

v_0 = maximum peripheral velocity attained,
l_0 = a typical length (the rotator radius),
t_0 = a typical time in which the velocity varies,
h_0 = the unit of magnetic field.

Multiplying (2·1) by l_0^2/h_0 we can rewrite it

$$(l_0^2\nabla^2)\left(\frac{\mathbf{H}_0}{h_0}\right)+(4\pi\sigma v_0 l_0)\,(l_0\nabla)\wedge\left(\frac{\mathbf{v}}{v_0}\wedge\frac{\mathbf{H}}{h_0}\right)-\left(\frac{4\pi\sigma l_0^2}{t_0}\right)\left(t_0\frac{\partial}{\partial t}\right)\left(\frac{\mathbf{H}}{h_0}\right)=0. \tag{2·2}$$

It follows from (2·2) that for given boundary conditions the solution of (2·1) is characterized by two non-dimensional parameters which we denote by

$$\alpha=\tfrac{1}{2}(4\pi\sigma v_0 l_0), \tag{2·3}$$

$$\mu=4\pi\sigma l_0^2/t_0. \tag{2·4}$$

The parameter α was introduced in § 1, and is a measure of the ratio of the size of the rotator to the electromagnetic skin depth; the parameter μ is essentially the ratio of the natural decay time of electromagnetic fields in the rotator to the time of acceleration.

The values of the parameters for our laboratory experiment, and estimates for an eddy in the earth's core are

$$\left.\begin{array}{lll} \alpha_{\text{lab.}}\leqslant 10 & \text{as} & \sigma=6{\cdot}2\times10^{-4}\text{ e.m.u. (copper)},\\ & & a=2{\cdot}0\text{ cm},\\ & & v_0\leqslant 1500\text{ cm s}^{-1}\text{ (7500 rev/min)},\\ \alpha_{\text{eddy}}\sim 50 & \text{taking} & \sigma\sim3\times10^{-6}\text{ e.m.u.},\\ & & a\sim 500\text{ km},\\ & & v_0\sim 0{\cdot}05\text{ cm s}^{-1},\\ \mu_{\text{lab.}}\sim 3\times10^{-2} & \text{taking} & t_0\sim 1\text{ s},\\ \mu_{\text{eddy}}\sim 30 & \text{taking} & t_0\sim 100\text{ years}. \end{array}\right\} \tag{2·5}$$

The values quoted for the experiment are the best that could be obtained with our apparatus.

We see that it is possible to obtain a value of α in the laboratory comparable with that for a typical core eddy. In fact, as we shall see later, the induced fields from a rotator are, depending on the symmetry, either proportional to α for all α, or independent of α for $\alpha\gg1$. Therefore, the laboratory experiment is adequate to reproduce effects which do not depend on time variations of the velocity. However, it is clearly impossible to reproduce time-dependent effects with the apparatus as constructed.

2·2. *Design considerations*

It would have been desirable to make the parameter $\alpha = 2\pi\sigma\omega a^2$ the same for the experiment as for a core eddy, in which case the steady-state induction phenomena would be exactly comparable. However, for a typical eddy $\alpha = 50$ to 100, and it proved impossible to obtain large enough experimental velocity and radius to give this value. The angular velocity was limited by mechanical considerations and power requirements. The surrounding conductor would have to be of dimensions several times that of the rotor, and too large a scale for the latter would have led to excessive material requirements, both for the rotor assembly and the inducing field coils. A short cylindrical rotor, of 2 cm radius, rotating about a vertical axis, with surrounding conductor of 6 cm radius, was finally adopted, the cylindrical rather than spherical shape simplifying contact problems.

The possibility of using mercury as the conductor, with rotating and stationary vanes to impress a suitable velocity distribution, was considered, but mechanical difficulties and the high resistivity of mercury led to the use of copper or brass conductors, separated by a thin uniform layer of mercury. Several outer conductors of different shapes could then be made interchangeable. It would have been preferable for all the solid conductors to be made of copper, but to avoid constructional delays it was necessary to use brass for the outer blocks.

The inducing fields were most conveniently produced by a vertical solenoid for axial field, and a pair of coils with horizontal axis for transverse field. To avoid spurious results due to distortion of the magnetic fields, no ferromagnetic materials could be used in the construction of the rotor assembly; the main problem which arose from this was that of the high-speed bearings, but it was found that satisfactory ball races could be made from phosphor bronze. To spin the rotor the use of air or water turbines, which could be mounted directly on the shaft, was considered, but for reasons of simplicity of control, speed regulation, power supply and availability it was decided to use a series-wound a.c. motor and a belt drive. Though such motors are not inherently speed-stable it was found that in practice the stability was quite good enough.

For inducing fields of 10 to 100 G induced fields somewhere in the range of 1 to 1000γ were to be expected near to the conductors ($1\gamma = 10^{-5}$ G). The choice of magnetometer was thus a primary consideration in the design of the apparatus; it was decided to use one of the fluxgate type. The detector element of the fluxgate magnetometer is a saturable core transformer (the core being a mu-metal wire or strip); a sinusoidal voltage of constant amplitude and frequency is applied to the primary, and the wave form in the secondary winding is modified by the presence of any external magnetic field. After suitable filtering and amplification, an output current is obtained which is proportional to the component of applied field in the direction of the transformer core (see, for example, Brewer, Squires & Ross, 1951). The sensitivity of this type of magnetometer could be easily varied over a wide range, and with a movable detector head any component of field at any place could be measured provided that a sufficiently stable backing off field could be applied, while no appreciable external field would be introduced by the head. Thus the fluxgate magnetometer had many advantages over suspension and rotating coil magnetometers.

PHILOSOPHICAL TRANSACTIONS OF THE ROYAL SOCIETY A MATHEMATICAL, PHYSICAL & ENGINEERING SCIENCES

2·3. *Description of apparatus*

Figure 1 shows a schematic diagram of the rotor assembly as constructed, and figures 2 and 3 are photographs of this and the coil assembly.

The cylindrical copper rotor, 4·00 cm diameter, was integral with the shaft, which rotated in two semi-thrust phosphor-bronze ball races in the brass bearing block. The copper rotor was enclosed in a hollow brass cylinder of external diameter 12·0 cm, the annular gap being 0·05 cm. Apart from the mercury in this annular space the large cylinder was insulated electrically from the rest of the assembly by the Perspex bushes. This whole assembly was bolted to a triangular Dural plate which was supported above the Dural base-plate by three brass pillars.

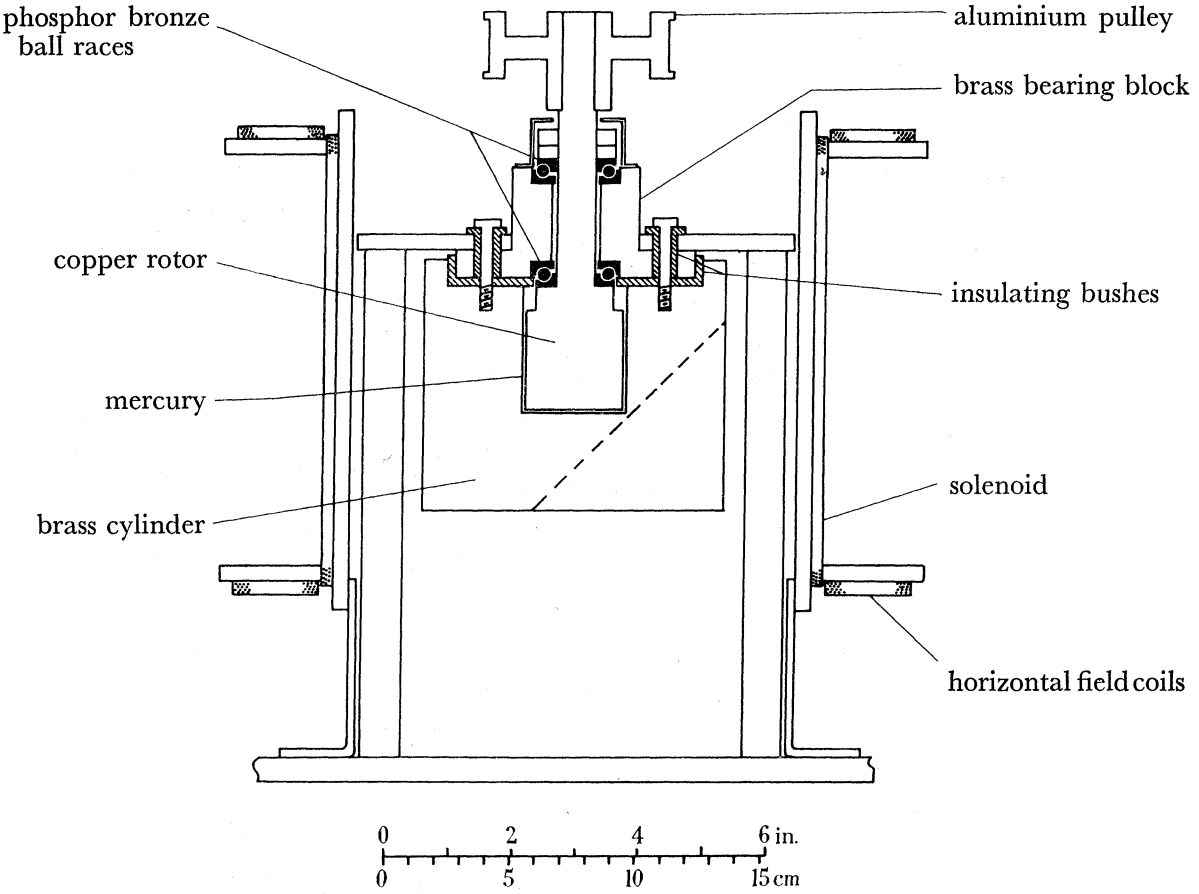

FIGURE 1. Rotor assembly.

Three interchangeable outer brass cylinders were used (figure 4): one, which will be called the symmetrical block, was a solid cylinder except for the internal cylindrical cavity; in the second, the hollow block, this cavity was bored right through, a brass or Perspex plug being inserted to provide the bottom surface of the cavity; the third, the asymmetrical block, was similar to the first except that it had been cut away at the bottom to give a plane surface at 45° to the axis, leaving a minimum thickness of 0·15 cm between the oblique surface and the bottom edge of the cavity.

The rotor was driven by an endless woven cotton belt from a series-wound reversible $\frac{1}{4}$ h.p. a.c. motor 1 m away, the speed being controlled by a variable transformer or a rheostat. Various pulleys were used on the motor and rotor shafts to give speed ratios of 1:2, 1:1 and 2:1, the speed of the motor pulley being measured by a commercial stroboscope.

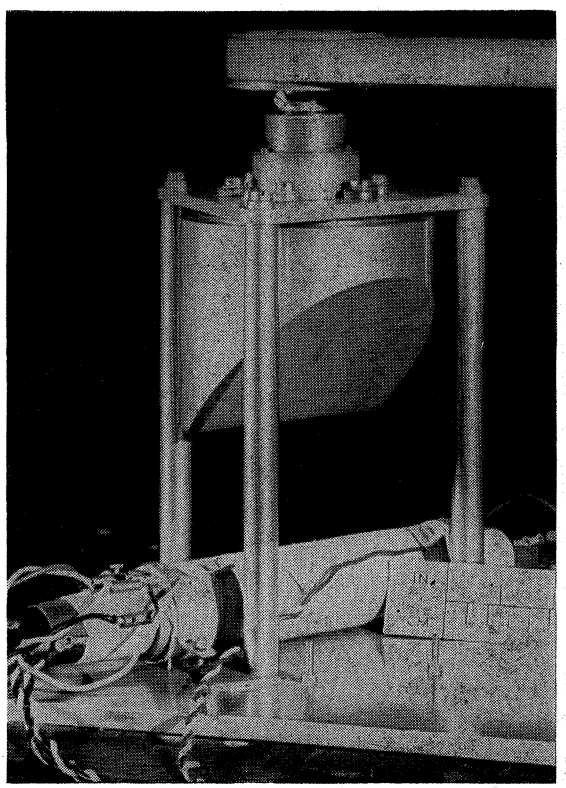

FIGURE 2. Fluxgate and rotor assembly.

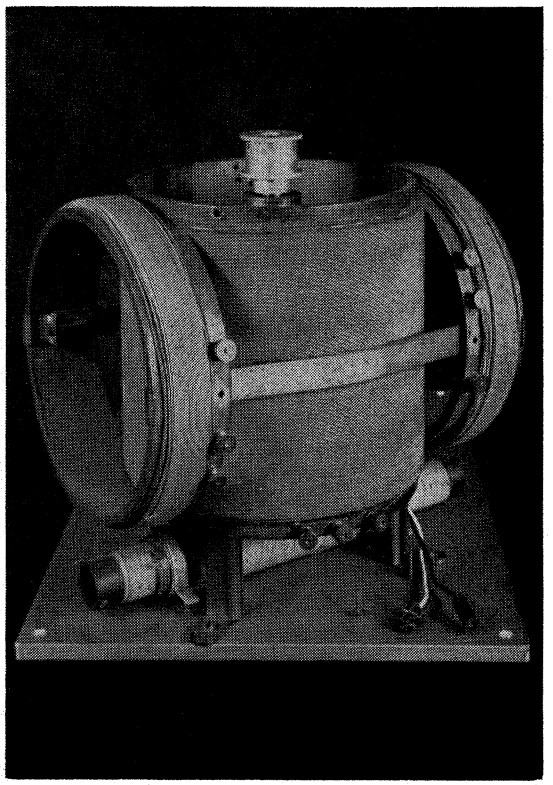

FIGURE 3. Inducing field coil assembly.

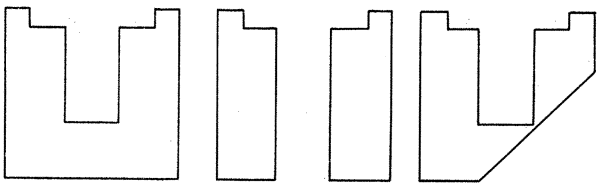

FIGURE 4. Outer conductors.

A vertical solenoid centrally placed about the rotor gave an axial inducing field, uniform to 2 % throughout the rotor, of up to 150 G at a power consumption of 250 W. Two coils strapped to the solenoid gave a transverse horizontal field of up to 20 G at 130 W, this field being uniform to 4 % throughout the rotor. This arrangement of coils enabled the transverse field to be applied in any horizontal direction, and also enabled both axial and transverse fields to be applied simultaneously if necessary.

The rotor assembly and motor were fastened to a wooden bench placed away from water pipes, electric conduits, etc., and the controls for the fluxgate, motor, field coil and stroboscope were on a bench several metres away.

PHILOSOPHICAL TRANSACTIONS OF THE ROYAL SOCIETY A MATHEMATICAL, PHYSICAL & ENGINEERING SCIENCES

The fluxgate was one which had been built by Goldsac (unpublished work); it had a sensitivity of about 20γ/mA, and the element would operate in fields of 0 to 50γ. By applying negative feedback through a solenoid round the fluxgate element, the sensitivity could be varied from 20 to 4000γ/mA, the feedback also stabilizing the overall sensitivity against variations of fluxgate sensitivity and amplifier gain. The necessary backing-off fields were conveniently applied using the same feedback solenoid, as were calibration fields. For most of the work the fluxgate was used at a sensitivity of about 1000γ/mA, and the output meter was a microammeter shunted to give 1 mA full-scale deflexion and a critically damped swing of 5 s. This damping effectively smoothed out short-period magnetic disturbances. The meter was read to 1 or 2 μA (i.e. 1 or 2γ) and was calibrated to this accuracy.

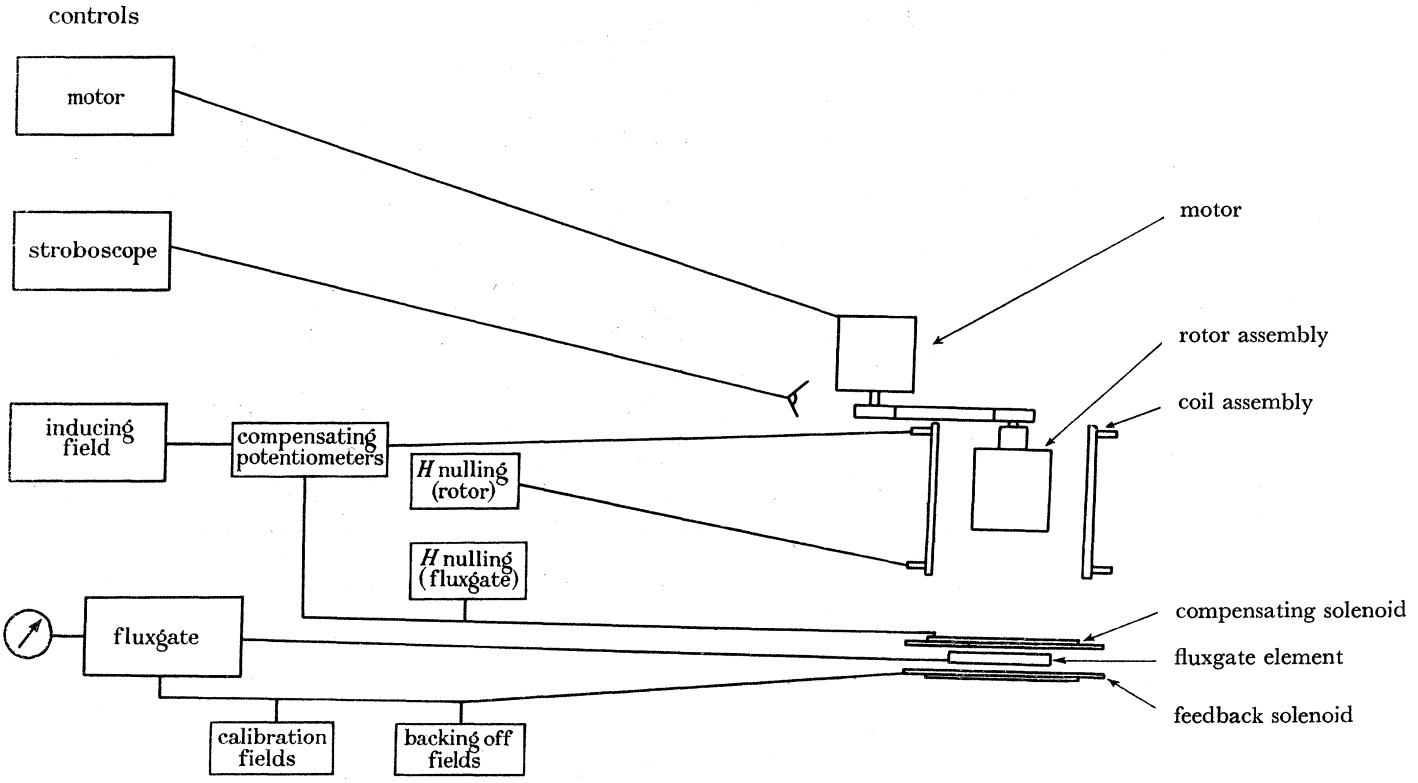

FIGURE 5. Block diagram of apparatus.

The fluxgate element was a tight push fit in the feedback solenoid, which was itself a tight push fit in a compensating solenoid, the whole being clamped wherever it was desired to measure the field, usually on the base-plate, under the axis of rotation. The compensating solenoid had two separate windings, one being split at the centre, and enabled the fluxgate to operate in the large inducing fields. When the vertical solenoid was being used, a current was passed through the split winding so as to annul, as far as possible, the diverging components of the inducing field, while the other winding was used to annul any field component along the fluxgate, which in this case was nominally perpendicular to the inducing field axis. Both these windings were fed from potentiometer circuits working from the potential drop across resistances in the inducing field circuit, so that, once set, the compensation automatically followed small changes in the inducing field current. With reasonable care in

centring the fluxgate and coils, the full fluxgate sensitivity of 20γ/mA could be obtained with an axial inducing field of 50 G, and, using similar compensating circuits, with a transverse inducing field of up to 20 G perpendicular to the fluxgate or 6 G parallel to it. The fluxgate element was normally alined E–W; when it was N–S the earth's field over it was cancelled by an additional current through the compensating solenoid.

Both the vertical solenoid and the horizontal field coils were wound in two sections, so the earth's field at the rotor could be annulled independently of producing the inducing field. Thus the field at the rotor could be exactly reversed merely by reversing the main inducing coil current. A block diagram of the various control and compensating circuits is given in figure 5. The stability of all the compensating circuits was such that the time variation of the field measured by the fluxgate was not appreciably greater when the inducing field was applied. Care had to be taken, however, to avoid vibration of the coil assembly, as the accompanying large changes of field at the fluxgate element could cause instability.

2·4. *Experimental method*

The stroboscope was calibrated from 500 to 3000 rev/min, and could be compared with the frequency of the mains at 1500 and 3000 rev/min. A spot determination of speed in this range was accurate to about ± 50 rev/min, with corresponding accuracy at the lower and higher submultiple and multiple speeds. For more accurate measurements the stroboscope was set at 3000 rev/min and the motor speed adjusted to a convenient submultiple or multiple of this. Thus, by using the several pulley ratios, rotor speeds of 500, 750, 1000, 1500, 2000, 2250, 3000, 3750, 4500, 6000, 7500, 9000 and 12000 rev/min were obtained, the reproducibility of speed when switching the motor on and off varying from about 25 to 50 rev/min through this range.

The experiments were performed in the Physical Laboratories, Manchester University, where during most of the day there was random magnetic noise of 5 to 20γ amplitude and field changes of up to 100γ/h, so frequent reference had to be made to the zero level of the field. Final measurements were made by working at one speed at a time, alternating 'at speed' and 'zero speed' readings at uniform time intervals, 8 to 10 double readings taking 3 to 5 min. This eliminated any zero drift linear with time, and any large non-linear change was generally noticed and the affected readings rejected and repeated. For each speed a mean deflexion was obtained with a standard deviation of about 2γ, the actual value varying between 1γ for very quiet periods and 5γ during very disturbed periods when measurements would not normally be made.

This method involved rapid switching of the motor, and this was in any case necessary at high speeds because the heating of the rotor assembly was very considerable. About 200 W was absorbed at 7500 rev/min, mainly in the mercury layer, giving a temperature rise of 3° C in the 40 s at full speed needed for one complete set of measurements at this speed for one direction of rotation. Copper, mercury and brass have appreciable temperature coefficients of resistivity, (1 to 4) $\times 10^{-3}$/° C, so the temperature of the rotor assembly was noted throughout the measurements and empirical corrections applied to the observed induced fields to refer them to a standard temperature, these corrections being obtained from auxiliary experiments in which the assembly was heated externally.

PHILOSOPHICAL TRANSACTIONS OF THE ROYAL SOCIETY A MATHEMATICAL, PHYSICAL & ENGINEERING SCIENCES

In the axial field investigations the fluxgate was horizontal and parallel to the plane of the oblique surface of the asymmetrical block, i.e. parallel to the direction of the induced field. In the transverse field investigations the inducing field was N–S, so that the earth's field could be annulled, and measurements of the induced field were made with the fluxgate element horizontal, parallel and perpendicular to the inducing field, the magnitude and direction of the total induced field then being computed. As it was not possible to set the fluxgate element to better than about 1°, measurements were made for both directions of rotation, the mean of the two giving the required value. This procedure is justified provided that the deviation from the desired position is small; for 3° deviation the error involved is less than 0·2 %.

In some measurements the usable speed range was limited by the breakdown of the mercury contact at high speeds. This was caused by the mercury moving away from the bottom of the rotor, the centrifugal force setting up a pressure distribution which reduced the pressure on the axis and tended to move the mercury outwards and up past the side of the rotor. The exact pressure distribution was not calculated, but a cavity was bound to form on the axis at some critical speed when the absolute pressure there became negative. Cavitation would occur at lower speeds if the mercury was dirty or any air was trapped in it, because the pressure gradient would draw less dense matter into the cavity. The formation of a cavity was confirmed by observing the bottom surface of the mercury through the Perspex plug in the hollow block. If the space between the rotor and block were completely filled with mercury, cavitation could not occur, but this was not feasible because of the difficulty of preventing mercury from being forced into the bottom bearing. However, an optimum quantity of mercury was found which could not escape into the bearings but which did increase the critical speed to a higher value, and a cleaning technique was evolved which gave the best possible contact. The rotor could then be spun up to about 5000 rev/min without cavitation occurring.

2·5. *Discussion of errors*

Measurements were made with inducing fields of 4 to 150 G such as to give a maximum induced field at the fluxgate element of about 500γ. The inducing field current of 1 to 5 A was kept constant to $\pm$0·005 A. The rotor speed was constant to $\pm$(20 to 50) rev/min at each speed, equivalent to variations of induced field of about $\pm 4\gamma$, but being random these will be included in the standard deviation of $\pm$(2 to 3) γ obtained for the mean of eight to ten readings at each speed. The error involved in applying the temperature correction was probably less than 3γ in most cases. The fluxgate sensitivity showed variations of about 1 %, and it was not easily possible to calibrate the fluxgate to better accuracy than this, so the standard deviation for the induced field at each speed may be put about 5γ. In the transverse inducing field investigations, the measurements for the fluxgate element parallel and perpendicular to the inducing field were combined to give the magnitude h and direction ζ of the total induced field, with standard deviations of about 5γ and 2° (at low speed) to 0·5° (for speeds greater than 1000 rev/min), respectively.

Systematic errors due to change in position of the coil assembly or fluxgate element, and dimensional changes at the higher temperatures, can be shown to be negligible. There were, however, two possible sources of systematic error the effect of which could not be reliably

estimated: in the speed range for which measurements were used the spurious field change given by the 50 c/s field of the motor was less than 5γ, but its magnitude and sign varied and no systematic attempt was made to allow for it; and, though the brass blocks were machined to close dimensional tolerances, there may have been internal variations in conductivity due to inhomogeneities in the casting from which they were made.

The experiments were designed primarily to measure the variation of induction with speed, and the standard deviations quoted above are for relative measurements only; absolute measurements were subject to much greater uncertainty. The constants of the field coils could not be calculated to better than 2 or 3 %. The fluxgate could be calibrated to 1 % for uniform fields but the observed field was non-uniform, approximating to that of a dipole about 12 cm from the centre of the fluxgate element, the mu-metal cores of which were 12 cm long, and it is estimated that the effective absolute sensitivity was not known to better than about $\pm 10\,\%$.

Measurements with the isolated rotor were made successfully up to 12000 rev/min, this limit being set by the safe working speed of the motor. With the mercury contact, the speed limit was set by the motor power at about 8000 rev/min. In the experiments using axial inducing field the maximum useful speed was 4500 rev/min, because of the breakdown of the contact, but in the transverse field measurements no change in the induced field due to this could be observed up to 8000 rev/min. This was understandable because in this case the current flow through the mercury would normally be concentrated at the outer part of the bottom surface of the rotor, and with the quantity of mercury used there would always be contact for at least 0·2 cm from the edge. However, measurements at 6000 and 7500 rev/min were not completely satisfactory, and have not been used, because at the highest motor powers, spurious field changes of up to 40γ were observed. These were due to the motor, and could not be completely eliminated or allowed for as they were critically dependent on the experimental conditions.

2·6. *Experimental results and discussion*

It is convenient to summarize and discuss separately the results for axial and transverse applied fields. For transverse field the discussion is independent of the rest of this paper. The discussion for axial inducing field does, however, draw on several results of the theoretical investigations described later in this paper, particularly in § 7.

Axial applied field

Preliminary experiments with the isolated rotor, and with this in the solid (symmetrical) block, showed that there was no detectable external induced field in these cases with axial symmetry. This was to be expected from the symmetry theorem proved in § 6·1.

With the rotor in the asymmetrical block, measurements were possible up to 4500 rev/min ($\alpha = 7$) and showed no appreciable departure from a linear relation between induced field and speed of rotation (figure 6). The observed relation was

$$h = (2{\cdot}3 \pm 0{\cdot}3) \times 10^{-4} H_0 \alpha', \qquad (2{\cdot}6)$$

where h, the horizontal component, was measured 12 cm under the bottom of the rotor.

(The copper rotor and brass block were separated by a small but appreciable thickness of mercury, all three metals having different conductivities. However, in this case almost all the induced currents flow through all three media, and one has to use an appropriate intermediate conductivity σ', and hence $\alpha' = 2\pi\sigma'\omega a^2$. The conductivity of copper is $6{\cdot}2 \times 10^{-4}$, of mercury $0{\cdot}1 \times 10^{-4}$, and of the brass used $1{\cdot}22 \times 10^{-4}$ e.m.u.; σ' was taken as $1{\cdot}50 \times 10^{-4}$ e.m.u. It must be emphasized, however, that the qualitative features of the induction phenomena, and in particular the effect of the transverse secondary inducing field, depend on the parameter $\alpha = 2\pi\sigma\omega a^2$, where σ is the rotor conductivity.)

The external induced field in this case may be estimated theoretically in several ways.

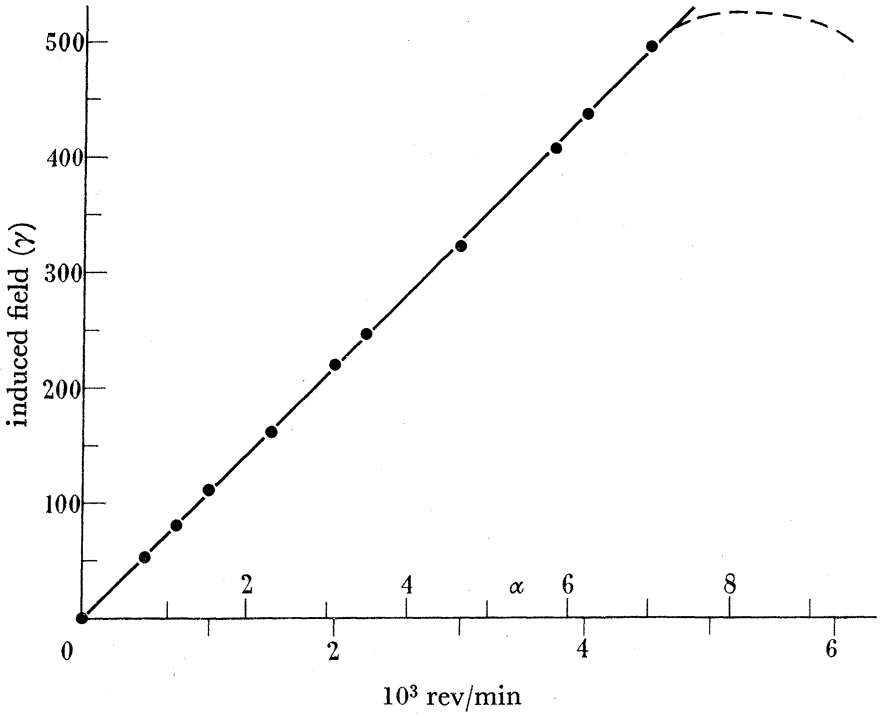

FIGURE 6. Induction in an axial inducing field.

Figure 7 shows one section of the experimental conductors superimposed on the theoretical current distribution in an infinite medium (figure 15). Various estimates of the effect of the finite boundary on the current distribution were made (e.g. that only those currents which would be completely inside the conductor would flow, or that the remaining currents were confined to flow just inside the boundary), allowing for the different boundaries in the different meridian sections. The resultant external magnetic field was then obtained by summing the dipole moments of the individual current circuits in each section. This method predicts fields at the point of observation lying in the range

$$h = (1 \text{ to } 2) \times 10^{-4} H_0 \alpha'. \qquad (2{\cdot}7)$$

An alternative method of taking account of the experimental boundary conditions is to approximate them by boundaries for which theoretical solutions are given in § 7, i.e. an

infinite plane boundary and a spherical boundary. These are indicated in figure 8. For the plane case (7·9) gives a field at the magnetometer of magnitude

$$h \simeq 6 \times 10^{-4} H_0 \alpha'. \tag{2·8}$$

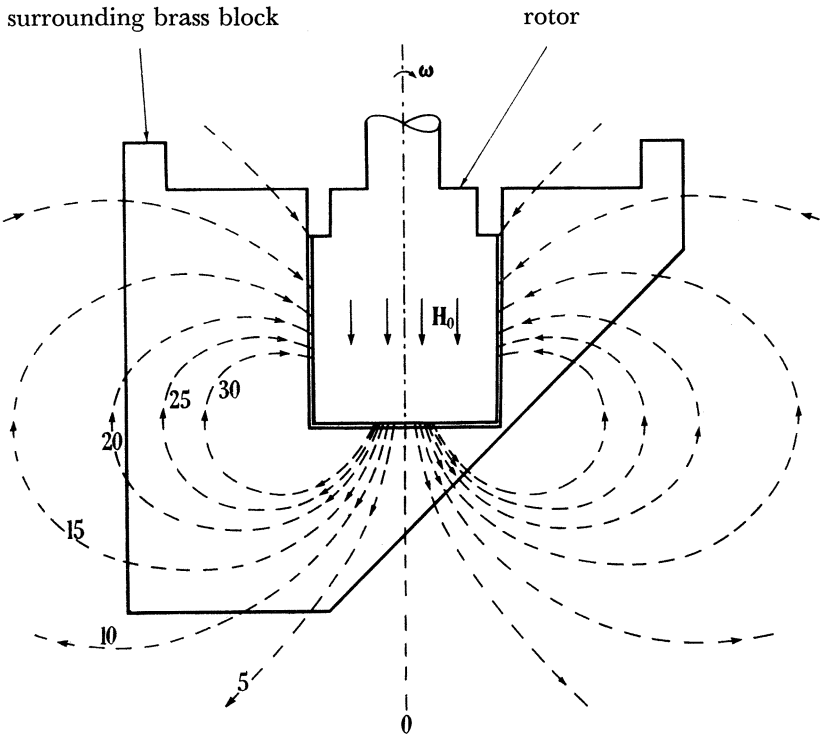

FIGURE 7. Limitation of current flow by the boundary of the outer conductor. The current distribution for a surrounding conductor of infinite extent is superposed on a cross-section of the asymmetrical block.

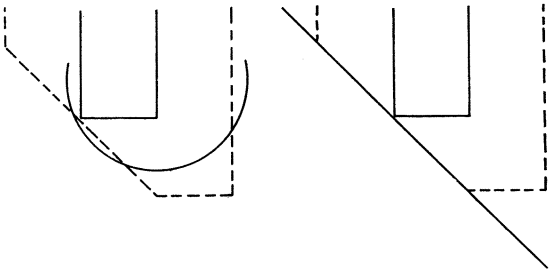

FIGURE 8. Approximation of the asymmetrical block by a sphere and by a half-space.

This is most probably an over-estimate, as no account is taken of the limitation of the currents by the cylindrical surface of the block. For the spherical boundary 7·7 gives

$$h \simeq 2 \times 10^{-4} H_0 \alpha', \tag{2·9}$$

taking $R \simeq 14$ cm, $L \simeq 3$ cm. The agreement between the theoretical estimates (2·7), (2·8), (2·9) and the experimental result (2·6) is surprisingly good considering the crudity of the approximations made.

The magnetic field at the rotor given by the current reflected at the outside boundary leads to a second-order external induced field. This can be estimated from the results of

§ 7·4. Equation (7·26) gives the mean field over the end of the rotator due to the currents reflected from an infinite plane boundary. This secondary inducing field is transverse to the axis of rotation, and the secondary induced field due to it may be estimated by approximating the experimental rotor by a sphere of radius 2 cm. This leads to a secondary induced field h_2 at the magnetometer of magnitude

$$h_2 \simeq 8 \times 10^{-6} H_0 \alpha' M(\alpha), \tag{2·10}$$

where $M(\alpha)$ is the magnitude function ($2M/H_0a^3 = h/h_{\max.}$) given in figure 9. The direction of $\mathbf{h}_2$ will rotate through $\frac{1}{2}\pi$ as α increases, but for high velocities it is parallel to the primary induced field $\mathbf{h}_1$. Thus the secondary field increases with $\mathbf{h}_1$ (which is proportional to $H_0\alpha'$) with the addition of the factor $M(\alpha)$. The effect of this will be to give an upward curvature to the induced field against speed graph, which will flatten into a straight line of increased slope as $M(\alpha)$ approaches its limiting value of 1·0 at high speeds. Combining (2·10) with the experimental result (2·6) we have

$$h_2/h_1 \sim 3{\cdot}5 \times 10^{-2} M(\alpha). \tag{2·11}$$

At $\alpha = 7$ (the maximum value in this experiment) $M(\alpha) = 0{\cdot}5$, and (2·11) predicts a difference between low and high speeds of only about 1%, which is too small to be observed. Any such difference of slope in the experimental results is only 2 or 3%; the standard deviation of the experimental points from a single straight line is 3γ, and the maximum deviation 6γ.

Transverse applied field

In this case the direction of the induced field varies with velocity, but the induced dipole moment $\mathbf{M}$ is always in the plane normal to the axis of rotation; the induced field may therefore be specified by h, its magnitude, and ζ, the angle between $\mathbf{h}$ and $-\mathbf{H}_0$.

The full theoretical solutions for an isolated sphere and an infinite cylinder have been given in a convenient form by Bullard (1949*b*, pp. 419–422). They are, for a sphere

$$(2M/H_0a^3)\, e^{i\zeta} = J_{\frac{5}{2}}[(-2i\alpha)^{\frac{1}{2}}]/J_{\frac{1}{2}}[(-2i\alpha)^{\frac{1}{2}}], \tag{2·12}$$

and for an infinite cylinder (M = dipole moment per unit length)

$$(2M/H_0a^2)\, e^{i\zeta} = J_2[(2i\alpha)^{\frac{1}{2}}]/J_0[(2i\alpha)^{\frac{1}{2}}]. \tag{2·13}$$

The experimental values of $h/h_{\max.}$ and ζ for the isolated finite cylinder, and the corresponding theoretical curves for a sphere ($2M/H_0a^3$ and ζ) and for an infinite cylinder ($2M/H_0a^2$ and ζ) are plotted in figure 9. The value of $h_{\max.}$, the magnitude of the induced field at infinite speed, was obtained with an accuracy of about 5% by extrapolation of a plot of h against $\alpha^{-\frac{1}{2}}$ (see (5·34)).

At low speeds the experimental curves lie between the theoretical ones, but at higher speeds tend very closely to those for a sphere, as would be expected. The actual value of $h_{\max.}$ agrees with the theoretical one to within the experimental accuracy of absolute measurements.

In the limit $\alpha \to \infty$ we have, from (2·12), $\zeta \to 0$. This agrees with the result of Thomson (1893). However, Gans (1921), quoted by Valentiner (1927), states that in the limit $\zeta \to 45°$.

That this latter result is incorrect is confirmed by the experiment, in which ζ decreased to 25° at $\alpha = 18$, in agreement with Bullard's result.

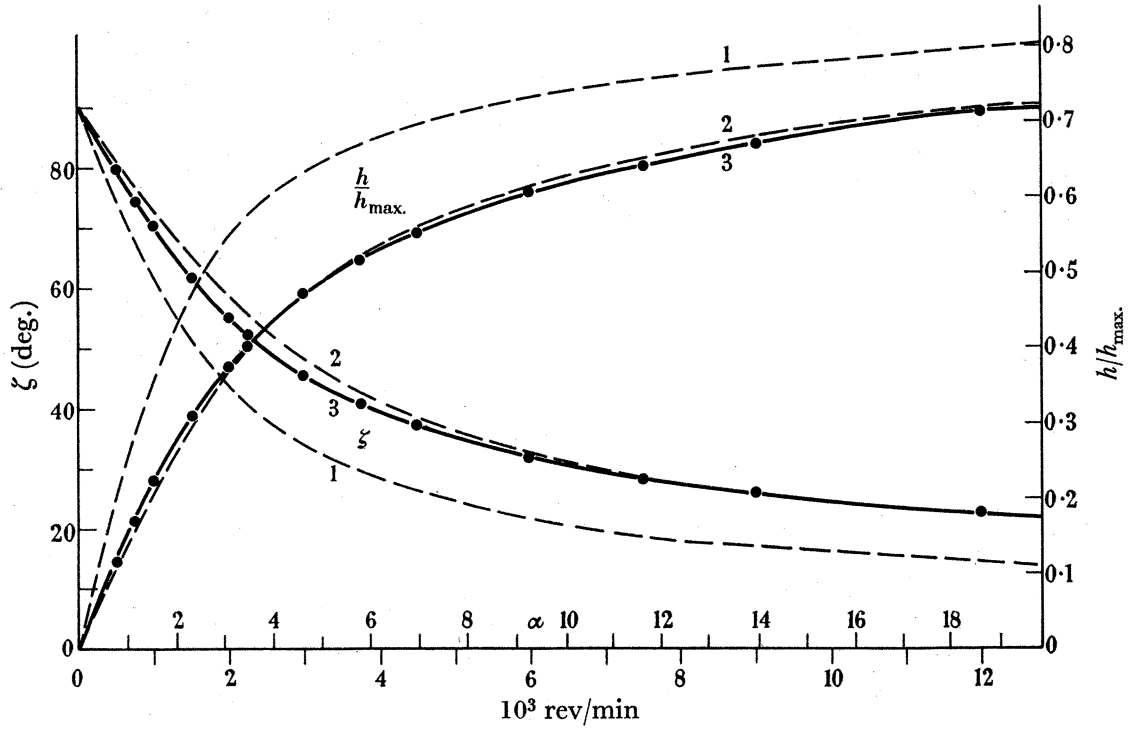

FIGURE 9. Induction in transverse field. Curves 1, theoretical (infinite cylinder); 2, theoretical (sphere); 3, experimental (cylinder).

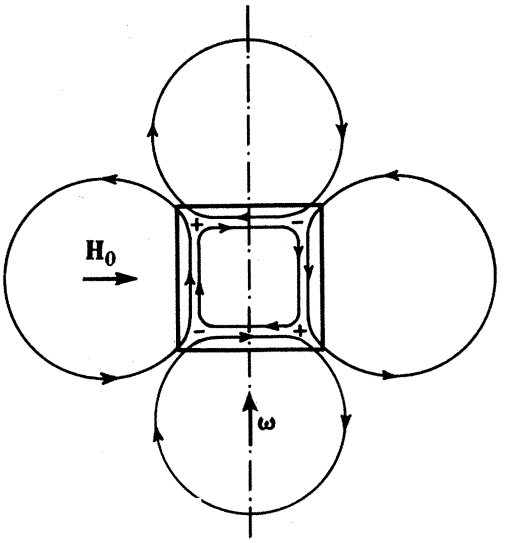

FIGURE 10. Schematic representation of the induced current system of a rotator in transverse field for $\alpha \ll 1$.

In this case of transverse inducing field the electric field outside the rotator is approximately that of a transverse central quadrupole, giving four external current circuits when the rotator is surrounded by a conducting medium. This is illustrated in figure 10, which shows schematically the surface-charge distribution and the four external current circuits

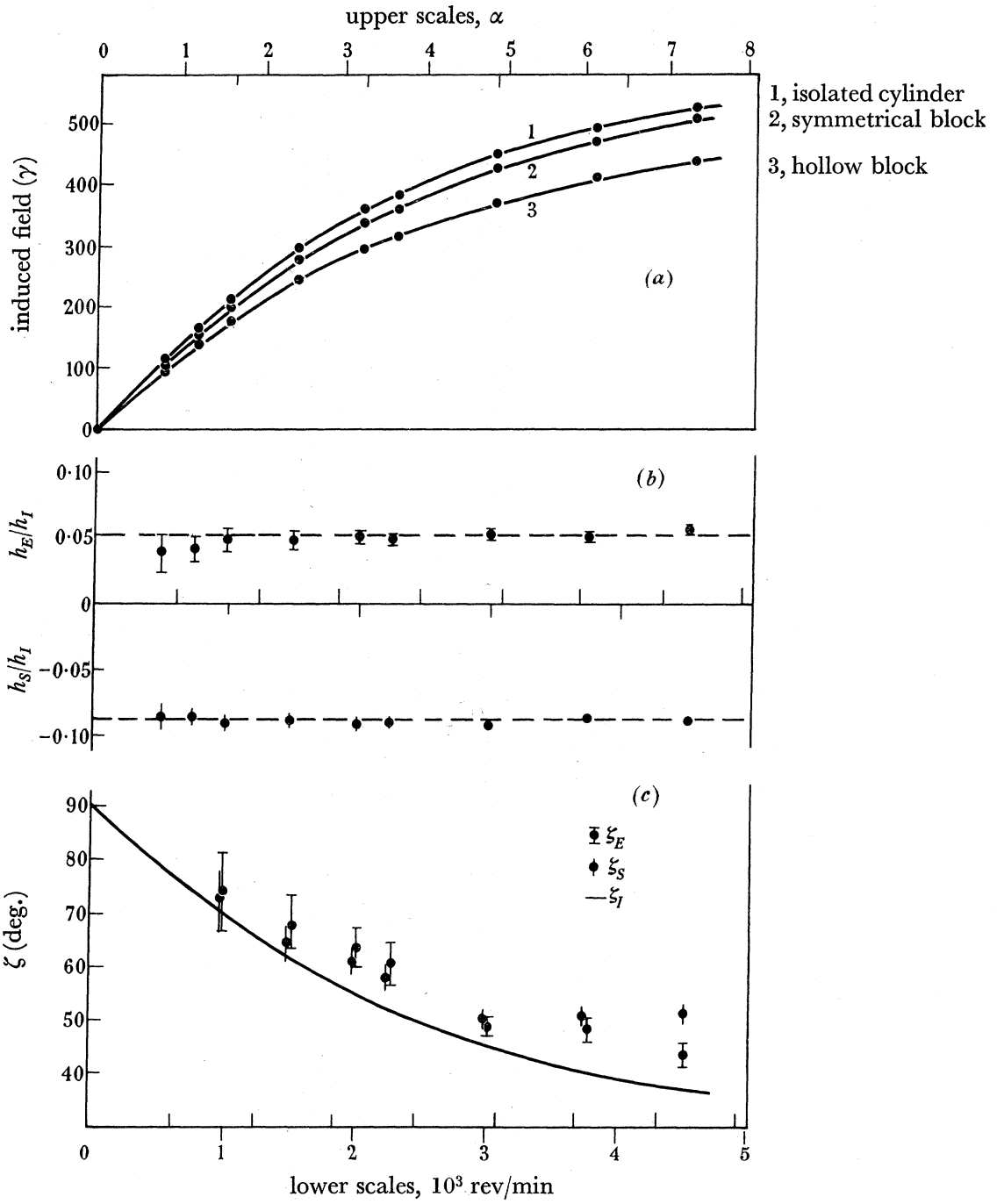

FIGURE 11. Induction in transverse field. Effect of outer conductors.

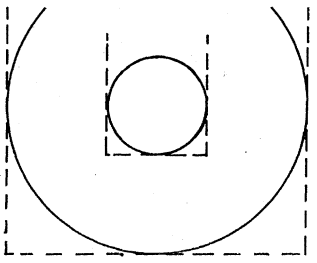

FIGURE 12. Approximation of experimental conductors by concentric spheres.

superimposed on the internal current circuit for an isolated rotator. The opposing currents shown inside the ends of the rotator would of course partially cancel, but it is convenient to visualize the current system as five separate loops. The two loops at the ends have the same direction as the internal one, while the two side loops have the opposite direction; the magnitudes of all five increase together to their limiting value attained when $\alpha \to \infty$. The experimental curves for h when the rotor was in the hollow block with Perspex plug, and in the symmetrical block, are compared with that for the isolated rotor in figure 11*a*. With the hollow block only the two side loops would be introduced, thus reducing the external induced field, while with the symmetrical block one end loop, which would increase the field, would be present as well. An indication of the separate contributions of these loops was obtained by subtracting the appropriate measurements. In figure 11*b* are plotted h_S/h_I and h_E/h_I, where h_S and h_E are the fields given by this method for the contribution of one side loop and one end loop, and h_I is the field given by the isolated cylinder, all normalized to the same distance from the magnetometer; in figure 11*c* the values of ζ_S and ζ_E are compared with the experimental curve for ζ_I. The errors are large, because we are now dealing with the small differences of large fields, but the field ratios appear to remain constant at about $-8{\cdot}8\,\%$ for the side loop and $+5{\cdot}0\,\%$ for the end loop. No great reliance can be placed on the values obtained, because this method of estimation ignores any distortion of the current distribution inside the rotor, but they should be of the right order of magnitude. When allowance is made for the difference in conductivity between the brass blocks and the copper rotor, for uniform conductivity and the particular boundary conditions of the experiment the fields of the external circuits would be 20 to 40 % of that given by the isolated cylinder. The exact solution has been given by Bullard (1949*b*, pp. 422–423, $n = m = 1$) for the similar case of a spherical rotator of radius a in a concentric spherical conductor of radius b (a and b are interchanged in Bullard's notation). Figure 12 compares the experimental case with the spherical one for $b = 3a$. For this theoretical case an estimate can be made of the induced field due to one of the external current circuits; this gives a value of 50 % of the field due to the internal current circuit, in good agreement with the experimental value considering the approximation made.

From this solution of Bullard's we see that, for an isolated rotator, the plane of the external electric quadrupole field rotates through only $\frac{1}{4}\pi$, while the plane of the internal current circuit rotates through $\frac{1}{2}\pi$, as α is varied from 0 to ∞. However, in an infinite conducting medium the plane of the external currents follows that of the internal currents as this rotates through $\frac{1}{2}\pi$, and this is very nearly the case for any conductor with $b > 2a$. Figure 11*c* shows that in the experiment ζ_S and ζ_E appear to decrease more slowly than ζ_I, but it is doubtful if the difference is significant, and it is not more than could be due to the particular geometry of the experimental conditions.

PART C. BASIC THEORY OF INDUCTION IN ROTATING CONDUCTORS

The following sections 3, 4 and 5 give an account of the theory of induction in rotators embedded in conductors of infinite extent. The results of these three sections are then extended in part D to rotators in finite conducting shells.

The results of §§ 3 to 5 overlap to a considerable extent those of Bullard's (1949*b*) treatment of induction in a rotating sphere. Bullard used generating functions from which **E** and **H**

can be derived; these generating functions can be expanded in series of terms each of which contains two factors: a radial function, which has to satisfy an ordinary differential equation with boundary conditions, and a spherical harmonic. The results are confined to bodies bounded by concentric spheres or coaxial cylinders. Our approach differs from Bullard's in that we start from integral solutions of the field equations, and work with the field vectors themselves rather than with generating functions. This procedure has two merits. First, some of the salient properties of the solutions are contained in the Green's functions of the integral solutions; as a consequence, the physical properties of the solutions come out of the theory in a clearer way than with Bullard's methods. Secondly, the work with the field vectors instead of the generating functions releases us from the constraint of having to start out from a co-ordinate system of spherical or cylindrical symmetry. The price we have to pay for these advantages is that when the applied field $\mathbf{H}_0$ does not have axial symmetry we can give the solutions only for the extreme cases of low and high angular velocity, whereas Bullard gave them for the complete range.

We saw in § 1·1 that the equations satisfied by the magnetic field have quite different characters according to whether the fields are axially symmetric or not. We shall deal with the case of axial symmetry in § 3, and with the case of no axial symmetry in §§ 4 and 5. As we have already mentioned in § 1·1 the case of transverse (i.e. without axial symmetry) inducing field may be subdivided into the cases of low angular velocity, when $\alpha \ll 1$ (§ 4) ($\alpha =$ (radius/skin depth)^2 is the parameter $2\pi\sigma\omega a^2$), and of high angular velocity, when $\alpha \gg 1$ (§ 5).

3. Axial symmetry ($m = 0$)

We consider a material of uniform conductivity σ filling all space. Part of the material is in rotational motion about an axis, and the remainder is stationary. The applied magnetic field $\mathbf{H}_0$ is assumed to be uniform, parallel to the axis of rotation, and time-independent. (Actually some of the results are valid for a non-uniform but axially symmetric $\mathbf{H}_0$.) As examples we take a semi-infinite cylinder, a finite cylinder and a sphere. We calculate the induced magnetic field, the accompanying current system and the electromagnetic couples. Finally, we discuss the case of a time-dependent angular velocity.

We use spherical polar co-ordinates (r, θ, λ) and cylindrical polar co-ordinates (ρ, z, λ) with the $\theta = 0$ and z axes coinciding with the axis of rotation.

3·1. *Field equations*

We saw in § 1·1 that the magnetic field $\mathbf{H}(= \mathbf{H}_0 + \mathbf{h})$ has to satisfy the equations

$$\frac{\partial \mathbf{H}}{\partial t} = \frac{1}{4\pi\sigma} \nabla^2 \mathbf{H} + \nabla \wedge (\mathbf{v} \wedge \mathbf{H}), \tag{3·1}$$

$$\nabla . \mathbf{H} = 0, \tag{3·2}$$

where v is the local velocity of the matter.

When a magnetic field satisfying (3·1) and the boundary conditions has been found, the corresponding electric field can be computed from (1·1). (The complete solution obtained may violate the conservation of charge because the displacement current is being neglected.)

In the case of an $\mathbf{H}_0$ with axial symmetry, the treatment of equation (3·1) is much simplified by the fact that the induced magnetic field $\mathbf{h}$ must everywhere be parallel to $\hat{\boldsymbol{\lambda}}$. For the time-independent case, the proof of this statement is as follows: E_λ vanishes because $\int \mathbf{E}.\mathrm{d}\mathbf{s}'$ taken around any circle centred on the axis and lying in a plane perpendicular to the axis is zero $\left(\int \mathbf{E}.\mathrm{d}\mathbf{s}' = -\int \mathrm{d}A'\hat{\mathbf{n}}'.\partial\mathbf{H}/\partial t = 0\right)$. Moreover, the vector $\mathbf{v}\wedge\mathbf{H}$ has no λ component. Thus the current density $\sigma(\mathbf{E}+\mathbf{v}\wedge\mathbf{H})$ has no λ component, and has axial symmetry because of the symmetry of the whole problem. After a little consideration, one can see from the Biot–Savart law that such a current system gives rise to a magnetic field pointing everywhere along $\hat{\boldsymbol{\lambda}}$.

If there is time-dependence the argument given in the preceding paragraph breaks down because $\int \mathbf{E}.\mathrm{d}\mathbf{s}' \neq 0$. If one nevertheless assumes the result to be true, then, as we shall see in § 3·5, one can find a solution of (3·1) which behaves in the prescribed way at infinity. Therefore if one assumes the uniqueness of the solution of the field equations corresponding to specified (axially symmetric) distributions of velocity and applied magnetic field, then it follows that the assumption of an induced field parallel to λ must be correct.

Thus with axial symmetry $\mathbf{v}\wedge\mathbf{h} = 0$, and we may replace the term $\boldsymbol{\nabla}\wedge(\mathbf{v}\wedge\mathbf{H})$ in (3·1) by $\boldsymbol{\nabla}\wedge(\mathbf{v}\wedge\mathbf{H}_0)$. The applied field $\mathbf{H}_0$ satisfies

$$\partial\mathbf{H}_0/\partial t = 0, \quad \nabla^2\mathbf{H}_0 = 0, \quad \boldsymbol{\nabla}.\mathbf{H}_0 = 0. \tag{3·3}$$

Therefore from (3·1) and (3·2) we see that the induced magnetic field $\mathbf{h}$ must satisfy

$$\frac{\partial\mathbf{h}}{\partial t} = \frac{1}{4\pi\sigma}\nabla^2\mathbf{h} + \boldsymbol{\nabla}\wedge(\mathbf{v}\wedge\mathbf{H}_0), \tag{3·4}$$

$$\boldsymbol{\nabla}.\mathbf{h} = 0. \tag{3·5}$$

Equation (3·5) is satisfied by a field $\mathbf{h}(r,\theta,\lambda) = h_\lambda(r,\theta)\,\hat{\boldsymbol{\lambda}}$, where h_λ is independent of λ.

Until we come to § 3·5 we shall confine ourselves to the time-independent case. If we write $\mathbf{v}(r,\theta,\lambda) = r\sin\theta\,\omega(r,\theta)\,\hat{\boldsymbol{\lambda}}$, equation (3·4) becomes

$$\nabla^2\mathbf{h} = -4\pi\sigma\boldsymbol{\nabla}\wedge(\mathbf{v}\wedge\mathbf{H}_0) = -4\pi\sigma r\sin\theta(\mathbf{H}_0.\boldsymbol{\nabla}\omega)\,\hat{\boldsymbol{\lambda}}. \tag{3·6}$$

The solution of (3·6) is

$$\mathbf{h}(\mathbf{r}) = \sigma \int_{\text{all space}} \mathrm{d}V' \frac{r'\sin\theta'[\mathbf{H}_0.\boldsymbol{\nabla}'\omega(r',\theta')]}{|\mathbf{r}-\mathbf{r}'|}\hat{\boldsymbol{\lambda}}', \tag{3·7}$$

where variables of integration are denoted by a prime. For a rigid rotator, ω changes only at the surface; equation (3·7) then reduces to

$$\mathbf{h}(\mathbf{r}) = -\sigma\omega \int_{\substack{\text{rotator}\\ \text{surface}}} \mathrm{d}A' \frac{r'\sin\theta'\mathbf{H}_0.\hat{\mathbf{n}}'}{|\mathbf{r}-\mathbf{r}'|}\hat{\boldsymbol{\lambda}}', \tag{3·8}$$

where $\hat{\mathbf{n}}$ is the unit vector pointing outwards normally to the rotator surface.

3·2. *Cylinder*

Semi-infinite cylinder

We now apply (3·6) and (3·8) to a semi-infinite cylinder of radius a, rotating with constant angular velocity ω, and embedded in rigid conducting surroundings of infinite extent. The origin of co-ordinates is taken at the centre of the end disk (see figure 13).

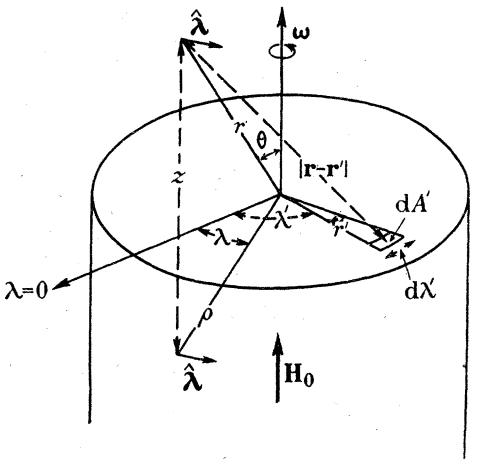

FIGURE 13. Co-ordinate system. End of cylinder.

The product $\mathbf{H}_0 . \hat{\mathbf{n}}$ is equal to $+H_0$ on the end disk of the cylinder, and is zero everywhere else. Equation (3·8) therefore simplifies to

$$\mathbf{h}(\mathbf{r}) = -\sigma\omega H_0 \int_{\text{end disk}} \mathrm{d}A' \frac{r'}{|\mathbf{r}-\mathbf{r}'|}\hat{\boldsymbol{\lambda}}'. \tag{3·9}$$

According to (3·6) we have $\nabla^2\mathbf{h} = 0$ everywhere except on the end disk; from (3·9) $\mathbf{h}$ is continuous there, while the derivative $\partial\mathbf{h}/\partial n$ along the outward normal has a discontinuity

$$\left(\frac{\partial\mathbf{h}}{\partial n}\right)_+ - \left(\frac{\partial\mathbf{h}}{\partial n}\right)_- = +4\pi\sigma\omega r H_0\hat{\boldsymbol{\lambda}}, \tag{3·10}$$

where the subscripts $(+, -)$ denote that the derivative is taken just outside or just inside the cylinder.

Now the vector function

$$\operatorname{sgn}(\cos\theta)\,\tfrac{2}{3}\pi\sigma\omega H_0 r^2 P_2^1(\cos\theta)\,\hat{\boldsymbol{\lambda}} \tag{3·11}$$

(where $\operatorname{sgn}(\cos\theta) = \pm 1$ when $\cos\theta \gtrless 0$) satisfies Laplace's equation everywhere except on the plane $\theta = \frac{1}{2}\pi$ (the end disk); the function (3·11) vanishes there and its normal derivative has the same discontinuity as $\mathbf{h}$. Therefore the vector function

$$\mathbf{h} - \operatorname{sgn}(\cos\theta)\,\tfrac{2}{3}\pi\sigma\omega H_0 r^2 P_2^1(\cos\theta)\,\hat{\boldsymbol{\lambda}} \tag{3·12}$$

satisfies Laplace's equation everywhere in $r<a$; for $r<a$ it is therefore possible to expand $\mathbf{h}$ in the series

$$\mathbf{h} = \operatorname{sgn}(\cos\theta)\,\tfrac{2}{3}\pi\sigma\omega H_0 r^2 P_2^1(\cos\theta)\,\hat{\boldsymbol{\lambda}} + \sum_{s=0}^{\infty} b_s \left(\frac{r}{a}\right)^{2s+1} P_{2s+1}^1(\cos\theta)\,\hat{\boldsymbol{\lambda}}. \tag{3·13}$$

(That $\mathbf{h}$ is parallel to $\hat{\boldsymbol{\lambda}}$ is a consequence of (3·9). The occurrence of P_n^m with only the value $m = 1$ follows from $\hat{\boldsymbol{\lambda}} = -\hat{\mathbf{x}}\sin\lambda + \hat{\mathbf{y}}\cos\lambda$. Because both $\mathbf{h}$ and the term containing sgn $(\cos\theta)$ are even in $\cos\theta$, we must have $n = 2s+1$ in $P_n^1(\cos\theta)$ in (3·13).)

For $r > a$, we have $\nabla^2\mathbf{h} = 0$ everywhere. Hence we can write, for $r > a$,

$$\mathbf{h} = \sum_{s=0}^{\infty} a_s \left(\frac{a}{r}\right)^{2s+2} P_{2s+1}^1(\cos\theta)\,\hat{\boldsymbol{\lambda}}. \tag{3·14}$$

The coefficients a_s, b_s can be determined from the behaviour of the integral solution (3·9) near the axis. Denoting by a prime the co-ordinates of the points of integration (which here lie in the end disk of the cylinder), we have

$$|\,\mathbf{r}-\mathbf{r}'\,|^2 = [r^2 - 2rr'\sin\theta\cos(\lambda-\lambda') + r'^2], \tag{3·15}$$

so that near $\theta = 0$ equation (3·9) gives

$$\begin{aligned}\mathbf{h} &= -\sigma\omega H_0\hat{\boldsymbol{\lambda}}\int_{\lambda'=0}^{2\pi} d\lambda' \int_{r'=0}^{a} r'\,dr' \frac{r'\cos(\lambda-\lambda')}{(r^2+r'^2)^{\frac{1}{2}}}\left[1 + \frac{rr'}{r^2+r'^2}\cos(\lambda-\lambda')\,\theta + O(\theta^2)\right] \\ &= -\sigma\omega H_0\hat{\boldsymbol{\lambda}}\pi\theta[1+O(\theta)]\,r[(a^2+r^2)^{\frac{1}{2}} + r^2(a^2+r^2)^{-\frac{1}{2}} - 2r],\end{aligned} \tag{3·16}$$

if we note that the contribution from the component of $\hat{\boldsymbol{\lambda}}'$ (at the point of integration) perpendicular to $\hat{\boldsymbol{\lambda}}$ (at the field point) vanishes on integration. By expanding (3·16) in ascending and descending powers of (r/a), putting

$$P_{2s+1}^1(\cos\theta) = (s+1)\,(2s+1)\,\theta[1+O(\theta^2)]$$

in (3·13) and (3·14), and equating coefficients of equal powers of (r/a), one finds

for $r < a$,

$$\begin{aligned}\mathbf{h} = 2\pi\sigma\omega a^2 H_0\hat{\boldsymbol{\lambda}}\Big[&\tfrac{1}{3}\,\mathrm{sgn}(\cos\theta)\left(\frac{r}{a}\right)^2 P_2^1(\cos\theta) - \tfrac{1}{2}\left(\frac{r}{a}\right)P_1^1(\cos\theta) \\ &+ \sum_{s=1}^{\infty}\frac{(-1)^s(2s-2)!}{2^{2s}(s+1)!\,(s-1)!}\left(\frac{r}{a}\right)^{2s+1} P_{2s+1}^1(\cos\theta)\Big];\end{aligned} \tag{3·17}$$

for $r > a$,

$$\begin{aligned}\mathbf{h} &= -2\pi\sigma\omega a^2 H_0\hat{\boldsymbol{\lambda}}\sum_{s=0}^{\infty}\frac{(-1)^s(2s)!}{2^{2s+2}(s+2)!\,s!}\left(\frac{a}{r}\right)^{2s+2} P_{2s+1}^1(\cos\theta) \\ &= -2\pi\sigma\omega a^2 H_0\hat{\boldsymbol{\lambda}}\left[\left(\frac{a^2}{8r^2}\right)\sin\theta + O\left(\frac{a^4}{r^4}\right)\right].\end{aligned} \tag{3·18}$$

This case of a single-ended cylinder is of particular interest as being most amenable to experimental investigation; the solution has therefore been studied in more detail. By using the terms with $s \leqslant 3$ of the expansions (3·17) and (3·18), numerical computations have been made with an accuracy of about 1 %. Figure 14 gives an axial section of the surfaces of constant h in units of $10^{-2}\sigma\omega a^2 H_0$.

The current density is given by $\mathbf{j} = (1/4\pi)\,\nabla\wedge\mathbf{h}$. We define a current function I by

$$I(r,\theta,\lambda) = \int_0^r dr' j_\theta(r',\theta,\lambda)\sin\theta. \tag{3·19}$$

The surfaces of constant I are parallel to the direction of current flow, and the current flowing between the surfaces I and $I+\delta I$ in a sector of angle $\delta\lambda$ is $\delta I\delta\lambda$. We have

$$I(r,\theta,\lambda) = \frac{\sin\theta}{4\pi}\int_0^r r'\,\mathrm{d}r'(\nabla\wedge\mathbf{h})_\theta(r',\theta,\lambda) = -\frac{r\sin\theta}{4\pi}h_\lambda(r,\theta,\lambda). \tag{3·20}$$

The function I has also been computed, and an axial section of the surfaces of constant I, expressed in units of $10^{-3}\sigma\omega a^3H_0$, is given in figure 15.

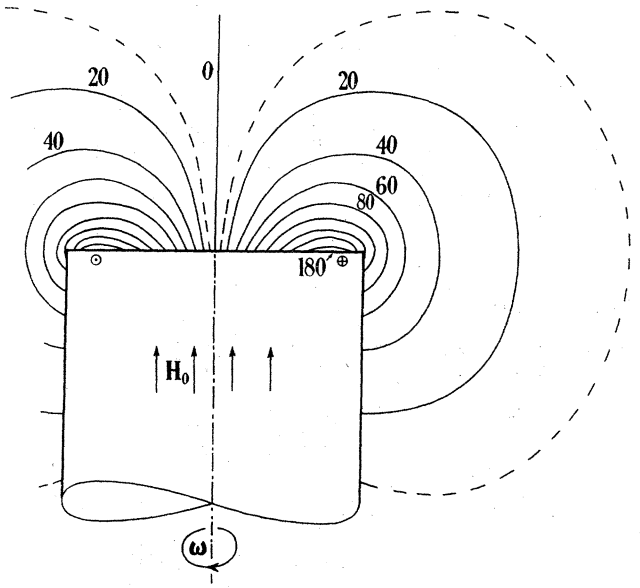

FIGURE 14. Contours of induced magnetic field. One end of a cylinder. Uniform axial inducing field. Surrounding conductor of infinite extent. The figures give the strength of h_λ in units of $10^{-2}H_0\sigma\omega a^2$.

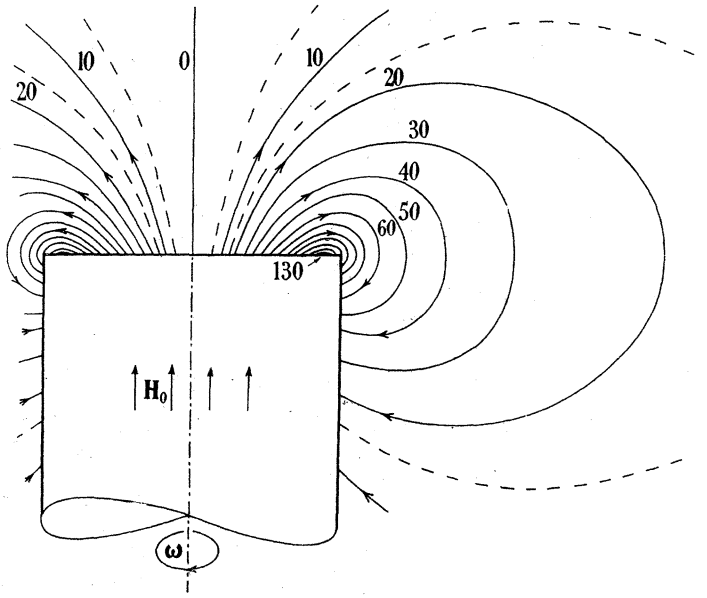

FIGURE 15. Lines of current flow. One end of a cylinder. Uniform axial inducing field. Surrounding conductor of infinite extent. The figures give the values of the current function I in units of $10^{-3}H_0\sigma\omega a^3$.

Finite cylinder

For this case an approximate solution can be obtained by combining the leading terms in the appropriate expansions (3·17) and (3·18) for the two ends. If we take the origin at the midpoint of the axis of a cylinder of radius a, length $2u$, we obtain, for large r,

$$\mathbf{h} = -2\pi\sigma\omega a^2 H_0 \hat{\boldsymbol{\lambda}}\left[\left(\frac{3ua^2}{4r^3}\right)\sin\theta\cos\theta + O\left(\frac{a^4}{r^4}\right) + O\left(\frac{a^2u^3}{r^5}\right)\right]. \tag{3·21}$$

In order to obtain numerical results it is more convenient, and also more accurate for small r, to make a graphical transformation of the semi-infinite cylinder solution from the spherical polar co-ordinate form to a cylindrical polar one; a simple axial displacement followed by addition then gives the solution for the finite cylinder. Figure 16 shows the current distribution for a cylinder of length $2a$.

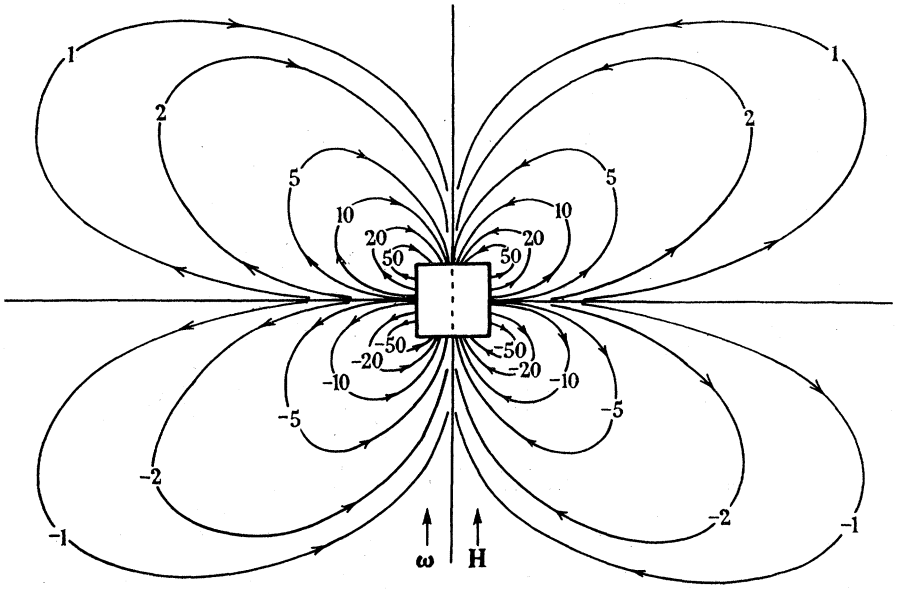

FIGURE 16. Lines of current flow; finite cylinder. Uniform axial inducing field. Surrounding conductor of infinite extent. The axial length is equal to the diameter. The figures give the values of the current function I in units of $10^{-3}H_0\sigma\omega a^3$.

3·3. *Sphere*

We consider a rigid conducting sphere of radius a rotating at constant angular velocity ω in a rigid conducting medium of infinite extent. The origin of co-ordinates is at the centre of the sphere (see figure 17).

Equation (3·8) reduces to

$$\begin{aligned}\mathbf{h} &= -\sigma\omega a H_0 \int_A \mathrm{d}A' \frac{\sin\theta'\cos\theta'}{|\mathbf{r}-\mathbf{r}'|}\hat{\boldsymbol{\lambda}}' \\ &= -\sigma\omega a^3 H_0 \hat{\boldsymbol{\lambda}} \int_A \mathrm{d}\theta'\,\mathrm{d}\lambda' \sin^2\theta' \cos\theta' \cos(\lambda-\lambda') \\ &\quad \times \sum_{n=0}^{\infty} \frac{a^n}{r^{n+1}}\left[P_n(\cos\theta')\,P_n(\cos\theta) + 2\sum_{s=1}^{n} P_n^s(\cos\theta')P_n^s(\cos\theta)\cos s(\lambda-\lambda')\right] \\ &= -\tfrac{4}{5}\pi\sigma\omega a^5 H_0 \hat{\boldsymbol{\lambda}} \frac{\sin\theta\cos\theta}{r^3}\end{aligned} \tag{3·22}$$

outside the sphere. Equation (3·22) is a special case of a result obtained by Bullard (1949*b*, p. 424).

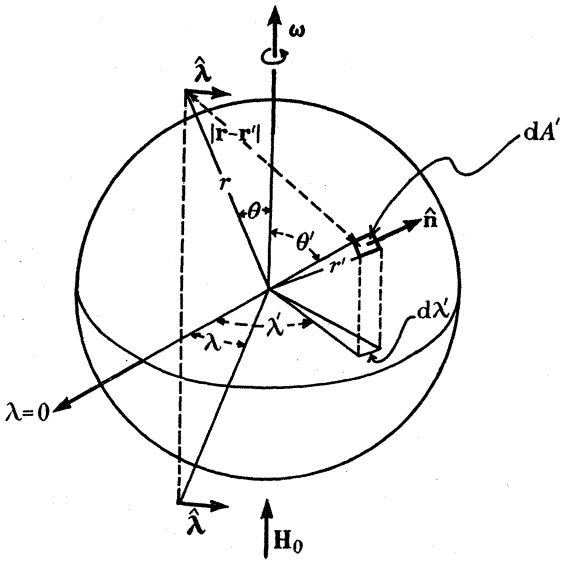

FIGURE 17. Co-ordinate system; sphere.

3·4. *Electromagnetic couples*

In this case of axial symmetry the electromagnetic couple $\boldsymbol{\Gamma}$ on a rotator in a conducting medium of infinite extent can be calculated as follows. We have, taking the origin of $\mathbf{r}$ on the axis of rotation and integrating over the volume of the rotator,

$$\boldsymbol{\Gamma} = \int_V \mathrm{d}V' \mathbf{r} \wedge (\mathbf{J} \wedge \mathbf{H}) = \frac{1}{4\pi} \int_V \mathrm{d}V' \mathbf{r} \wedge [(\nabla \wedge \mathbf{H}) \wedge \mathbf{H}]$$

$$= \frac{1}{4\pi} \int_A \mathrm{d}A' (\mathbf{r} \wedge \mathbf{H}\, \hat{\mathbf{n}}' . \mathbf{H} - \tfrac{1}{2} \mathbf{r} \wedge \hat{\mathbf{n}}' H^2), \tag{3·23}$$

where the intregal is now taken over the rotator surface (see, for example, Stratton 1941, chap. II). In our case of axial symmetry, the second term vanishes on integration. Since $\hat{\mathbf{n}} . \mathbf{H}$ can be replaced by $\hat{\mathbf{n}} . \mathbf{H}_0$, the $\mathbf{r} \wedge \mathbf{H}_0$ part of the first term also vanishes on integration. Thus (3·23) can be written in the form

$$\boldsymbol{\Gamma} = \frac{1}{4\pi} \int_A \mathrm{d}A' \mathbf{r} \wedge \mathbf{h}\, \hat{\mathbf{n}}' . \mathbf{H}_0. \tag{3·24}$$

We shall estimate $\boldsymbol{\Gamma}$ for a thin cylinder in a uniform field $\mathbf{H}_0$ parallel to the axis; (3·24) then breaks up into separate contributions from the two end disks. If we use the fact that $\mathbf{h} = h_\lambda(\rho, z)\, \hat{\boldsymbol{\lambda}}$, we have

$$\boldsymbol{\Gamma} \simeq 2 . \tfrac{1}{2} H_0 \hat{\mathbf{z}} \int_0^a r' \mathrm{d}r' r' h_\lambda(\rho', 0), \tag{3·25}$$

where $h_\lambda \hat{\boldsymbol{\lambda}}$ is the induced field calculated in § 3·2 for a semi-infinite cylinder. (We make the approximation of neglecting at each end disk the induced field given by the other end disk.) If we insert for h_λ the term of lowest order in (r/a) from the series (3·17), we obtain

$$\boldsymbol{\Gamma} \simeq H_0 \hat{\mathbf{z}} \int_0^a r' \mathrm{d}r' r' \left(-\alpha H_0 \frac{r'}{2a}\right) = -\tfrac{1}{8} \alpha H_0^2 a^3 \hat{\mathbf{z}}, \tag{3·26}$$

where $\alpha = 2\pi\sigma\omega a^2$. For the opposite extreme of a spherical rotator Bullard (1949*b*, p. 431) obtained $\boldsymbol{\Gamma} = -(4/75)\, \alpha H_0^2 a^3 \hat{\mathbf{z}}$. Thus $\boldsymbol{\Gamma}$ is roughly independent of the length of a cylinder.

3·5. *Time-dependent angular velocity*

When the angular velocity of the rotator is time-dependent, equation (3·6) ceases to be valid and we have to work with the full equation (3·4):

$$\nabla^2\mathbf{h}-4\pi\sigma\frac{\partial\mathbf{h}}{\partial t}=-4\pi\sigma\nabla\wedge(\mathbf{v}\wedge\mathbf{H}_0). \tag{3·27}$$

Sinusoidal angular velocity

A solution of equation (3·27) has been given by Bullard (1949*b*) for a sphere rotating with sinusoidally varying angular velocity. We shall treat this problem by another method. When $\mathbf{v}$ is proportional to $e^{i\nu t}$, the solution of (3·27) is

$$\mathbf{h}(\mathbf{r},t)=+\sigma\int_{\text{rotator}}dV'\frac{\exp[-(1+i)(2\pi\sigma\nu)^{\frac{1}{2}}|\mathbf{r}-\mathbf{r}'|]}{|\mathbf{r}-\mathbf{r}'|}\nabla'\wedge[\mathbf{v}(\mathbf{r}',t)\wedge\mathbf{H}_0]. \tag{3·28}$$

(The solution corresponding to the real part of $\mathbf{v}$ is the real part of (3·28), (3·29) and (3·30).) As in the time-independent case, for a rigid rotator, equation (3·28) reduces to a surface integral. If the angular velocity is $\omega_0 e^{i\nu t}$, we have

$$\mathbf{h}(\mathbf{r},t)=-\sigma\omega_0\int_{\substack{\text{rotator}\\\text{surface}}}dA'\frac{\exp[-(1+i)(2\pi\sigma\nu)^{\frac{1}{2}}|\mathbf{r}-\mathbf{r}'|]}{|\mathbf{r}-\mathbf{r}'|}\rho'\mathbf{H}_0.\hat{\mathbf{n}}'\hat{\boldsymbol{\lambda}}'e^{i\nu t}. \tag{3·29}$$

If $2\pi\sigma\nu a^2\gg1$, where a is the radius of the rotator, then the exponential in (3·29) is negligible except in a relatively thin surface layer of thickness $\sim d=(2\pi\sigma\nu)^{-\frac{1}{2}}$ on both sides of the rotator surface; the induced field is confined to this surface layer. Only surface points within a distance not larger than about $(2\pi\sigma\nu)^{-\frac{1}{2}}$ from a given field point contribute to the induced field at that field point. For a field point whose perpendicular distance from the rotator surface is $p(\ll a)$, we can evaluate (3·29) by taking the factor $(\rho\mathbf{H}_0.\hat{\mathbf{n}}\hat{\boldsymbol{\lambda}})$ outside the integral and assigning to this factor its value at the foot of the perpendicular from the field point to the rotator surface; the remaining surface integral converges so rapidly that the curved surface can be replaced by an infinite plane; we then easily obtain

$$\mathbf{h}(\mathbf{r},t)\simeq-\sigma\omega_0\rho\mathbf{H}_0.\hat{\mathbf{n}}\hat{\boldsymbol{\lambda}}.2\pi\frac{\exp[+(1-i)(2\pi\sigma\nu)^{\frac{1}{2}}p]}{(1+i)(2\pi\sigma\nu)^{\frac{1}{2}}}e^{i\nu t}. \tag{3·30}$$

The maximum induced field therefore occurs on the surface and is

$$|\mathbf{h}(\mathbf{r},t)|_{\text{max.}}=\left|\left(\frac{\pi\sigma}{\nu}\right)^{\frac{1}{2}}\rho\omega_0\mathbf{H}_0.\hat{\mathbf{n}}\right|_{\text{max.}}. \tag{3·31}$$

On the other hand, if $2\pi\sigma\nu a^2\ll1$ then we have $d\gg a$. The exponential in (3·29) can be replaced by 1 when $\mathbf{r}$ is within a distance of $\sim d$ from all points of the rotator surface. Therefore when $2\pi\sigma\nu a^2\ll1$ the pattern of $\mathbf{h}$ is the time-independent pattern in and near the rotator, and follows the angular velocity adiabatically.

Short pulse

The general solution of equation (3·27) is

$$\mathbf{h}(\mathbf{r},t)=\sigma^{\frac{3}{2}}\int_{-\infty}^{t}dt'\int_{\text{all space}}dV'\nabla\wedge[\mathbf{v}(\mathbf{r}',t')\wedge\mathbf{H}_0]\frac{\exp\left[-\frac{|\mathbf{r}-\mathbf{r}'|^2\pi\sigma}{t-t'}\right]}{(t-t')^{\frac{3}{2}}}. \tag{3·32}$$

As it stands, equation (3·32) is useful for obtaining the effect of a short pulse of rotation which occurs during the time $(t_0-\frac{1}{2}\Delta T)<t<(t_0+\frac{1}{2}\Delta T)$. If $(t-t_0)\gg\Delta T$, then (3·32) becomes

$$\mathbf{h}(\mathbf{r},t)\simeq\left(\frac{\sigma}{t-t_0}\right)^{\frac{3}{2}}\Delta T\int_{\text{all space}}\mathrm{d}V'\exp\left[-\frac{|\mathbf{r}-\mathbf{r}'|^2\pi\sigma}{(t-t_0)}\right]\nabla\wedge[\bar{\mathbf{v}}(\mathbf{r}')\wedge\mathbf{H}_0(\mathbf{r}')],\qquad(3\cdot33)$$

where $\bar{\mathbf{v}}(\mathbf{r})$ is the time average of $\mathbf{v}(\mathbf{r},t)$ over the duration of the pulse.

Step function

The solution for a step function angular velocity ($\omega=0$ for $t<0$, $\omega=$ constant for $t>0$) can be obtained either by integrating with respect to time in (3·32) and using the formula

$$t^{-\frac{3}{2}}\exp\left[-\frac{R^2\pi\sigma}{t}\right]=-\frac{1}{R\sigma^{\frac{1}{2}}}\frac{\partial}{\partial t}\operatorname{erf}\left[R\left(\frac{\pi\sigma}{t}\right)^{\frac{1}{2}}\right],\qquad(3\cdot34)$$

or directly from (3·27) by the use of well-known operator methods (see, for example, Jeffreys & Jeffreys 1950). We obtain

$$\mathbf{h}(\mathbf{r},t)=\sigma\int\mathrm{d}V'\frac{\{1-\operatorname{erf}[R(\pi\sigma/t)^{\frac{1}{2}}]\}}{R}\nabla\wedge(\mathbf{v}\wedge\mathbf{H}_0),\qquad(3\cdot35)$$

where we have put $|\mathbf{r}-\mathbf{r}'|\equiv R$.

Since for small and large x respectively we have

$$\begin{aligned}1-\operatorname{erf}(x)&=1-\frac{2}{\sqrt{\pi}}\left(x-\frac{x^3}{3}+\frac{x^5}{10}-\ldots\right)\quad\text{for } x\ll1,\\&=\frac{\exp(-x^2)}{x\sqrt{\pi}}\left(1-\frac{1}{2x^2}+\frac{3}{4x^4}-\ldots\right)\quad\text{asymptotically for } x\gg1,\end{aligned}\qquad(3\cdot36)$$

it follows from (3·35) (putting $x=(R^2\pi\sigma/t)^{\frac{1}{2}}$) that

$$\mathbf{h}(\mathbf{r},t)=\sigma\int_{\text{rotator}}\mathrm{d}V'\frac{1}{R}\nabla\wedge(\mathbf{v}\wedge\mathbf{H}_0)\frac{\exp(-R^2\pi\sigma/t)}{\pi^{\frac{1}{2}}(R^2\pi\sigma/t)^{\frac{1}{2}}}\left(1-\frac{t}{2R^2\pi\sigma}+\ldots\right),\qquad(3\cdot37)$$

when $t\ll R^2\pi\sigma$ for all points of the rotator, and

$$\mathbf{h}(\mathbf{r},t)=\sigma\int_{\text{rotator}}\mathrm{d}V'\frac{1}{R}\nabla\wedge(\mathbf{v}\wedge\mathbf{H}_0)\left[1-\frac{2}{\sqrt{\pi}}\left(\frac{R^2\pi\sigma}{t}\right)^{\frac{1}{2}}+\frac{2}{\sqrt{\pi}}\frac{1}{3}\left(\frac{R^2\pi\sigma}{t}\right)^{\frac{3}{2}}-\ldots\right],\qquad(3\cdot38)$$

when $t\gg R^2\pi\sigma$ for all points of the rotator. By (3·37), $\mathbf{h}$ will be exponentially small at any point until $t\sim R^2\pi\sigma$. The second term in (3·38) vanishes since $\int\mathrm{d}V'\nabla\wedge(\mathbf{v}\wedge\mathbf{H}_0)=0$ (by partial integration); the induced field therefore has the asymptotic value of the time-independent case when $t\gg R^2\pi\sigma$ for all points of the rotator. The deviation from the asymptotic value decreases as $t^{-\frac{3}{2}}$.

Finite pulse

The induced field due to an angular velocity $\omega=0$ for $t<0$ and $t>T$, $\omega=\omega_0$ (constant) for $0<t<T$ can be found by superimposing two solutions (3·35). During the time $0<t<T$ the induced field is given by (3·35). For $t>T$, we have

$$\mathbf{h}(\mathbf{r},t)=\sigma\int_{\text{rotator}}\mathrm{d}V'\frac{1}{R}\left[\operatorname{erf}\left(\frac{R^2\pi\sigma}{t-T}\right)^{\frac{1}{2}}-\operatorname{erf}\left(\frac{R^2\pi\sigma}{t}\right)^{\frac{1}{2}}\right]\nabla\wedge(\mathbf{v}\wedge\mathbf{H}_0).\qquad(3\cdot39)$$

The functions

$$1-\operatorname{erf}\left[\left(\frac{R^2\pi\sigma}{t}\right)^{\frac{1}{2}}\right] \qquad \text{for all } t>0,$$

and

$$f(t,T,R)\equiv 1-\operatorname{erf}\left[\left(\frac{R^2\pi\sigma}{t}\right)^{\frac{1}{2}}\right] \qquad \text{for } 0<t<T$$

$$\equiv \operatorname{erf}\left[\left(\frac{R^2\pi\sigma}{t-T}\right)^{\frac{1}{2}}\right]-\operatorname{erf}\left[\left(\frac{R^2\pi\sigma}{t}\right)^{\frac{1}{2}}\right] \quad \text{for } t>T \tag{3·40}$$

are shown in figures 18 and 19. Curves are given for $f(t, T, R)$ corresponding to a number of values of $R^2\pi\sigma$.

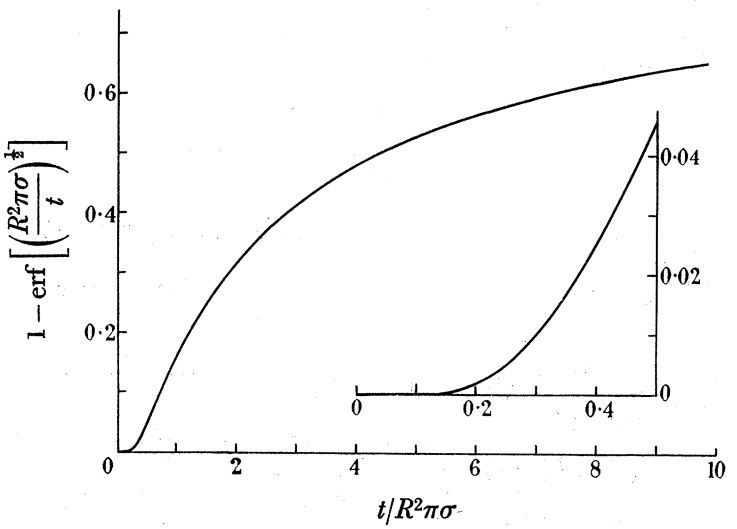

FIGURE 18. Propagation of a step-function disturbance.

For $t \gtrsim T$, $R^2\pi\sigma \gtrsim T$, we have

$$f(t,T,R) \simeq \frac{(R^2\pi\sigma)^{\frac{1}{2}}T}{(t-\frac{1}{2}T)^{\frac{3}{2}}\sqrt{\pi}} \exp\left(-\frac{R^2\pi\sigma}{t-\frac{1}{2}T}\right). \tag{3·41}$$

This approximation could be obtained directly from (3·32) if we treated the disturbance as a short pulse; it is in fact just another way of writing (3·33). The approximation (3·41) is shown in figure 19 for $R^2\pi\sigma = T$, $t > T$.

The maximum value of $f(t, T, R)$ at a fixed point occurs at time

$$t \simeq T \qquad \text{if} \quad R^2\pi\sigma \lesssim \tfrac{1}{3}T, \tag{3·42}$$

$$t \simeq \tfrac{2}{3}R^2\pi\sigma \qquad \text{if} \quad R^2\pi\sigma \gtrsim 3T. \tag{3·43}$$

At the shorter distances the observed disturbance lasts for a time $\sim T$; at the larger distances the interval between the instants at which $f(t, T, R)$ has half its maximum value is $1{\cdot}8R^2\pi\sigma$. Thus at the larger distances the time scale of the observed disturbance depends on the distance from the original disturbance rather than on the duration of the source pulse. Figure 19 shows that it is not possible to estimate T from the observed disturbance if $R^2\pi\sigma \gtrsim T$.

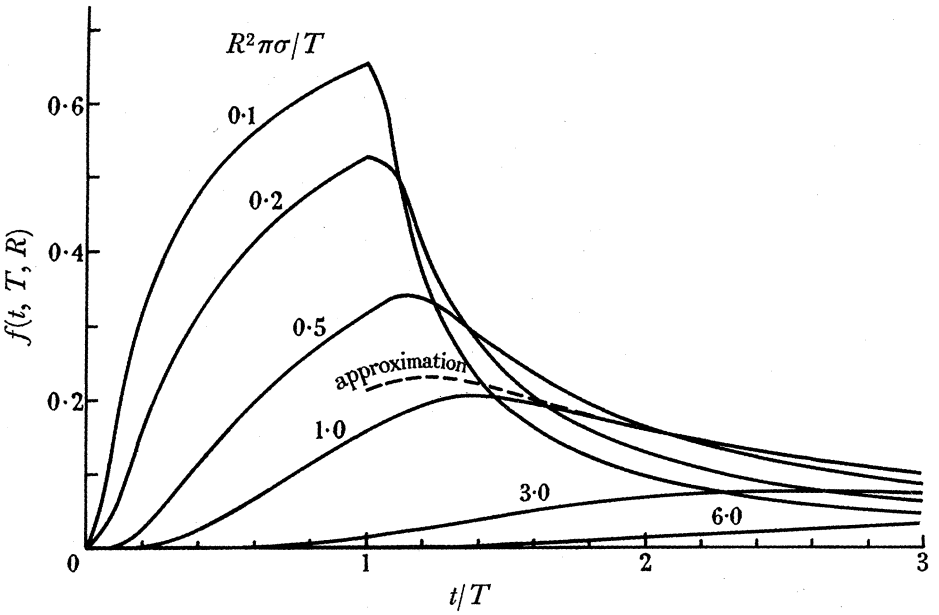

FIGURE 19. Propagation of a square-pulse disturbance of period T.

$$f(t, T, R) = 1 - \operatorname{erf}\left[\left(\frac{R^2\pi\sigma}{t}\right)^{\frac{1}{2}}\right] \qquad \text{for} \quad 0 < t < T,$$

$$= \operatorname{erf}\left[\left(\frac{R^2\pi\sigma}{t-T}\right)^{\frac{1}{2}}\right] - \operatorname{erf}\left[\left(\frac{R^2\pi\sigma}{t}\right)^{\frac{1}{2}}\right] \quad \text{for} \quad t > T.$$

The approximation is

$$f(t, T, R) \simeq \frac{1}{\sqrt{\pi}} \frac{T}{R^2\pi\sigma} \left(\frac{R^2\pi\sigma}{t - \frac{1}{2}T}\right)^{\frac{3}{2}} \exp\left(-\frac{R^2\pi\sigma}{t - \frac{1}{2}T}\right),$$

and is drawn for $t > T$, $R^2\pi\sigma = T$.

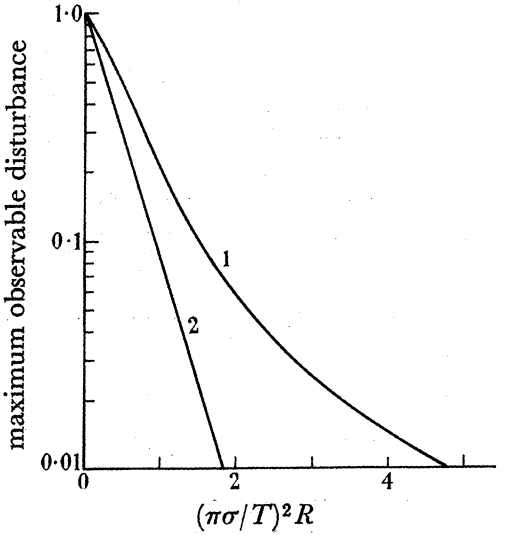

FIGURE 20. Attenuation of square pulse and sinusoidal disturbances. The curves drawn are

(1) square-pulse disturbance, duration T: $\left\{\operatorname{erf}\left[\left(\frac{R^2\pi\sigma}{t-T}\right)^{\frac{1}{2}}\right] - \operatorname{erf}\left[\left(\frac{R^2\pi\sigma}{t}\right)^{\frac{1}{2}}\right]\right\}_{\text{max.}}$,

(2) sinusoidal disturbance, period $2T$: $\exp\left(-2\pi\frac{R^2\pi\sigma}{T}\right)$.

The actual maximum value at a fixed point is

$$[f(t, T, R)]_{\max.} \simeq 1 - \left(\frac{4}{\pi}\frac{R^2\pi\sigma}{T}\right)^{\frac{1}{2}} \quad \text{if} \quad R^2\pi\sigma \lesssim \tfrac{1}{3}T, \tag{3·44}$$

$$\simeq 0{\cdot}23\,\frac{T}{R^2\pi\sigma} \quad \text{if} \quad R^2\pi\sigma \gtrsim 3T. \tag{3·45}$$

Equation (3·45) shows that for large R the maximum varies as $1/R^2$. This is in contrast to a maintained sinusoidal disturbance, for which the attenuation with distance is exponential. In figure 20 the attentuation of a square pulse of duration T is compared with that of a sinusoidal disturbance of period $2T$. The difference can be understood if we note that the Fourier transform of a pulse of length T is proportional to $\sin(\nu T/2)/(\nu T/2)$, and therefore does not change in order of magnitude from $\nu = 0$ to $\nu \sim 2/T$.

The effect of a finite acceleration time may be considered by building up the angular velocity in a series of steps. If the acceleration takes place in a time T', the remarks following equation (3·43) show that the details of the acceleration cannot be observed at distance R such that $R^2\pi\sigma \gtrsim T'$.

4. Transverse magnetic field at low angular velocity ($m \neq 0$, $\alpha \ll 1$)

We now turn to the more complicated case of fields without axial symmetry. The extra complication arises because the induced magnetic field $\mathbf{h}$ now interacts with $\mathbf{v}$ to give induced currents, in contrast to the axially symmetric case where $\mathbf{v} \wedge \mathbf{h} = 0$. However, if the velocities are sufficiently small, then the secondary induction effects are also small, and it is possible to obtain a solution expressed a a power series in the angular velocity. The first term in this solution is just what would have been obtained by neglecting the induction due to the induced field, that is, by replacing the term $(\mathbf{v} \wedge \mathbf{H})$ in the field equations by $(\mathbf{v} \wedge \mathbf{H}_0)$.

We start with the time-independent case, and obtain a criterion for the convergence of the power-series solution. We then relate this criterion to the skin depth observed by an observer moving with the rotator (see § 1·1). The solutions for a finite cylinder are then worked out in first approximation. The method which we use to treat the convergence is also used to prove a condition under which a dynamo process in a conductor of infinite extent is impossible. The section closes with some remarks on the time-dependent case.

4·1. *Time-independent case: solution in powers of ω*

We consider a finite steadily rotating region of axial symmetry (but of otherwise arbitrary shape and angular velocity distribution) within a conductor of the same uniform conductivity σ and of infinite extent. There is applied a steady magnetic field $\mathbf{H}_0$ which has no component with axial symmetry about the axis of rotation.

Equation (1·6) reduces to

$$\nabla^2\mathbf{H} + 4\pi\sigma\nabla \wedge (\mathbf{v} \wedge \mathbf{H}) = 0. \tag{4·1}$$

This equation can be replaced by the following integral equation, whose solutions automatically satisfy the boundary condition $\mathbf{H} \to \mathbf{H}_0$ at infinity:

$$\mathbf{H}(\mathbf{r}) = \mathbf{H}_0 + \sigma \int \mathrm{d}V' \frac{1}{|\mathbf{r}-\mathbf{r}'|} \nabla' \wedge (\mathbf{v} \wedge \mathbf{H})$$

$$= \mathbf{H}_0 - \sigma \int \mathrm{d}V' \nabla' \left(\frac{1}{|\mathbf{r}-\mathbf{r}'|}\right) \wedge (\mathbf{v} \wedge \mathbf{H}) \tag{4·2}$$

by partial integration. The field $\mathbf{H}$ given by (4·2) satisfies $\nabla.\mathbf{H}=0$ because

$$\begin{aligned}\nabla.\int \mathrm{d}V'\,\frac{1}{|\mathbf{r}-\mathbf{r}'|}\,\nabla'\wedge(\mathbf{v}\wedge\mathbf{H}) &= -\int \mathrm{d}V'\nabla'\left(\frac{1}{|\mathbf{r}-\mathbf{r}'|}\right).\nabla'\wedge(\mathbf{v}\wedge\mathbf{H})\\ &= -\int \mathrm{d}V'\,\nabla'.\left[\frac{1}{|\mathbf{r}-\mathbf{r}'|}\,\nabla'\wedge(\mathbf{v}\wedge\mathbf{H})\right]\\ &= 0\end{aligned}$$

by partial integration.

To emphasize the fact that $\mathbf{v}\propto\boldsymbol{\omega}$, we introduce a new vector $\mathbf{U}$ defined by

$$\mathbf{v}=\omega\mathbf{U}. \tag{4·3}$$

We now attempt a solution $$\mathbf{H}=\sum_{n=0}^{\infty}(\sigma\omega)^n\,\mathbf{H}^{(n)}. \tag{4·4}$$

If we substitute (4·4) in (4·2) and equate equal powers of $(\sigma\omega)$, then we obtain the recurrence relation

$$\mathbf{H}^{(n+1)}=-\int \mathrm{d}V'\nabla'\left(\frac{1}{|\mathbf{r}-\mathbf{r}'|}\right)\wedge[\mathbf{U}\wedge\mathbf{H}^{(n)}]. \tag{4·5}$$

The convergence of (4·4) can now be demonstrated. From (4·5) we have

$$|\mathbf{H}^{(n+1)}|\leqslant\int \mathrm{d}V'\left|\nabla'\left(\frac{1}{|\mathbf{r}-\mathbf{r}'|}\right)\wedge(\mathbf{U}\wedge\mathbf{H}^{(n)})\right|\leqslant\int \mathrm{d}V'\,\frac{|\mathbf{U}||\mathbf{H}^{(n)}|}{|\mathbf{r}-\mathbf{r}'|^2}\leqslant|\mathbf{U}|_{\max.}|\mathbf{H}^{(n)}|_{\max.}\int\frac{\mathrm{d}V'}{|\mathbf{r}-\mathbf{r}'|^2},$$

and hence $$|\mathbf{H}^{(n+1)}|_{\max.}\leqslant|\mathbf{U}|_{\max.}|\mathbf{H}^{(n)}|_{\max.}\left(\int\frac{\mathrm{d}V'}{|\mathbf{r}-\mathbf{r}'|^2}\right)_{\max.}. \tag{4·6}$$

The integration is to be carried out over the moving region, and the point $\mathbf{r}$ so chosen as to make $\int \mathrm{d}V'/|\mathbf{r}-\mathbf{r}'|^2$ a maximum. The integral is $4\pi a$ for a sphere of radius a (origin at the centre) and $2\pi^2 a$ for an infinite cylinder of radius a (origin on the axis). Hence we may put

$$\left(\int\frac{\mathrm{d}V'}{|\mathbf{r}-\mathbf{r}'|^2}\right)_{\max.}=Aa,$$

where $A\lesssim 6\pi$ and a is a typical radius of the moving region, measured perpendicular to the axis. It now follows from repeated application of (4·6) that for a rigid rotator of radius a (for which $|\mathbf{U}|\sim a$)

$$(\sigma\omega)^n|\mathbf{H}^{(n)}|_{\max.}\leqslant(6\pi a^2)^n(\sigma\omega)^n|\mathbf{H}_0|_{\max.}, \tag{4·7}$$

so that the series (4·4) converges uniformly when

$$6\pi a^2\sigma\omega=3\alpha<1. \tag{4·8}$$

If we sum (4·5) from $n=0$ to $n=\infty$, and add $\mathbf{H}_0$ to both sides of the result, then the uniform convergence of the series (4·4) permits us to exchange order of summation and integration, so that the series (4·4) is indeed a solution of (4·2).

The argument leading to this convergence condition shows that the first approximation, in which one puts $\mathbf{v}\wedge\mathbf{H}_0$ for $\mathbf{v}\wedge\mathbf{H}$ in (4·2), is valid provided $\alpha\ll 1$. In fact, for $\alpha\ll 1$, the magnetic field permeates the whole rotator (§ 1·1) and the induced field is very small compared with $\mathbf{H}_0$.

We may note that a rough argument to deduce the features of the induced field will usually follow the method of successive approximations, i.e. it will use (4·4) with a small number of terms, and will therefore give a valid result only if (4·8) is satisfied. Equation (4·2) is valid also in the symmetric case discussed in § 3, but there the series (4·4) breaks off after the second term. The distinctive feature of the asymmetric case is that the induced magnetic field gives rise to a Lorentz force in all orders of $(\sigma\omega)$.

4·2. *Examples*

We now apply (4·2) to calculate in first approximation the induced magnetic field given by spherical and finite cylindrical rotators.

Sphere

We consider a rigid sphere of radius a and conductivity σ rotating at constant angular velocity ω in a rigid conductor of the same conductivity and of infinite extent. A uniform magnetic field $\mathbf{H}_0$ is applied perpendicularly to the axis of rotation. We use spherical polar co-ordinates (r, θ, λ) with the origin at the centre of the sphere, and denote the axis of rotation $(\theta = 0)$ by $\hat{\mathbf{z}}$. The applied field $\mathbf{H}_0$ points in the direction $(\theta = \frac{1}{2}\pi, \lambda = 0)$.

Equation (4·2) can be rewritten in the form

$$\mathbf{h} \simeq \sigma \nabla \wedge \int_{\text{rotator}} \mathrm{d}V' \frac{\mathbf{v} \wedge \mathbf{H}_0}{|\mathbf{r}-\mathbf{r}'|}, \tag{4·9}$$

to first approximation. Putting $\mathbf{v} = \omega\hat{\mathbf{z}} \wedge \mathbf{r}$ in (4·9), we have

$$\mathbf{h} = \sigma\omega H_0 \hat{\mathbf{z}} \wedge \nabla \int_{\text{rotator}} \mathrm{d}V' \frac{r' \sin\theta' \cos\lambda'}{|\mathbf{r}-\mathbf{r}'|}$$

$$= \tfrac{2}{15}\alpha H_0 a^3 \hat{\mathbf{z}} \wedge \nabla \left(\frac{\sin\theta\cos\lambda}{r^2}\right). \tag{4·10}$$

The integration is carried out by substituting an expansion for $(1/|\mathbf{r}-\mathbf{r}'|)$ as in (3·22).

The electric field $\mathbf{e}$ associated with $\mathbf{h}$ outside the rotator is given by (1·1) and (4·10) as

$$\mathbf{e} = \tfrac{1}{5}\omega a^5 H_0 \nabla \left(\frac{\cos\theta \sin\theta \cos\lambda}{r^3}\right). \tag{4·11}$$

This is the field of an electric quadrupole in the plane $\lambda = 0$.

Equations (4·10) and (4·11) are special cases of results given by Bullard (1949 *b*).

Finite cylinder

We now replace the sphere of the previous problem by a rigid cylinder of radius a and length $2u$. Equation (4·9) gives

$$\mathbf{h} = \tfrac{1}{4}\alpha H_0 a^2 u \hat{\mathbf{z}} \wedge \nabla \left(\frac{\sin\theta\cos\lambda}{r^2}\right) + O\left(\frac{1}{r^4}\right), \tag{4·12}$$

the origin being taken on the axis half-way between the ends.

At large distances $\mathbf{h}$ is proportional to the volume of the rotator and to the parameter α for both sphere and cylinder. In both cases $\mathbf{h}$ bears a crude resemblance to the field of

a dipole pointing perpendicularly to the applied field, although in this approximation, $\mathbf{h}$ is everywhere perpendicular to the axis of rotation. It is proved in § 5·5 that the result $\mathbf{h}.\boldsymbol{\omega} = 0$ is in fact exact for any rotator in a conducting region of infinite extent.

4·3. *Dynamo processes*

Another interesting result follows from (4·2). For a stationary magnetic field vanishing at infinity, we have

$$|\mathbf{H}(\mathbf{r})| \leqslant \sigma \int dV' \frac{|\mathbf{v}||\mathbf{H}|}{|\mathbf{r}-\mathbf{r}'|^2} \leqslant \sigma |\mathbf{v}|_{\max.} |\mathbf{H}|_{\max.} \left(\int \frac{dV'}{|\mathbf{r}-\mathbf{r}'|^2}\right)_{\max.}, \tag{4·13}$$

and hence

$$|\mathbf{H}|_{\max.} \leqslant \left[\sigma |\mathbf{v}|_{\max.} \left(\int \frac{dV'}{|\mathbf{r}-\mathbf{r}'|^2}\right)_{\max.}\right] |\mathbf{H}|_{\max.}. \tag{4·14}$$

Therefore we can only have $\mathbf{H} \neq 0$ if the quantity in square brackets is greater than unity. It follows that it is impossible to find a set of motions in a conducting medium of infinite extent which will steadily maintain a magnetic field by a dynamo process if

$$\sigma |\mathbf{v}|_{\max.} \left(\int \frac{dV'}{|\mathbf{r}-\mathbf{r}'|^2}\right)_{\max.} < 1,$$

or

$$4\pi\sigma |\mathbf{v}|_{\max.} l \lesssim 1, \tag{4·15}$$

where l is a typical linear dimension of the moving region. The integral is to be taken over the region in motion, and the point $\mathbf{r}$ chosen so as to make $\int dV'/|\mathbf{r}-\mathbf{r}'|^2$ a maximum. The expression for which the inequality is obtained is of the same order of magnitude as the parameter α for the moving region. For the earth's core we have $\alpha \sim 50$.

4·4. *Time-dependent angular velocity*

The full time-dependent equation (1·6) can also be solved in first approximation. If we put $\mathbf{v} \wedge \mathbf{H}_0$ for $\mathbf{v} \wedge \mathbf{H}$ in (1·6), this equation again becomes analogous to the inhomogeneous heat-conduction equation; integral solutions can be written down as in § 3·5. The theory of § 3·5 can be taken over almost word for word, except that the source density ($\mathbf{v} \wedge \mathbf{H}_0$) of the induced field is now distributed over the region of uniform as well as of variable angular velocity (see (1·8)).

In general it is to be expected that if the angular velocity varies sufficiently slowly, then the induced magnetic field will follow the variations of angular velocity adiabatically as in the time-independent condition, no matter what the symmetry or the magnitude of the angular velocity. (We have already had an instance of this behaviour in the axially symmetric case discussed in § 3·5.) In § 9 we shall need to understand under just what conditions the time-independent solution can be used as a valid approximation when the angular velocity is variable. In a conducting medium of infinite extent one can replace equation (1·6) by the integral equation

$$\mathbf{H}(\mathbf{r}, t) = \mathbf{H}_0 + \sigma^{\frac{3}{2}} \int_{-\infty}^{t} dt' \int_{\text{all space}} dV' \nabla' \wedge [\mathbf{v}(\mathbf{r}', t') \wedge \mathbf{H}(\mathbf{r}', t')] \frac{\exp\left(-\frac{|\mathbf{r}-\mathbf{r}'|^2 \pi\sigma}{t-t'}\right)}{(t-t')^{\frac{3}{2}}}, \tag{4·16}$$

as one can verify by differentiation. If conditions are steady, then the integration over t' gives

$$\int \mathrm{d}t' \exp(\ )/(t-t')^{\frac{3}{2}} = \sigma^{-\frac{1}{2}} |\mathbf{r}-\mathbf{r}'|^{-1},$$

giving the time-independent integral equation (4·2). For a particular pair of points $(\mathbf{r}, \mathbf{r}')$, 90% of the value of the t' integral comes from $(t-t') < 400\sigma|\mathbf{r}-\mathbf{r}'|^2$. Therefore, provided that conditions are substantially steady during a characteristic time T, the t' integral and the factor $\exp(\ )/(t-t')^{\frac{3}{2}}$ can be replaced by $\sigma^{-\frac{1}{2}}|\mathbf{r}-\mathbf{r}'|^{-1}$ for all pairs of points $(\mathbf{r}, \mathbf{r}')$ for which

$$|\mathbf{r}-\mathbf{r}'| < \frac{1}{20}\left(\frac{T}{\sigma}\right)^{\frac{1}{2}} = \frac{\pi}{10} \times (\text{skin depth corresponding to period } T).$$

It follows that the integral equation (4·16) can be replaced by the time-independent integral equation (4·2) for any point $\mathbf{r}$ in the rotating region provided that the dimensions of the rotator are appreciably smaller than the skin depth corresponding to the characteristic time T; since the induction process is dominated by the form of the integral equation for $\mathbf{H}$ in the rotating region, the condition that the field should follow the variations of angular velocity adiabatically in the neighbourhood of the rotator is that the dimensions of the rotator should be smaller than a skin depth. The argument can easily be extended to show that the time-independent solutions will also describe the field satisfactorily out to a distance of the order of the skin depth away from the rotator.

These conclusions are in no way affected by the symmetry or the magnitude of the velocity.

5. Transverse field at high angular velocity ($m \neq 0$, $\alpha \gg 1$)

We now discuss the case of an axially asymmetric $\mathbf{H}_0$ at high angular velocity. This case differs from those of §§ 3 and 4 in that the induced magnetic field $\mathbf{h}$ now gives important induction effects. Throughout this section (except in § 5·5) we shall use $(\mathbf{E}, \mathbf{H})$ and $(\mathbf{E}', \mathbf{H}')$ to denote the fields outside and inside the rotator respectively.

We shall restrict the discussion to the time-independent case except in § 5·7, where we discuss the behaviour of $\mathbf{h}$ when the rotator starts up. Our treatment is based on the fact that if the angular velocity is sufficiently large, $\mathbf{E}'$ and $\mathbf{H}'$ are confined to a boundary layer of thickness $\sim d \propto \omega^{-\frac{1}{2}}$ on the inside of the surface of the rotating conductor. A simple expression can then be given for $\mathbf{H}'$ at any point in this boundary layer in terms of $\mathbf{H}$ at adjacent points of the boundary. We shall use this expression to eliminate $(\mathbf{E}', \mathbf{H}')$ from the boundary conditions at the rotator surface. The boundary conditions obtained from the elimination contain only the external fields $(\mathbf{E}, \mathbf{H})$ and are useful in the limit as $\omega \to \infty$.

In this section we treat not only the rotator embedded in a conductor of infinite extent but also the isolated rotator. These two cases require separate treatment because current can flow across the boundary in the first but not in the second, a difference which leads to different behaviours of $\mathbf{E}$ and $\mathbf{H}$ at the boundary.

Except where otherwise stated, we shall use either cylindrical polar co-ordinates (ρ, z, λ) or spherical polar co-ordinates (r, θ, λ). The axis of rotation will contain the origin, and will coincide with the z or $\theta = 0$ axis. We shall discuss fields in which each component in either of the polar co-ordinate systems contains λ in a factor $\mathrm{e}^{\mathrm{i}m\lambda}$ only.

The field equations are

$$\nabla \wedge \mathbf{H} = 4\pi\sigma(\mathbf{E}+\mathbf{v}\wedge\mathbf{H}), \tag{5·1}$$

$$\nabla \wedge \mathbf{E} = 0, \tag{5·2}$$

$$\nabla . \mathbf{E} = 4\pi q c^2, \tag{5·3}$$

$$\nabla . \mathbf{H} = 0. \tag{5·4}$$

Equations (5·1) to (5·4) are valid both inside and outside the rotator, with the provisos that $\mathbf{v} = 0$ outside the rotator, and that $\sigma = 0$ outside the isolated rotator.

5·1. *The boundary layer*

If we eliminate $(\mathbf{E}, \mathbf{E}')$ from (5·1) and (5·2), and remember that the field components are proportional to $e^{im\lambda}$, then the equations for $(\mathbf{H}, \mathbf{H}')$ become

$$\nabla^2\mathbf{H} = 0, \quad \nabla^2\mathbf{H}' - (2im/d^2)\,\mathbf{H}' = 0, \tag{5·5}$$

and

$$\nabla . (\mathbf{H}, \mathbf{H}') = 0, \tag{5·6}$$

where d is the skin depth for $m = 1$, that is,

$$d \equiv (2\pi\sigma\omega)^{-\frac{1}{2}}. \tag{5·7}$$

The solution of (5·5) for $\mathbf{H}'$ is

$$\mathbf{H}'(\mathbf{r}) = \frac{1}{4\pi}\int_{\substack{\text{rotator}\\ \text{surface}}} \mathrm{d}A' \left\{ \frac{\exp\left[-(1+\mathrm{i})\,|\,\mathbf{r}-\mathbf{r}'\,|\sqrt{m/d}\right]}{|\,\mathbf{r}-\mathbf{r}'\,|}\,\frac{\partial \mathbf{H}'(\mathbf{r}')}{\partial n'} - \mathbf{H}'(\mathbf{r}')\,\frac{\partial}{\partial n'}\,\frac{\exp\left[-(1+\mathrm{i})|\mathbf{r}-\mathbf{r}'|\sqrt{m/d}\right]}{|\,\mathbf{r}-\mathbf{r}'\,|}\right\}, \tag{5·8}$$

where $\partial/\partial n$ signifies differentiation along the outward normal. It follows from (5·8) that $\mathbf{H}'$ is appreciable only within a boundary layer of thickness $(d/\sqrt{m})$. This boundary layer is thin compared to the radius a of the rotator if

$$ma^2/d^2 = m2\pi\sigma\omega a^2 = m\alpha \gg 1, \tag{5·9}$$

where α is the non-dimensional parameter $2\pi\sigma\omega a^2$.

Since $\mathbf{E}'$ is related to $\mathbf{H}'$ by equation (5·1), $\mathbf{E}'$ is also confined to this boundary layer.

5·2. *Solution near the boundary*

We next obtain an approximate solution of (5·5) valid inside the rotator. This solution contains only the boundary values of $\mathbf{H}'$ and not of $\partial\mathbf{H}'/\partial n$. Take Cartesian co-ordinates (x, y, z) with the origin in the rotator surface, and with the positive z direction pointing along the outward normal. Let l be the characteristic length in which $\mathbf{H}'$ varies along the rotator surface. (The characteristic length of variation in the $\hat{\boldsymbol{\lambda}}$ direction is of order (ρ/m), and we shall see from examples in § 5·6 that the characteristic length along a meridian (λ = constant) on the rotator surface is determined by the rotator shape and by the symmetry of $\mathbf{H}_0$ at infinity in such a way as to remain finite and non-zero as $\omega \to \infty$.) Since $(\partial^2\mathbf{H}'/\partial x^2 + \partial^2\mathbf{H}'/\partial y^2)$ is $O(1/l^2)\,\mathbf{H}'$, equation (5·5) may be written

$$\frac{\partial^2\mathbf{H}'}{\partial z^2} - \frac{2im}{d^2}\left[1 + O\left(\frac{d^2}{ml^2}\right)\right]\mathbf{H}' = 0. \tag{5·10}$$

The solution of (5·10) is

$$\mathbf{H}'(0,0,z) = \mathbf{H}'(0,0,0)\exp\left\{+z\frac{(1+\mathrm{i})\sqrt{m}}{d}\left[1+O\left(\frac{d^2}{ml^2}\right)\right]\right\}. \tag{5·11}$$

(We have chosen the plus sign in the argument of the exponential so as to make $\mathbf{H}'$ decrease inwards.) From (5·11) we deduce that at the surface (where $z = 0$ and $\partial/\partial z = \partial/\partial n$) we have

$$\frac{\partial \mathbf{H}'}{\partial n} = \frac{(1+\mathrm{i})\sqrt{m}}{d}\left[1+O\left(\frac{d^2}{ml^2}\right)\right]\mathbf{H}'. \tag{5·12}$$

This result will be needed in the next two subsections.

5·3. *Boundary conditions for the isolated rotator as* $\omega \to \infty$

For the isolated rotator we shall need boundary conditions for the magnetic field only. It follows from (5·1) and (5·4) that

$$\mathbf{H} = \mathbf{H}' \tag{5·13}$$

on the rotator boundary.

Another boundary condition can be obtained from (5·4). Let us introduce an orthogonal curvilinear co-ordinate system (u_1, u_2, u_3) such that u_1 is constant on the rotator surface, u_2 on surfaces normal to the vector $\hat{\mathbf{n}} \wedge \hat{\boldsymbol{\lambda}}$ where they intersect the rotator surfaces, and u_3 on planes of constant λ. Then (5·4) becomes, in the usual notation (see, for example, Stratton 1941, p. 49),

$$\frac{1}{h_1 h_2 h_3}\left[\frac{\partial}{\partial u_1}(h_2 h_3 H_1) + \frac{\partial}{\partial u_2}(h_3 h_1 H_2) + \frac{\partial}{\partial u_3}(h_1 h_2 H_3)\right] = 0, \tag{5·14}$$

and a similar equation holds for $\mathbf{H}'$. At the rotator surface equation (5·14) is valid for both $\mathbf{H}$ and $\mathbf{H}'$; by equating the left-hand sides, we obtain, on using (5·13),

$$\frac{1}{h_1}\frac{\partial H_1}{\partial u_1} + \frac{1}{h_2}\frac{\partial H_2}{\partial u_2} + \frac{1}{h_3}\frac{\partial H_3}{\partial u_3} = \frac{1}{h_1}\frac{\partial H_1'}{\partial u_1} + \frac{1}{h_2}\frac{\partial H_2'}{\partial u_2} + \frac{1}{h_3}\frac{\partial H_3'}{\partial u_3}. \tag{5·15}$$

Now (5·13) tells us that

$$\frac{\partial H_2}{\partial u_2} = \frac{\partial H_2'}{\partial u_2}, \quad \frac{\partial H_3}{\partial u_3} = \frac{\partial H_3'}{\partial u_3}, \tag{5·16}$$

since the partial differentiations $\partial/\partial u_2$, $\partial/\partial u_3$ are carried out along curves lying in the rotator surface. It therefore follows from (5·15) that

$$\frac{\partial H_n}{\partial n} = \frac{\partial H_n'}{\partial n} \tag{5·17}$$

(note that $\partial/\partial n = \partial/h_1 \partial u_1$ and $H_1 = H_n$, $H_1' = H_n'$).

With the aid of the normal component of (5·12) we can eliminate the internal field $\mathbf{H}'$ from the boundary conditions (5·13) and (5·17). We obtain

$$\frac{\partial H_n}{\partial n} = \frac{(1+\mathrm{i})\sqrt{m}}{d} H_n\left[1+O\left(\frac{d^2}{ml^2}\right)\right]. \tag{5·18}$$

Since $\mathbf{H}$ (outside the rotator) is irrotational we can write

$$\mathbf{H} = -\nabla\Psi, \tag{5·19}$$

where Ψ' is a scalar potential function. Inserting (5·19) into (5·18), we have

$$\frac{\partial \Psi'}{\partial n} - \frac{d}{(1+\mathrm{i})\sqrt{m}}\left[1+O\left(\frac{d^2}{ml^2}\right)\right]\frac{\partial^2 \Psi'}{\partial n^2} = 0. \tag{5·20}$$

According to (5·4) and (5·19) we have $\nabla^2\Psi' = 0$, so that $\partial^2\Psi'/\partial n^2 = O(1/l^2)\,\Psi'$ near the rotator surface, and, neglecting the higher order terms, (5·20) can be rewritten

$$\frac{\partial \Psi'}{\partial n} + \frac{1}{l}O\left(\frac{d}{l\sqrt{m}}\right)\Psi' = 0. \tag{5·21}$$

Therefore, provided l remains finite as $\omega \to \infty$, we have $\lim_{\omega\to\infty} \partial\Psi'/\partial n = 0$, so that in the limit the rotator behaves as a perfect diamagnetic. This asymptotic condition is approached only slowly as ω increases, since $d \propto \omega^{-\frac{1}{2}}$.

5·4. *Boundary conditions as $\omega \to \infty$ for the rotator embedded in conducting material*

When the rotator is embedded in conducting material, the boundary conditions (5·13) and (5·18) continue to be valid. The difference between the isolated and embedded rotators is that outside the embedded rotator we have

$$\nabla \wedge \mathbf{H} = 4\pi\sigma\mathbf{E} \tag{5·22}$$

in place of $\nabla \wedge \mathbf{H} = 0$ for the isolated rotator. Due to the link (5·22) between $\mathbf{E}$ and $\mathbf{H}$, the boundary condition

$$\hat{\mathbf{n}} \wedge \mathbf{E} = \hat{\mathbf{n}} \wedge \mathbf{E}' \tag{5·23}$$

implies an additional condition on $\mathbf{H}$ and $\mathbf{H}'$. The equality $E_\lambda = E'_\lambda$, which does not contain $\mathbf{v}$, gives us $(\nabla \wedge \mathbf{H})_\lambda = (\nabla \wedge \mathbf{H}')_\lambda$. If we introduce orthogonal curvilinear co-ordinates as in the previous § 5·3 we obtain for the u_3 component

$$\frac{1}{h_1 h_2}\left[\frac{\partial}{\partial u_1}(h_2 H_2) - \frac{\partial}{\partial u_2}(h_1 H_1)\right] = \frac{1}{h_1 h_2}\left[\frac{\partial}{\partial u_1}(h_2 H'_2) - \frac{\partial}{\partial u_2}(h_1 H'_1)\right]. \tag{5·24}$$

Putting $H_2 = H'_2$, $H_1 = H'_1$ and $\partial H_1/\partial u_2 = \partial H'_1/\partial u_2$, we have

$$\frac{1}{h_1}\frac{\partial H_2}{\partial u_1} = \frac{1}{h_1}\frac{\partial H'_2}{\partial u_1},$$

or

$$\frac{\partial H_t}{\partial n} = \frac{\partial H'_t}{\partial n}, \tag{5·25}$$

where (H_t, H'_t) are the components of $(\mathbf{H}, \mathbf{H}')$ in the tangential direction $\hat{\mathbf{u}}_3 = \hat{\boldsymbol{\lambda}} \wedge \hat{\mathbf{n}}$. If we insert (5·25) and the condition $H_t = H'_t$ in (5·12), then we obtain

$$\frac{\partial H_t}{\partial n} = \frac{(1+\mathrm{i})\sqrt{m}}{d}\left[1+O\left(\frac{d^2}{ml^2}\right)\right]H_t. \tag{5·26}$$

The boundary conditions (5·18) and (5·26) affect only those components of $\mathbf{H}$ which lie in planes of constant λ. Nevertheless, these two boundary conditions are all we need since the divergence equation (5·4) expresses H_λ in terms of the components H_n and H_t.

Since $d \propto \omega^{-\frac{1}{2}}$, (5·18) and (5·26) imply the two asymptotic boundary conditions

$$\left.\begin{aligned} H_n &\to 0 \\ H_t &\to 0 \end{aligned}\right\} \quad \text{as} \quad \omega \to \infty, \tag{5·27}$$

in contrast to the case of the isolated rotator where we had only the single condition $H_n \to 0$. The physical reason for the difference lies in the patterns of the induced currents produced in the rotator by the induction term $\mathbf{v} \wedge \mathbf{H}'$; these currents tend to annul the components of $\mathbf{H}'$ and therefore $\mathbf{H}$ perpendicular to $\mathbf{v}$. In the isolated rotator, currents in the surface layer can flow only parallel to the surface, and so can annul only H_n; in the embedded rotator currents can flow through the surface and can therefore annul both H_n and H_t.

5·5. *A theorem about* $\mathbf{h}$

We now prove the following theorem: The induced field due to a steadily rotating region of axial symmetry but otherwise arbitrary shape and velocity distribution in uniformly conducting surroundings of infinite extent, and in a time-independent uniform applied field $\mathbf{H}_0$ of any direction, is everywhere perpendicular to the axis of rotation.

In this subsection we do not make any distinction between the fields inside and outside the rotator; the theorem is valid in both regions.

Let the axis of rotation be the z axis. From (1·6) and (1·9) we obtain, in the time-independent case,

$$\nabla^2 H_z - 4\pi\sigma\omega \frac{\partial H_z}{\partial \lambda} = 0, \tag{5·28}$$

as the z component of $\nabla \wedge (\mathbf{v} \wedge \mathbf{H})$ is $-\omega \partial H_z/\partial\lambda$. If we multiply (5·28) by H_z, and integrate over all space, we have

$$\int \mathrm{d}V'(H_z \nabla^2 H_z) - 4\pi\sigma \int \mathrm{d}V' \omega(\rho', z')\, H_z \frac{\partial H_z}{\partial \lambda} = 0$$

or

$$\int \mathrm{d}V' \nabla' . (H_z \nabla' H_z) - \int \mathrm{d}V' (\nabla' H_z)^2 - 2\pi\sigma \int \mathrm{d}V' \frac{\partial}{\partial \lambda}(\omega H_z^2) = 0. \tag{5·29}$$

The first integral in (5·29) vanishes. (It can be transformed into a surface integral at infinity; this surface integral vanishes because $\nabla H = O(r^{-3})$ for a semi-infinite cylinder, and $\nabla H = O(r^{-4})$ for finite rotators.) The third integral in (5·29) vanishes since (ωH_z^2) is single-valued (integrate first with respect to λ). Hence (5·29) reduces to

$$\int \mathrm{d}V' (\nabla' H_z)^2 = 0. \tag{5·30}$$

Therefore ∇H_z is zero everywhere, and since $H_z = H_{0z}$ at infinity it follows that $H_z = H_{0z}$ everywhere. But $H_z = H_{0z} + h_z$, and therefore $h_z = 0$ everywhere.

5·6. *Examples*

Isolated sphere

We now calculate the induced field outside an isolated rigid conducting sphere of radius a rotating at large constant angular velocity ω. A uniform magnetic field H_0 is applied perpendicular to the axis of rotation ($\theta = 0$) in the direction ($\theta = \frac{1}{2}\pi$, $\lambda = 0$).

If we put $\mathbf{H} = -\nabla\Psi$ outside the sphere we have

$$\nabla^2 \Psi = 0, \quad \Psi \to -H_0 r \sin\theta \cos\lambda \quad \text{as} \quad r \to \infty, \tag{5·31}$$

and from (5·21)

$$\left[\frac{\partial \Psi}{\partial r} + \frac{1}{l} O\left(\frac{d}{l\sqrt{m}}\right) \Psi\right]_{r=a} = 0, \tag{5·32}$$

where l is a characteristic distance of variation of Ψ along the surface of the sphere. In the limit as $\omega \to \infty$, we can neglect the second term in (5·32) provided that $[\Psi(r=a)/l^2\omega^{\frac{1}{2}}] \to 0$ as $\omega \to \infty$. If we make this approximation, we find from (5·31) and (5·32) that

$$\lim_{\omega\to\infty} \Psi = -H_0 r \sin\theta\cos\lambda - \tfrac{1}{2}H_0 a^3 \frac{\sin\theta\cos\lambda}{r^2}. \tag{5·33}$$

From (5·33) we see that $l \sim a$, which is consistent with $\lim_{\omega\to\infty} [\Psi(r=a)/l^2\omega^{\frac{1}{2}}] = 0$.

From (5·33), and including an error term from (5·32), we have

$$\mathbf{h} = \tfrac{1}{2}H_0 a^3 \nabla\left(\frac{\sin\theta\cos\lambda}{r^2}\right) + O(\omega^{-\frac{1}{2}}). \tag{5·34}$$

The sphere therefore behaves as a magnetic dipole of moment $-\tfrac{1}{2}\mathbf{H}_0 a^3$ as $\omega \to \infty$.

Sphere embedded in conductor

We next calculate the external induced magnetic field when the sphere of the previous example is surrounded by rigid conducting matter of infinite extent.

The asymptotic boundary conditions (5·27) show that on the rotator surface we have $\lim_{\omega\to\infty} (H_\rho, H_z) = 0$. We know already from the theorem of § 5·5 that $H_z = 0$ everywhere, and are therefore led to consider H_ρ. If we write out the equation $\nabla^2\mathbf{H} = 0$ in cylindrical polar co-ordinates, take the ρ component, and substitute for H_λ from the divergence equation, we obtain

$$\nabla^2(\rho H_\rho) + 2\partial H_z/\partial z = 0,$$

or

$$\nabla^2(\rho H_\rho) = 0, \tag{5·35}$$

since $H_z = 0$. We have to solve (5·35), subject to the boundary conditions

$$\rho H_\rho \to H_0 r \sin\theta\cos\lambda \quad \text{as} \quad r \to \infty, \tag{5·36}$$

and

$$(\rho H_\rho)_{r=a} = 0. \tag{5·37}$$

The last equation follows from the boundary conditions (5·27), and is valid provided that

$$\left.\begin{aligned} \lim_{\omega\to\infty}\left(\frac{d}{\sqrt{m}}\right)\frac{\partial H_n}{\partial n} &= 0, \\ \lim_{\omega\to\infty}\left(\frac{d}{\sqrt{m}}\right)\frac{\partial H_t}{\partial n} &= 0. \end{aligned}\right\} \tag{5·38}$$

The solution of (5·35), (5·36) and (5·37) is

$$\rho H_\rho = H_0 r\sin\theta\cos\lambda - H_0 a^3 \sin\theta\cos\lambda/r^2, \tag{5·39}$$

so that

$$H_\rho = H_0\cos\lambda - H_0 a^3\cos\lambda/r^3. \tag{5·40}$$

The divergence equation in cylindrical polar co-ordinates is

$$\frac{1}{\rho}\frac{\partial}{\partial\rho}(\rho H_\rho) + \frac{\partial H_z}{\partial z} + \frac{1}{\rho}\frac{\partial H_\lambda}{\partial\lambda} = 0,$$

so that since $H_z = 0$, we have from (5·39)

$$H_\lambda = H_0 a^3 \sin\lambda(1 - 3\sin^2\theta)/r^3. \tag{5·41}$$

Equations (5·40) and (5·41) are consistent with (5·38).

We can write (5·40) and (5·41) in the alternative form

$$\mathbf{H} = \mathbf{H}_0 + \mathbf{h}, \quad \mathbf{h} = H_0 a^3 \hat{\mathbf{z}} \wedge \nabla \left(\frac{\sin\theta \sin\lambda}{r^2} \right) + O(\omega^{-\frac{1}{2}}). \tag{5·42}$$

By comparison of (4·10) and (5·42) we see that the induced fields at low velocity and at high velocity differ by a factor $2\alpha/15$ and a rotation through 90°.

Prolate spheroid embedded in conductor

If the sphere of the last problem is replaced by a prolate spheroid rotating about the symmetry axis, one can solve (5·35) and the asymptotic boundary condition $(\rho H_\rho)_{\text{surface}} = 0$ in spheroidal co-ordinates. H_λ can then be found from the divergence equation. The result one finds is, when expressed in spherical polar co-ordinates,

$$\mathbf{h} \simeq \tfrac{2}{3} H_0 a^2 u \hat{\mathbf{z}} \wedge \nabla \left(\frac{\sin\theta \sin\lambda}{r^2} \right) \quad \text{as} \quad r \to \infty, \tag{5·43}$$

where $2u$ is the length and a the maximum radius (in a plane perpendicular to $\hat{\mathbf{z}}$) of the spheroid. From (5·42) and (5·43) we see that $\mathbf{h}$ is roughly proportional to the volume of the rotator, regardless of the shape.

5·7. *Time-dependent angular velocity: a particular problem*

We shall not attempt a thoroughgoing analysis of induction in a rotator with a variable angular velocity which reaches high values of α. We shall merely try to get a partial answer to the question: How does the magnetic field behave when the rotation starts? It was suggested to us by Mr T. Gold that the steady state which we have been discussing so far might in fact never be reached, or might be reached only after a complicated interim period during which the lines of force are wound up by the rotator; this is a process which might lead to a very large induced magnetic field. (We already know from § 4·4 that if the angular velocity varies sufficiently slowly, then the induced field follows the angular velocity adiabatically; we are here concerned with rapid accelerations.)

To see whether, and under what conditions, this winding up process in fact occurs, we consider the following situation. An infinite rigid cylinder of radius a is embedded in conducting matter and lies in a uniform magnetic field $\mathbf{H}_0$ applied perpendicular to the axis. The cylinder starts to rotate at time $t = 0$ with constant angular velocity ω_0. Outside the cylinder there is a boundary layer of thickness Δ in which the angular velocity decreases linearly to zero, i.e. we have

$$\omega(\rho) = \omega_0 \qquad \text{for} \quad \rho < a,$$

$$\omega(\rho) = \omega_0 \left[1 - \frac{\rho - a}{\Delta} \right] \qquad \text{for} \quad a < \rho < a + \Delta,$$

and

$$\omega(\rho) = 0 \qquad \text{for} \quad \rho > a + \Delta,$$

where ρ is the distance from the axis of the cylinder. It is convenient to take Cartesian co-ordinates (x, y) in a plane perpendicular to the axis of the cylinder, and with the origin at the centre of the cylinder, as shown in figure 21.

To start with, we ignore the diffusion term ($\nabla^2\mathbf{H}/4\pi\sigma$) in equation (1·6); the remaining terms then show that the lines of force are dragged round with the conducting matter so that two particles which lie on the same line of force at any one time always remain on that line (Dungey 1950). We shall later return to an estimate of the diffusion term. Figure 21 shows the lines of force schematically after the cylinder has completed one and N revolutions. The lines of force in the boundary region have length $\sim\Delta$ at time $t = 0$, and are stretched out to a length $2\pi aN$ after N revolutions. Since the field strength at any point is proportional to the distance between two fluid particles placed infinitesimally close together on a field line passing through that point (Dungey 1950), the maximum value of the magnetic field in the boundary layer after N revolutions is

$$H_{\max.} \simeq \left(\frac{2\pi aN}{\Delta}\right) H_0 = \left(\frac{v_0 t}{\Delta}\right) H_0 \tag{5·44}$$

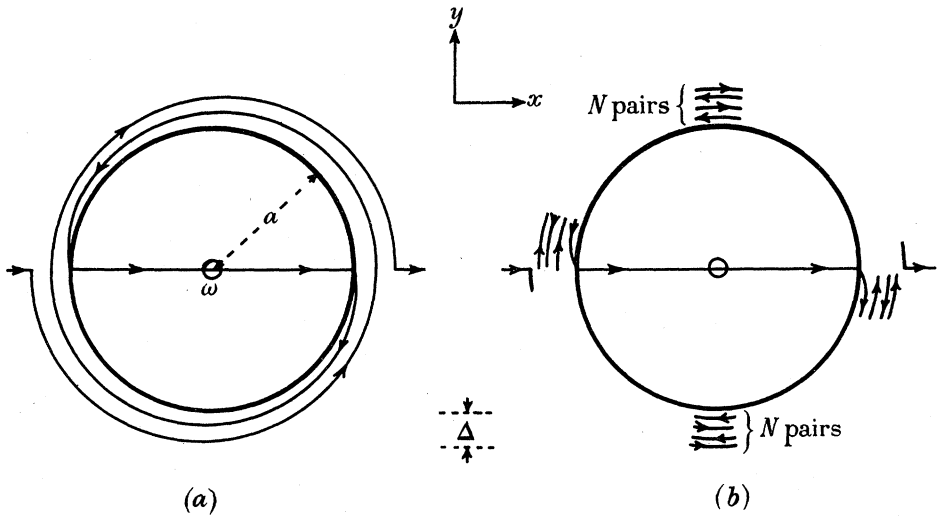

FIGURE 21. Lines of force in the velocity transition layer. (*a*) After one rotation. (*b*) After N rotations.

(v_0 is the peripherical velocity of the cylinder). Therefore it is possible to produce in the velocity transition layer induced magnetic fields much larger than the applied magnetic field $\mathbf{H}_0$ provided that

$$\frac{v_0 t}{\Delta} \gg 1. \tag{5·45}$$

We now estimate when the diffusion term becomes important. We have, in the neighbourhood of a point on the circumference of the cylinder and on the y-axis,

$$[\nabla\wedge(\mathbf{v}\wedge\mathbf{H})]_x \sim v_0 H_0 \frac{2\pi(N+\frac{1}{2})}{\Delta},$$

$$[\nabla\wedge(\mathbf{v}\wedge\mathbf{H})]_y \sim v_0 H_0 \frac{1}{a},$$

$$\frac{1}{4\pi\sigma}(\nabla^2\mathbf{H})_x \sim \frac{H_0}{4\pi\sigma}\frac{2\pi aN}{\Delta}\left[\frac{2\pi(N+\frac{1}{2})}{\Delta}\right]^2,$$

$$\frac{1}{4\pi\sigma}(\nabla^2\mathbf{H})_y \sim \frac{H_0}{4\pi\sigma}\left[\frac{2\pi(N+\frac{1}{2})}{\Delta}\right]^2.$$

(In these estimates we have used the fact that the field lines make an angle $\Delta/2\pi aN$ with the tangents of circles centred on the origin.) Diffusion is negligible if

$$|\,[\nabla\wedge(\mathbf{v}\wedge\mathbf{H})]_{x,y}\,|\gg\left|\frac{1}{4\pi\sigma}(\nabla^2\mathbf{H})_{x,y}\right|.$$

This condition is fulfilled for both the x and y components if

$$\left(\frac{v_0 t}{\Delta}\right)^2\frac{1}{4\pi\sigma a v_0}\ll 1. \tag{5·46}$$

We see from (5·45) and (5·46) that it is possible to choose the parameters in such a way as to have large amplification of the field while the diffusion process remains negligible. Of course, after a sufficiently long time, (5·46) must be violated. (We note that for a rotator with a sharp boundary ($\Delta=0$), condition (5·46) is violated so that the peculiar behaviour associated with the boundary layer does not occur.)

Unfortunately, it was not possible to investigate this winding up process experimentally because the necessary values of the non-dimensional parameters could not be obtained. If we express v_0 and t in terms of the non-dimensional parameters α and μ introduced in (2·3) and (2·4), and the other parameters occurring in these equations, then if we put t_0 for t the conditions (5·45) and (5·46) become

$$\mu\left(\frac{\Delta}{l_0}\right)\ll 2\alpha\ll\left[\mu\left(\frac{\Delta}{l_0}\right)\right]^2. \tag{5·47}$$

To satisfy this condition, it is clearly necessary that $\mu(\Delta/l_0)\gg 1$, and $\alpha\gg 1$. Since the boundary-layer thickness is smaller than the radius $a(=l_0)$, it is therefore necessary that $\mu\gg 1$. As we saw in (2·5), this condition could not be achieved in the experiment; (2·5) also shows that (5·47) might be satisfied in the earth's core.

PART D. INDUCTION IN ROTATORS EMBEDDED IN FINITE CONDUCTING SHELLS

In part C we saw that when a rotating conductor is surrounded by conducting matter, currents emerge from the rotator and contribute to the induced magnetic field. These currents are due to an electric field whose sources lie in a charge distribution of density $-(1/4\pi c^2)\,\nabla.\,(\mathbf{v}\wedge\mathbf{H})$ in the rotator and on its surface. These charges are maintained by the Lorentz forces in the rotator. The boundary of a finite conducting shell restricts the flow of the currents; there is built up a surface-charge distribution on the boundary whose electric field reflects the currents emerging from the rotator. We now calculate the contribution of these reflected currents to the induced magnetic field.

The basic approximation in this treatment is the neglect of the interaction of the magnetic field of the reflected current with the motion of the rotator. We give two methods which are complementary. The first, which is applicable only to plane boundaries, is based on the Biot–Savart integral. The second method, applicable to both plane and spherical boundaries, is based on the use of generating functions from which the fields can be derived. These methods lead to the simple relations (6·6) and (6·25) by which the induced magnetic field outside the conductor can be readily calculated from the induced magnetic field for a conductor of infinite extent. These calculations, for some specific cases, are given in § 7. The first method enables us to estimate the error in the approximation; this is done in § 7·4. The second method is easily extended to the time-dependent case.

6. General analysis

In this section we develop the basis of the method. In § 6·1 a symmetry theorem is proved. The time-independent case is dealt with in §§ 6·2, 6·3 and 6·4; the time-dependent problem is then discussed in §§ 6·5 and 6·6.

6·1. *A symmetry theorem*

If the shell boundary and the applied field both have axial symmetry about the axis of rotation, then we can show that there is no induced field outside the shell. This result does *not* depend on the approximation used in the rest of this section.

It is true for a finite shell as well as for an infinite one that the induced currents must flow in planes which pass through the axis of rotation. Because of this, and of the axial symmetry, we have $\mathbf{h} = h_\lambda \hat{\boldsymbol{\lambda}}$, where h_λ is constant along any circle C centred on the axis and lying in a plane perpendicular to it. Now outside the conducting shell we have $\int \mathbf{h}.\mathrm{d}\mathbf{s} = 0$, and therefore $\mathbf{h} = 0$.

This result was obtained by Bullard (1949*b*) for the particular case of a sphere rotating in a spherical shell.

6·2. *Plane boundary, first method*

We consider a conductor rotating at constant angular velocity in a uniform constant applied magnetic field $\mathbf{H}_0$, and in rigid conducting material of the same conductivity filling the half-space $z<0$. The space $z>0$ is assumed to be insulating. We define a value $z_1(<0)$ such that all of the rotator is in $z<z_1$. We use V_∞ and V_σ to denote all space and the conducting domain respectively. Functions in the insulating region are distinguished by a prime. The induced magnetic field will be denoted by $\mathbf{h}$, and the accompanying current density and electric field by $\mathbf{j}$ and $\mathbf{e}$ respectively; the corresponding quantities for a conducting shell filling all space will be denoted by $\mathbf{h}_\infty$, $\mathbf{j}_\infty$ and $\mathbf{e}_\infty$. We shall call the reflected current, magnetic field and electric field $\mathbf{j}_r$, $\mathbf{h}_r$ and $\mathbf{e}_r$, so that inside the conducting matter

$$\mathbf{j} = \mathbf{j}_\infty + \mathbf{j}_r, \quad \mathbf{h} = \mathbf{h}_\infty + \mathbf{h}_r, \quad \mathbf{e} = \mathbf{e}_\infty + \mathbf{e}_r. \tag{6·1}$$

The Biot–Savart integral gives

$$\begin{aligned}\mathbf{h}(\mathbf{r}) &= \int_{V_\sigma} \mathrm{d}V' \mathbf{j}(\mathbf{r}') \wedge \nabla' \frac{1}{|\mathbf{r}-\mathbf{r}'|} \\ &= \int_{V_\infty} \mathrm{d}V' \mathbf{j}_\infty(\mathbf{r}') \wedge \nabla' \frac{1}{|\mathbf{r}-\mathbf{r}'|} + \int_{V_\sigma} \mathrm{d}V' \mathbf{j}_r(\mathbf{r}') \wedge \nabla' \frac{1}{|\mathbf{r}-\mathbf{r}'|} - \int_{(V_\infty - V_\sigma)} \mathrm{d}V' \mathbf{j}_\infty(\mathbf{r}') \wedge \nabla' \frac{1}{|\mathbf{r}-\mathbf{r}'|}. \end{aligned} \tag{6·2}$$

The first term on the right in (6·2) is $\mathbf{h}_\infty(\mathbf{r})$. The second term can be transformed into an integral over the boundary of the conductor,

$$\int_{V_\sigma} \mathrm{d}V' \mathbf{j}_r \wedge \nabla' \frac{1}{|\mathbf{r}-\mathbf{r}'|} = \int_{V_\sigma} \mathrm{d}V' \left[\frac{1}{|\mathbf{r}-\mathbf{r}'|} \nabla' \wedge \mathbf{j}_r - \nabla' \wedge \frac{\mathbf{j}_r}{|\mathbf{r}-\mathbf{r}'|} \right] = -\int_A \mathrm{d}A' \frac{\hat{\mathbf{n}}' \wedge \mathbf{j}_r}{|\mathbf{r}-\mathbf{r}'|},$$

because our basic approximation implies that $\nabla \wedge \mathbf{j}_r = 0$. (If we did not neglect the induction effects of $\mathbf{j}_r$, we should have $\nabla \wedge \mathbf{j}_r = \nabla \wedge [\sigma(\mathbf{e}_r + \mathbf{v} \wedge \mathbf{h}_r)] = \sigma \nabla \wedge (\mathbf{v} \wedge \mathbf{h}_r)$ in the rotator. The

third term in (6·2) can similarly be transformed into a surface integral because $\mathbf{j}_\infty = \sigma\mathbf{e}_\infty$ in $(V_\infty - V_\sigma)$, and $\nabla \wedge \mathbf{e}_\infty = 0$. We can therefore rewrite (6·2) in the form

$$\mathbf{h}(\mathbf{r}) = \mathbf{h}_\infty(\mathbf{r}) - \int_{\substack{\text{conductor}\\\text{surface}}} dA' \frac{\hat{\mathbf{n}}' \wedge [\mathbf{j}_\infty(\mathbf{r}') + \mathbf{j}_r(\mathbf{r}')]}{|\mathbf{r} - \mathbf{r}'|}, \tag{6·3}$$

where $\hat{\mathbf{n}}'$ is the unit vector pointing outwards normally to the conductor surface. This expression is valid, to our approximation, both outside and inside the conductor.

Equation (6·3) is true for a conducting shell of arbitrary shape. If, however, we take the conductor surface to be the plane $z = 0$, then $\hat{\mathbf{n}}' = \hat{\mathbf{z}} =$ constant in the surface integral in (6·3), so that we obtain

$$\hat{\mathbf{z}} . \mathbf{h}(\mathbf{r}) = \hat{\mathbf{z}} . \mathbf{h}_\infty(\mathbf{r}). \tag{6·4}$$

The component of the induced magnetic field normal to the boundary is therefore unaffected by the introduction of the boundary.

Equation (6·4) is sufficient to define the induced field outside the conductor. If we put (in $z > 0$)

$$\mathbf{h} = - \quad \Psi, \tag{6·5}$$

then

$$\Psi(x, y, z) = \Psi(x, y, \infty) + \int_\infty^z dz' \frac{\partial \Psi(x, y, z')}{\partial z'} = \Psi(x, y, \infty) - \int_\infty^z dz' \hat{\mathbf{z}} . \mathbf{h}_\infty(x, y, z'),$$

from (6·4). Provided that $\mathbf{h} = O(R^{-n})$ as $R \to \infty$, where $n > 1$ and where R is the distance from the rotator, the potential $\Psi(x, y, z)$ becomes constant over the (x, y) plane when $z \to \infty$. We can therefore put $\Psi(x, y, \infty) = 0$, so that

$$\Psi(x, y, z) = - \int_\infty^z dz' \, \hat{\mathbf{z}} . \mathbf{h}_\infty(x, y, z'). \tag{6·6}$$

The result (6·6) does not contain the position of the boundary in any way. The induced field outside the conductor is therefore independent of the exact position of the conductor boundary between the rotator and the point of observation, as long as the normal to the boundary is fixed. (It has to be emphasized that this result is valid only in the time-independent case and in our approximation.)

From (6·3) we can obtain a starting point for an estimate of the error involved in our approximation. The values of the integral in (6·3) are symmetrical about the plane $z = 0$; therefore if $\mathbf{r}_I$ is the image of $\mathbf{r}$ in this plane, we have

$$\mathbf{h}(\mathbf{r}) - \mathbf{h}_\infty(\mathbf{r}) = \mathbf{h}(\mathbf{r}_I) - \mathbf{h}_\infty(\mathbf{r}_I). \tag{6·7}$$

Equation (6·7) enables us to calculate the reflected magnetic field $\mathbf{h}_r \, (= \mathbf{h} - \mathbf{h}_\infty)$ inside the conductor when we have calculated $\mathbf{h}$ at the corresponding points outside by means of (6·6). This $\mathbf{h}_r$ can now be regarded as an additional applied field, and the consequent induced fields can in turn be calculated, so that we obtain a measure of the error in the first approximation. This procedure is carried out in § 7·4.

6·3. *Plane boundary, second method*

We now treat the problem of § 6·2 by a second method capable of being extended to a spherical boundary.

In the conductor ($z<0$), but outside the rotator, the field equations are

$$\nabla \wedge \mathbf{H} = 4\pi\sigma\mathbf{E}, \tag{6·8}$$

$$\nabla \wedge \mathbf{E} = 0, \tag{6·9}$$

$$\nabla . \mathbf{E} = 0, \tag{6·10}$$

$$\nabla . \mathbf{H} = 0. \tag{6·11}$$

In the insulator ($z>0$) equation (6·8) is replaced by

$$\nabla \wedge \mathbf{H} = 0. \tag{6·12}$$

In this second method we again start with the fields $\mathbf{E} = \mathbf{e}_\infty$ and $\mathbf{H} = \mathbf{H}_0 + \mathbf{h}_\infty$ for a rotator embedded in a conductor of infinite extent. In the space $z<0$ we add to them a 'reflected' field, a solution of the field equations (6·8) to (6·11) in which the fields tend to zero as $R \to \infty$; in the space $z>0$ we replace $(\mathbf{e}_\infty, \mathbf{h}_\infty)$ by a 'transmitted' field, a solution of the free-space equations (6·9) to (6·12) in which also the fields vanish as $R \to \infty$. The boundary conditions at infinity are therefore satisfied, and the boundary conditions at $z = 0$ then define the 'reflected' and 'transmitted' fields uniquely in terms of $\mathbf{h}_\infty$. Since the fields we add inside the conductor satisfy (6·8), which does not contain the $(\mathbf{v} \wedge \mathbf{H})$ term, we are again neglecting the interaction of the 'reflected' field with the rotator.

In this and the following subsections we first discuss the general solutions of the field equations, and then find the particular solutions which give us the 'transmitted' field.

*General form of solutions**

Let us consider the possible types of solution of the field equations (6·8) to (6·12). A general solution of (6·9) and (6·10) is $\mathbf{E} = +\nabla(\partial\psi/\partial z)$, where ψ is a scalar function which satisfies $\nabla^2\psi = 0$, and is otherwise arbitrary. (The use of $\partial\psi/\partial z$ instead of just ψ, and the similar definitions in (6·14) to (6·16), are convenient to bring out the analogy to the time-dependent case. The use of $\partial\psi/\partial z$ is sufficiently general because functions independent of z do not occur in our problems.) Equations (6·8) and (6·11) are then satisfied by $\mathbf{H} = 4\pi\sigma\nabla\psi \wedge \hat{\mathbf{z}}$. This combination of $\mathbf{E}$ and $\mathbf{H}$ will be called a type 1 solution. The general solution of (6·8) and (6·11) is then obtained by adding to $\mathbf{H}$ a field $\nabla(\partial\phi/\partial z)$, where ϕ is a scalar function which satisfies $\nabla^2\phi = 0$, and is otherwise arbitrary. This addition to $\mathbf{H}$ does not affect $\mathbf{E}$. This second solution will be called a type 2 solution. We have then

$$\left.\begin{aligned} \mathbf{H}_1 &= 4\pi\sigma\nabla\psi \wedge \hat{\mathbf{z}} \\ \mathbf{E}_1 &= \nabla\frac{\partial\psi}{\partial z} \\ \nabla^2\psi &= 0 \end{aligned}\right\} \quad \text{(type 1 solution for } \sigma \neq 0); \tag{6·13}$$

$$\left.\begin{aligned} \mathbf{H}_2 &= \nabla\frac{\partial\phi}{\partial z} \\ \mathbf{E}_2 &= 0 \\ \nabla^2\phi &= 0 \end{aligned}\right\} \quad \text{(type 2 solution for } \sigma \neq 0). \tag{6·14}$$

In type 1 solutions $\mathbf{H}$ lies in planes of constant z.

* Literature references for the solutions used here and in §§ 6·4 to 6·6 are given in §6·6.

The solutions of the free-space equations (6·9) to (6·12) can be obtained by an analogous argument. We distinguish these solutions and their generating functions by a prime. The solutions are

$$\left.\begin{aligned} \mathbf{H}_1' &= 0 \\ \mathbf{E}_1' &= \boldsymbol{\nabla}\frac{\partial\psi'}{\partial z} \\ \nabla^2\psi' &= 0 \end{aligned}\right\} \quad \text{(type 1 solution for } \sigma = 0); \tag{6·15}$$

$$\left.\begin{aligned} \mathbf{H}_2' &= \boldsymbol{\nabla}\frac{\partial\phi'}{\partial z} \\ \mathbf{E}_2' &= 0 \\ \nabla^2\phi' &= 0 \end{aligned}\right\} \quad \text{(type 2 solution for } \sigma = 0). \tag{6·16}$$

In this time-independent case type 2 solutions are of the same form inside and outside the conductor.

Boundary conditions at the surface of the shell

These are $\mathbf{H} = \mathbf{H}'$, $\mathbf{E}\wedge\hat{\mathbf{n}} = \mathbf{E}'\wedge\hat{\mathbf{n}}$ and $\mathbf{E}\,.\,\hat{\mathbf{n}} = 0$ on the plane $z = 0$ (where $\hat{\mathbf{n}} = \hat{\mathbf{z}}$). Using $\nabla^2(\psi, \phi, \phi') = 0$, we find that the boundary conditions are satisfied if

$$\left.\begin{aligned} \psi = 0, \quad \frac{\partial\psi}{\partial z} &= \frac{\partial\psi'}{\partial z} \\ \phi = \phi', \quad \frac{\partial\phi}{\partial z} &= \frac{\partial\phi'}{\partial z} \end{aligned}\right\} \quad \text{at} \quad z = 0. \tag{6·17}$$

Particular solution

For the rotator embedded in a conductor of infinite extent the solution $(\mathbf{e}_\infty, \mathbf{h}_\infty)$ in $z > z_1$ can be expressed as a superposition of type 1 fields (6·13) and type 2 fields (6·14). If the conductor in $z > 0$ is now removed we obtain, in our approximation, a new solution of the field equations and boundary conditions as follows. The type 2 part of $(\mathbf{e}_\infty, \mathbf{h}_\infty)$ is valid as it stands in both $z < 0$ and $z > 0$, and it also satisfies the boundary conditions; it is unaltered by the insertion of the boundary. The type 1 part of $(\mathbf{e}_\infty, \mathbf{h}_\infty)$ is still a valid solution in $z < 0$, but it does not satisfy the boundary condition $\psi = 0$ at $z = 0$; it is not a valid solution in $z > 0$. A reflected type 1 field has to be added in $z < 0$ to satisfy $\psi = 0$ at $z = 0$, and an external type 1 field has to be put in $z > 0$ to satisfy $\partial\psi/\partial z = \partial\psi'/\partial z$ at $z = 0$. Both these additional fields must vanish as $R \to \infty$.

The normal component of the electric field of the type 1 part of the solution has a discontinuity at $z = 0$; this is due to a surface-charge distribution whose field reflects the current system of the rotator. The type 2 part has no electric field.

The type 1 fields do not give any magnetic components outside the conductor; the only magnetic field there is that of the type 2 part of $\mathbf{h}_\infty$. The z component of $\mathbf{h}_\infty$ comes only from the type 2 part, and as we have seen this is unaffected by the insertion of the boundary. Therefore we have $\hat{\mathbf{z}}\,.\,\mathbf{h}(\mathbf{r}) = \hat{\mathbf{z}}\,.\,\mathbf{h}_\infty(\mathbf{r})$ as in (6·4). In practice it is not necessary to resolve $(\mathbf{e}_\infty, \mathbf{h}_\infty)$ in terms of generating functions; equation (6·4) is sufficient to define the induced field outside the conductor.

6·4. *Spherical boundary*

We next consider a conductor rotating at constant angular velocity in a uniform constant applied magnetic field $\mathbf{H}_0$, and in a rigid conducting spherical shell of the same conductivity as the rotator. We do *not* assume the rotator to be at the centre of the shell. We take spherical polar co-ordinates (r, θ, λ) with the origin at the centre of the shell. The radius of the shell is r_0, and the rotator lies entirely in $r<r_1$, where $r_1<r_0$. The field equations are (6·8) to (6·11) in the conductor $(r<r_0)$ but outside the rotator, and (6·9) to (6·12) in the insulator $(r>r_0)$.

General form of solution

An argument analogous to that which led to the general solutions (6·13) to (6·16) shows that the solution of the field equations can be classified into two types as before.

In the conductor

$$\left.\begin{aligned} \mathbf{H}_1 &= 4\pi\sigma\nabla\psi\wedge\mathbf{r} \\ \mathbf{E}_1 &= \nabla\left[\frac{\partial}{\partial r}(r\psi)\right] \\ \nabla^2\psi &= 0 \end{aligned}\right\} \quad \text{(type 1 solution for } \sigma\neq 0); \tag{6·18}$$

$$\left.\begin{aligned} \mathbf{H}_2 &= \nabla\left[\frac{\partial}{\partial r}(r\phi)\right] \\ \mathbf{E}_2 &= 0 \\ \nabla^2\phi &= 0 \end{aligned}\right\} \quad \text{(type 2 solution for } \sigma\neq 0). \tag{6·19}$$

In type 1 solutions $\mathbf{H}$ is always perpendicular to $\mathbf{r}$.

In the insulator

$$\left.\begin{aligned} \mathbf{H}_1' &= 0 \\ \mathbf{E}_1' &= \nabla\left[\frac{\partial}{\partial r}(r\psi')\right] \\ \nabla^2\psi' &= 0 \end{aligned}\right\} \quad \text{(type 1 solution for } \sigma = 0); \tag{6·20}$$

$$\left.\begin{aligned} \mathbf{H}_2' &= \nabla\left[\frac{\partial}{\partial r}(r\phi')\right] \\ \mathbf{E}_2' &= 0 \\ \nabla^2\phi' &= 0 \end{aligned}\right\} \quad \text{(type 2 solution for } \sigma = 0). \tag{6·21}$$

(The use of these expressions for $\mathbf{E}_1, \mathbf{H}_2, \mathbf{E}_1', \mathbf{H}_2'$ excludes fields of the form $\nabla(1/r)$. Such fields do not occur in our problems.)

Boundary conditions at the surface of the shell

These are $\mathbf{H}=\mathbf{H}'$, $\mathbf{E}\wedge\hat{\mathbf{r}}=\mathbf{E}'\wedge\hat{\mathbf{r}}$, $\mathbf{E}.\hat{\mathbf{r}}=0$, and are satisfied if we put

$$\left.\begin{aligned} \psi &= 0, \quad \frac{\partial}{\partial r}(r\psi) = \frac{\partial}{\partial r}(r\psi') \\ \phi &= \phi', \quad \frac{\partial\phi}{\partial r} = \frac{\partial\phi'}{\partial r} \end{aligned}\right\} \quad \text{at } r = r_0. \tag{6·22}$$

Particular solution

An approximate solution for the finite shell can be obtained from $\mathbf{h}_\infty$ and $\mathbf{e}_\infty$ in a manner analogous to that of § 6·3. The removal of the conductor in $r>r_0$ leaves the type 2 part of $(\mathbf{h}_\infty, \mathbf{e}_\infty)$ unchanged; a type 1 field regular at $r=0$ has to be added in $r<r_0$ to satisfy the boundary condition $\psi=0$, and a further type 1 field which vanishes as $r\to\infty$ has to be put in $r>r_0$ to satisfy $\partial(r\psi)/\partial r = \partial(r\psi')/\partial r$. Outside the shell, the type 1 part of $(\mathbf{h}, \mathbf{e})$ gives an electric field only, while the type 2 part gives a magnetic field only.

We see from (6·18) and (6·19) that in $r>r_1$ the radial component of $\mathbf{h}_\infty$ is contained in the type 2 part, and therefore remains unaltered when the conductor in $r>r_0$ is removed; that is, in our approximation,

$$\mathbf{h}.\hat{\mathbf{r}} = \mathbf{h}_\infty.\hat{\mathbf{r}} \quad (\text{in } r>r_0). \tag{6·23}$$

If we put, in $r>r_0$,

$$\mathbf{h} = -\nabla\Psi, \tag{6·24}$$

as in (6·5), we obtain analogously to (6·6)

$$\Psi(r,\theta,\lambda) = -\int_\infty^r \mathrm{d}r'\hat{\mathbf{r}}.\mathbf{h}_\infty(r',\theta,\lambda). \tag{6·25}$$

The absence of r_0 from (6·25) shows that if the relative positions of the rotator, shell centre and point of observation (r,θ,λ) are fixed, then the induced field outside the shell is independent of r_0 (as long as $r_1<r_0<r$). Formula (6·25) forms the basis of our detailed calculations of field patterns in § 7.

6·5. *Time-dependent case, plane boundary*

The methods of §§ 6·3 and 6·4 can be extended to the time-dependent case. We now consider again the problem of § 6·3 but this time for a rotator with time-dependent angular velocity. As before all the rotator is in $z<z_1$ (<0), and $\sigma=0$ for $z>0$.

The field equations in the conductor $(z<0)$ but outside the rotator are now

$$\nabla\wedge\mathbf{H} = 4\pi\sigma\mathbf{E}, \tag{6·26}$$

$$\nabla\wedge\mathbf{E} = -\frac{\partial\mathbf{H}}{\partial t}, \tag{6·27}$$

$$\nabla.\mathbf{E} = 0, \tag{6·28}$$

$$\nabla.\mathbf{H} = 0. \tag{6·29}$$

In the insulator $(z>0)$ equation (6·26) is replaced by

$$\nabla\wedge\mathbf{H} = 0. \tag{6·30}$$

General form of solution

Without loss of generality, we may restrict the discussion to fields containing the time in a factor $\mathrm{e}^{-\mathrm{i}\nu t}$ only. The appropriate solutions of (6·26) to (6·30) are of two basic types,

analogous to the time-independent solutions (6·13) to (6·16) of (6·8) to (6·12). In the conductor we have

$$\left.\begin{aligned} &\mathbf{H}_1 = 4\pi\sigma\nabla\psi\wedge\hat{\mathbf{z}} \\ &\mathbf{E}_1 = \nabla\frac{\partial\psi}{\partial z} + \mathrm{i}4\pi\sigma\nu\psi\hat{\mathbf{z}} \\ &\nabla^2\psi + \mathrm{i}4\pi\sigma\nu\psi = 0, \quad \psi \propto \mathrm{e}^{-\mathrm{i}\nu t} \end{aligned}\right\} \quad \text{(type 1 solution for } \sigma \neq 0); \tag{6·31}$$

$$\left.\begin{aligned} &\mathbf{H}_2 = \nabla\frac{\partial\phi}{\partial z} + \mathrm{i}4\pi\sigma\nu\phi\hat{\mathbf{z}} \\ &\mathbf{E}_2 = \mathrm{i}\nu\nabla\phi\wedge\hat{\mathbf{z}}, \\ &\nabla^2\phi + \mathrm{i}4\pi\sigma\nu\phi = 0, \quad \phi \propto \mathrm{e}^{-\mathrm{i}\nu t} \end{aligned}\right\} \quad \text{(type 2 solution for } \sigma \neq 0). \tag{6·32}$$

In the insulator

$$\left.\begin{aligned} &\mathbf{H}_1' = 0 \\ &\mathbf{E}_1' = \nabla\frac{\partial\psi'}{\partial z} \\ &\nabla^2\psi' = 0, \quad \psi' \propto \mathrm{e}^{-\mathrm{i}\nu t} \end{aligned}\right\} \quad \text{(type 1 solution for } \sigma = 0); \tag{6·33}$$

$$\left.\begin{aligned} &\mathbf{H}_2' = \nabla\frac{\partial\phi'}{\partial z} \\ &\mathbf{E}_2' = \mathrm{i}\nu\nabla\phi'\wedge\hat{\mathbf{z}} \\ &\nabla^2\phi' = 0, \quad \phi' \propto \mathrm{e}^{-\mathrm{i}\nu t} \end{aligned}\right\} \quad \text{(type 2 solution for } \sigma = 0). \tag{6·34}$$

The magnetic field of type 1 solutions and the electric field of type 2 solutions lie in planes of constant z.

The functions (ψ, ϕ) and (ψ', ϕ') can be expressed as linear superpositions of functions of the form

$$(\psi, \phi) = \exp\left[\mathrm{i}(\xi x + \eta y) \pm (\xi^2 + \eta^2 - \mathrm{i}4\pi\sigma\nu)^{\frac{1}{2}} z\right] \mathrm{e}^{-\mathrm{i}\nu t}, \tag{6·35}$$

$$(\psi', \phi') = \exp\left[\mathrm{i}(\xi x + \eta y) \pm (\xi^2 + \eta^2)^{\frac{1}{2}} z\right] \mathrm{e}^{-\mathrm{i}\nu t}, \tag{6·36}$$

where ξ and η are arbitrary real parameters.

Boundary conditions at the surface of the shell

These are $\mathbf{E}\wedge\hat{\mathbf{n}} = \mathbf{E}'\wedge\hat{\mathbf{n}}$, $\mathbf{E}.\hat{\mathbf{n}} = 0$ and $\mathbf{H} = \mathbf{H}'$ at $z = 0$ and are satisfied by

$$\left.\begin{aligned} &\psi = 0, \quad \frac{\partial\psi}{\partial z} = \frac{\partial\psi'}{\partial z} \\ &\phi = \phi', \quad \frac{\partial\phi}{\partial z} = \frac{\partial\phi'}{\partial z} \end{aligned}\right\} \quad \text{at} \quad z = 0. \tag{6·37}$$

The boundary conditions (6·37) are the same as in the time-independent case.

Particular solution

To solve the problem of the bounded conductor let us again start with a conductor filling all space, and with induced fields $\mathbf{h}_\infty$ and $\mathbf{e}_\infty$. We now remove the conductor in $z > 0$,

and neglect the induction effects of the reflected current; we see that the type 2 part of $(\mathbf{h}_\infty, \mathbf{e}_\infty)$ *is* changed in its passage through the boundary, because ϕ and ϕ' now satisfy different differential equations. In contrast to the situation in the time-independent case of § 6·3, both the type 1 and type 2 parts of $(\mathbf{h}, \mathbf{e})$ are now modified by the boundary.

The type 1 field does not give a magnetic field in $z>0$ (although it does give an electric field) and will not be discussed further. To discuss the type 2 field, which gives both electric and magnetic fields, let us consider a component of $\mathbf{h}_\infty$ which is, in $z>z_1$, derived from the following function:

$$\phi_\infty \exp\left[\mathrm{i}(\xi x+\eta y)-(\xi^2+\eta^2-\mathrm{i}4\pi\sigma\nu)^{\frac{1}{2}} z\right] \mathrm{e}^{-\mathrm{i}\nu t}, \tag{6·38}$$

where ϕ_∞ is a constant, and where the real part of $(\xi^2+\eta^2-\mathrm{i}4\pi\sigma\nu)^{\frac{1}{2}}$ is positive. In order to construct an approximate solution (in the sense of §§ 6·2, 6·3 and 6·4) from (6·38), we have to add a reflected function

$$\mathscr{R}_2\phi_\infty \exp\left[\ldots+(\xi^2+\eta^2-\mathrm{i}4\pi\sigma\nu)^{\frac{1}{2}} z\right] \mathrm{e}^{-\mathrm{i}\nu t} \quad \text{in} \quad z<0, \tag{6·39}$$

and replace (6·38) by a transmitted function

$$\mathscr{T}_2\phi_\infty \exp\left[\ldots-(\xi^2+\eta^2)^{\frac{1}{2}} z\right] \mathrm{e}^{-\mathrm{i}\nu t} \quad \text{in} \quad z>0. \tag{6·40}$$

From the boundary conditions (6·37) we find that

$$\mathscr{T}_2 = \frac{2}{\left[1+\left(1-\dfrac{\mathrm{i}4\pi\sigma\nu}{\xi^2+\eta^2}\right)^{-\frac{1}{2}}\right]}, \quad \mathscr{R}_2 = \mathscr{T}_2-1. \tag{6·41}$$

The normal component of $\mathbf{h}$ at $z=0$ is

$$\left.\begin{aligned} \hat{\mathbf{z}}.\mathbf{h}(x,y,z=0;\nu) &= \mathscr{T}_2\hat{\mathbf{z}}.\mathbf{h}_\infty(x,y,z=0;\nu) \\ &\simeq \hat{\mathbf{z}}.\mathbf{h}_\infty \quad \text{if} \quad 4\pi\sigma\nu \ll (\xi^2+\eta^2), \\ &\simeq 2\hat{\mathbf{z}}.\mathbf{h}_\infty \quad \text{if} \quad 4\pi\sigma\nu \gg (\xi^2+\eta^2); \end{aligned}\right\} \tag{6·42}$$

intermediate Fourier components give $1 \leqslant |\mathscr{T}_2| \leqslant 2$.

The physical significance of the results (6·42) is as follows. Since $(\xi^2+\eta^2)^{-\frac{1}{2}}$ is the characteristic distance in which $\mathbf{h}$ varies along the plane $z=0$ (the conductor surface) and $(2\pi\sigma\nu)^{-\frac{1}{2}}$ is the skin depth, it follows from (6·42) that when the conductor in $z>0$ is removed, then $\hat{\mathbf{z}}.\mathbf{h}_\infty$ still penetrates unchanged into the region $z>0$ provided that the skin depth is much greater than the typical distance of variation along the surface of the conductor. We shall need this result in § 9.

According to (6·42) the surface transmission for different Fourier components does not vary greatly, so that a rough approximation to the solution for the induced magnetic field in $z>0$ could be obtained by neglecting this variation and fitting an external potential field to the normal component of $\mathbf{h}_\infty$ at $z=0$.

In contrast to the time-independent case, the depth of the rotator below the conductor surface is now important. In the time-dependent case, the induced field outside the conductor clearly depends on where between the rotator and the point of observation the boundary is placed, for, due to the skin effect in the conducting domain, $\mathbf{h}_\infty$ diminishes as $\exp[-R(2\pi\sigma\nu)^{\frac{1}{2}}]$ with distance R from the rotator.

6·6. *Time-dependent case, spherical boundary*

We now treat the problem of § 6·4 when the angular velocity of the rotator is variable. The field equations are (6·26) to (6·29) in the conducting domain ($r<r_0$) but outside the rotator, and (6·27) to (6·30) in the insulator ($r>r_0$). As in § 6·5, we consider fields containing the time in a factor $e^{-i\nu t}$ only.

General form of solution

The solutions of the field equations are of two basic types. (This form of solution was first introduced by Lamb (1881) and was elaborated by Hansen (1935). Stratton (1941, chap. VII) gives a general treatment, including plane solutions analogous to those we have used in §§ 6·3 and 6·5. Elsasser (1946*a*) gives spherical solutions analogous to those we have used here and in § 6·4; Bullard (1949*b*) gives a detailed list of the respective field components. A useful account, including a proof of completeness, is given by Blatt & Weisskopf (1952, appendix B).) In the conductor we have

$$\left.\begin{aligned} \mathbf{H}_1 &= 4\pi\sigma\nabla\psi\wedge\mathbf{r} \\ \mathbf{E}_1 &= \nabla\left[\frac{\partial}{\partial r}(r\psi)\right]+i4\pi\sigma\nu\mathbf{r}\psi \\ \nabla^2\psi+i4\pi\sigma\nu\psi &= 0, \quad \psi\propto e^{-i\nu t} \end{aligned}\right\} \quad \text{(type 1 solution for } \sigma\neq 0); \tag{6·43}$$

$$\left.\begin{aligned} \mathbf{H}_2 &= \nabla\left[\frac{\partial}{\partial r}(r\phi)\right]+i4\pi\sigma\nu\mathbf{r}\phi \\ \mathbf{E}_2 &= i\nu\nabla\phi\wedge\mathbf{r} \\ \nabla^2\phi+i4\pi\sigma\nu\phi &= 0, \quad \phi\propto e^{-i\nu t} \end{aligned}\right\} \quad \text{(type 2 solution for } \sigma\neq 0). \tag{6·44}$$

In the insulator we have

$$\left.\begin{aligned} \mathbf{H}_1' &= 0 \\ \mathbf{E}_1' &= \nabla\left[\frac{\partial}{\partial r}(r\psi')\right] \\ \nabla^2\psi' &= 0, \quad \psi'\propto e^{-i\nu t} \end{aligned}\right\} \quad \text{(type 1 solution for } \sigma=0); \tag{6·45}$$

$$\left.\begin{aligned} \mathbf{H}_2' &= \nabla\left[\frac{\partial}{\partial r}(r\phi')\right] \\ \mathbf{E}_2' &= i\nu\nabla\phi'\wedge\mathbf{r}, \\ \nabla^2\phi' &= 0, \quad \phi'\propto e^{-i\nu t} \end{aligned}\right\} \quad \text{(type 2 solution for } \sigma=0). \tag{6·46}$$

The magnetic field of type 1 solutions and the electric field of type 2 solution are everywhere perpendicular to $\mathbf{r}$. Such fields were called toroidal, and the others poloidal, by Elsasser and Bullard. Bullard writes $\mathbf{H}_T, \mathbf{H}_S, \mathbf{E}_S, \mathbf{E}_T$ for our $\mathbf{H}_1, \mathbf{H}_2, \mathbf{E}_1, \mathbf{E}_2$.

The functions (ψ,ϕ) and (ψ',ϕ') can be expressed as linear superpositions of functions of the form

$$(\psi,\phi) = (kr)^{-\frac{1}{2}}\begin{matrix} J_{n+\frac{1}{2}}(kr) \\ H^{(1)}_{n+\frac{1}{2}}(kr) \end{matrix} P_n^m(\cos\theta)\begin{matrix} \cos m\lambda \\ \sin m\lambda \end{matrix} e^{-i\nu t}, \tag{6·47}$$

where

$$k^2 = i4\pi\sigma\nu, \tag{6·48}$$

$$(\psi',\phi') = \begin{matrix} (r/r_0)^n \\ (r_0/r)^{n+1} \end{matrix} P_n^m(\cos\theta)\begin{matrix} \cos m\lambda \\ \sin m\lambda \end{matrix} e^{-i\nu t}. \tag{6·49}$$

The functions containing $J_{n+\frac{1}{2}}(kr)$ or $(r/r_0)^n$ are regular at $r=0$, and the alternatives $H^{(1)}_{n+\frac{1}{2}}(kr)$ (where the imaginary part of k is positive) or $(r_0/r)^{n+1}$ vanish as $r\to\infty$.

Boundary conditions at the surface of the shell

These are $\mathbf{E}\wedge\hat{\mathbf{n}}=\mathbf{E}'\wedge\hat{\mathbf{n}}$, $\mathbf{E}.\hat{\mathbf{n}}=0$ and $\mathbf{H}=\mathbf{H}'$ on the surface $r=r_0$, and are satisfied if we put

$$\left.\begin{aligned}\psi=0,\quad &\frac{\partial}{\partial r}(r\psi)=\frac{\partial}{\partial r}(r\psi')\\ \phi=\phi',\quad &\frac{\partial\phi}{\partial r}=\frac{\partial\phi'}{\partial r}\end{aligned}\right\}\quad\text{at}\quad r=r_0. \tag{6·50}$$

The boundary conditions (6·50) are the same as in the time-independent case.

Particular solution

We can now construct an approximate solution of the problem of the bounded conductor in a way analogous to the method of § 6·5 by starting with the infinite conductor and then removing the conductor in $r>r_0$. The boundary conditions are again satisfied by adding reflected fields regular at $r=0$ and transmitted fields which vanish at infinity.

In contrast with the time-independent case both the type 1 and type 2 parts of $(\mathbf{h}_\infty,\mathbf{e}_\infty)$ are again modified by the boundary.

The type 1 solution does not give a magnetic field outside the shell. This solution will therefore not be considered further. For the type 2 solution, which gives both electric and magnetic fields, let us consider a component of $\mathbf{h}_\infty$ which is derived, in $r>r_1$, from a function

$$\phi_\infty(kr)^{-\frac{1}{2}}H^{(1)}_{n+\frac{1}{2}}(kr)\,P^m_n(\cos\theta)\,\mathrm{e}^{\mathrm{i}m\lambda}\,\mathrm{e}^{-\mathrm{i}\nu t}, \tag{6·51}$$

where ϕ_∞ is a constant. In order to obtain an approximate solution, we must add to (6·51) a reflected field

$$\mathscr{R}_2\phi_\infty(kr)^{-\frac{1}{2}}J_{n+\frac{1}{2}}(kr)\,P^m_n(\cos\theta)\,\mathrm{e}^{\mathrm{i}m\lambda}\,\mathrm{e}^{-\mathrm{i}\nu t} \tag{6·52}$$

in $r<r_0$, and replace (6·51) by a transmitted field

$$\mathscr{T}_2\phi_\infty(r_0/r)^{n+1}\,P^m_n(\cos\theta)\,\mathrm{e}^{\mathrm{i}m\lambda}\,\mathrm{e}^{-\mathrm{i}\nu t} \tag{6·53}$$

in $r>r_0$. The boundary conditions (6·50) give

$$\left.\begin{aligned}\mathscr{R}_2&=-\frac{H^{(1)}_{n-\frac{1}{2}}(kr_0)}{J_{n-\frac{1}{2}}(kr_0)},\\ \mathscr{T}_2&=(kr_0)^{-\frac{1}{2}}[H^{(1)}_{n+\frac{1}{2}}(kr_0)+\mathscr{R}_2J_{n+\frac{1}{2}}(kr_0)].\end{aligned}\right\} \tag{6·54}$$

The normal component of the induced magnetic field outside the conductor is, at the boundary $r=r_0$,

$$\left.\begin{aligned}\mathbf{h}(r_0,\theta,\lambda;\nu).\hat{\mathbf{r}}&=\mathbf{h}_\infty(r_0,\theta,\lambda;\nu).\hat{\mathbf{r}}\left[1-\frac{H^{(1)}_{n-\frac{1}{2}}(kr_0)\,J_{n+\frac{1}{2}}(kr_0)}{H^{(1)}_{n+\frac{1}{2}}(kr_0)\,J_{n-\frac{1}{2}}(kr_0)}\right]\\ &\simeq\mathbf{h}_\infty(r_0,\theta,\lambda;\nu).\hat{\mathbf{r}}\quad\text{if}\quad|kr_0|\ll n,\\ &\simeq 2\mathbf{h}_\infty(r_0,\theta,\lambda;\nu).\hat{\mathbf{r}}\quad\text{if}\quad|kr_0|\gg n.\end{aligned}\right\} \tag{6·55}$$

We can apply remarks analogous to those following equation (6·42) on the surface transmission and effect of position of the boundary to the present case of the spherical shell.

In particular, we may note that (r_0/n) is the characteristic distance in which $\mathbf{h}_\infty$ varies along the surface r_0 of the conducting sphere. Therefore the physical interpretation of (6·55) is that when the conductor in $r>r_0$ is removed, then $\mathbf{h}_\infty.\hat{\mathbf{r}}$ continues to penetrate into the insulator unchanged provided that $(r_0/n)\ll 1/\sqrt{(2\pi\sigma\nu)}$, i.e. that the characteristic distance of variation along the conductor surface is much smaller than the skin depth. We shall need this result in § 9.

7. The external field due to a rotator near a boundary of a conducting region

Introduction

In §§ 3, 4 and 5 solutions were obtained for a rotator in an infinite conducting medium for the three cases of axial applied field, transverse applied field with low angular velocity, and transverse applied field with high velocity. In § 6 we showed how one can use these results for the infinite shell as a starting point of an approximate treatment of a rotator in a finite shell. We now use this treatment to calculate the induced field due to a rigid rotator in a rigid sphere. (This model is the approximation used in part E for the discussion of induction in eddies in the core of the earth.) Only the time-independent case is considered.

In §§ 7·1, 7·2 and 7·3 solutions are given for the three simplest geometrical configurations; all others can be derived by a linear combination of these. For transverse applied field the solutions are given for $\alpha\gg 1$, the simple modifications necessary for $\alpha\ll 1$ being indicated. For simplicity, a spherical rotator is assumed, but the results will not be greatly different for an ellipsoidal or short finite cylindrical rotator; induction in one end of a cylindrical rotator is also discussed for comparison with the experimental work.

The approximation involved in obtaining these results is to neglect the induction effects associated with the magnetic field of the system of reflected currents. The errors involved in this approximation are estimated in § 7·4 and shown to be small in nearly all cases. Charts of the induced field on an external spherical surface concentric with the conducting shell (induced field on the surface of the earth due to a rotating eddy in the core) are given and discussed in § 7·5. A general discussion is given in § 7·6, and in § 7·7 the most important results of this section are summarized.

Co-ordinate system

See figure 22. Let a sphere of radius a, centre Q, rotate at constant angular velocity ω in a stationary sphere of radius R_C, the centre Q of the small sphere being at a distance L from that of the larger at O. (The limit $L\to 0$ gives the case of concentric spheres; the limit $R_C\to\infty$, $(R_C-L)\to D$ gives a rotator a distance D inside a plane boundary.) Denote the unit vector in the direction OQ by $\hat{\mathbf{p}}$, in the direction $\hat{\mathbf{p}}\wedge\boldsymbol{\omega}$ by $\hat{\mathbf{q}}$, and in the direction $\boldsymbol{\omega}\wedge\hat{\mathbf{q}}$ by $\hat{\mathbf{s}}$. (The results of this section are primarily intended for application to the theory of induction processes in the earth's core. It will therefore be convenient to use the terms vertical and horizontal to denote directions parallel and perpendicular respectively to the local radius vector. Thus the unit vector $\hat{\mathbf{p}}$ is the vertical through Q, $\hat{\mathbf{q}}$ lies in the horizontal plane through Q, and $\hat{\mathbf{s}}$ lies in a vertical plane through Q.) Take spherical polar co-ordinates (r,θ,λ) with the origin at O, and the origin of λ in the direction $\hat{\mathbf{q}}$. Let $QP=r'$, the angle $OQP=\pi-\beta$, and let the angle between $\boldsymbol{\omega}$ and $\hat{\mathbf{p}}$ be ξ. In §§ 7·1, 7·2 and 7·3 we shall consider

the following three cases of relative orientation of $\mathbf{H}_0$ (the applied magnetic field at the rotator, assumed constant and uniform), $\boldsymbol{\omega}$ (the angular velocity vector of the rotator), and the radial vector $\hat{\mathbf{p}}$: $\mathbf{H}_0$ parallel to $\boldsymbol{\omega}$ (case A); $\mathbf{H}_0$ perpendicular to both $\boldsymbol{\omega}$ and $\hat{\mathbf{p}}$, i.e. horizontal and parallel to $\hat{\mathbf{q}}$ (case B); $\mathbf{H}_0$ perpendicular to both $\boldsymbol{\omega}$ and $\hat{\mathbf{p}} \wedge \boldsymbol{\omega}$, i.e. in the vertical plane and parallel to $\hat{\mathbf{s}}$ (case C).

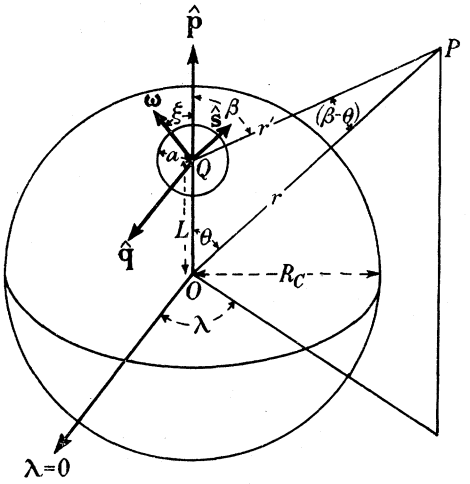

FIGURE 22. Co-ordinate system. Spherical rotator in spherical shell. The vectors $\hat{\mathbf{p}}$, $\hat{\mathbf{s}}$, $\boldsymbol{\omega}$ lie in the plane of the diagram. The vector $\hat{\mathbf{q}}$ and the direction $\lambda = 0$ are perpendicular to the plane of the diagram and are directed towards the reader.

7·1. *Axial applied field (case A)* ($\mathbf{H}_0 \wedge \boldsymbol{\omega} = 0$)

From (3·22) we find, after some calculation,

$$\mathbf{h}_\infty \cdot \hat{\mathbf{r}} = -\tfrac{2}{5}\alpha \frac{H_0 a^3 L \sin\xi}{2} \frac{1}{r'^5} \{2\cos\xi (r\cos\theta - L)\sin\theta\cos\lambda - \sin\xi\, r\sin^2\theta \sin 2\lambda\}, \quad (7\cdot1)$$

where $\mathbf{h}_\infty$ is the induced field due to a rotator in a conducting medium of infinite extent. The integration (6·25) can be carried out by elementary methods, and one finds for the potential Ψ' of the external induced field (in $r > R_C$), after some transformation,

$$\Psi' = \tfrac{2}{15}\alpha \frac{H_0 a^3 \sin\xi}{2} \frac{1}{r'^2} \left\{ 2\cos\xi \left[\frac{2\sin\theta}{1+\cos(\beta-\theta)} - \sin\beta \right] \cos\lambda + \sin\xi \left[\frac{2\cos\theta}{1+\cos(\beta-\theta)} - \cos\beta \right] \sin 2\lambda \right\}. \quad (7\cdot2)$$

The limiting case $L \to 0$ gives $\mathbf{h}_\infty \cdot \mathbf{r} = 0$, and hence

$$\mathbf{h} = 0. \quad (7\cdot3)$$

(The induced field also vanishes when $\xi = 0$ in the general case, i.e. when the axis of rotation is along a radius of the surrounding shell. Both these results are consequences of the symmetry theorem of § 6·1.)

In the limit $R_C \to \infty$, $(R_C - L) \to D$, we have

$$\mathbf{h}_\infty \cdot \hat{\mathbf{r}} \to -\tfrac{2}{5}\alpha \frac{H_0 a^3 \sin\xi}{2} \frac{1}{r'^3} \{\cos\xi \sin^2\beta \cos\lambda - \sin\xi \sin^2\beta \sin 2\lambda\}, \quad (7\cdot4)$$

$$\Psi' \to \tfrac{2}{15}\alpha \frac{H_0 a^3 \sin\xi}{2} \frac{1}{r'^2} \left\{ -2\cos\xi \sin\beta \cos\lambda - \sin\xi \left[\cos\beta - \frac{2}{1+\cos\beta} \right] \sin 2\lambda \right\}. \quad (7\cdot5)$$

Similar results can be obtained for the induced field $\mathbf{h}$ due to one end of a rotating cylinder in a conducting spherical shell. We shall denote the centre of the end disk by Q, and the angle between the axis of rotation and OQ by ξ, as with the sphere. We find from (3·18), after some calculation,

$$\mathbf{h}_\infty . \hat{\mathbf{r}} \simeq -\tfrac{1}{8}\alpha H_0 a^2 L \sin\xi \frac{\sin\theta\cos\lambda}{r'^3}. \tag{7·6}$$

The corresponding potential outside the shell is

$$\Psi' \simeq -\tfrac{1}{8}\alpha \frac{H_0 a^2 \sin\xi}{L} \frac{[1-\cos(\beta-\theta)]}{\sin\theta} \cos\lambda. \tag{7·7}$$

The limiting case $L \to 0$ gives $\mathbf{h}_\infty . \hat{\mathbf{r}} = 0$, and hence $\mathbf{h} = 0$ outside the shell.

In the limit $R_C \to \infty$, $(R_C - L) \to D$, we have

$$\mathbf{h}_\infty . \hat{\mathbf{r}} \to -\tfrac{1}{8}\alpha H_0 a^2 \sin\xi \frac{\sin\beta\cos\lambda}{r'^2}, \tag{7·8}$$

$$\Psi' \to -\tfrac{1}{8}\alpha H_0 a^2 \sin\xi \frac{(1-\cos\beta)\cos\lambda}{r'\sin\beta}. \tag{7·9}$$

The maximum value of $\mathbf{h}_\infty . \hat{\mathbf{r}}$ on $r = R$ becomes, by (7·6),

$$(\mathbf{h}_\infty . \hat{\mathbf{r}})_{\max.} = -\frac{0{\cdot}2\alpha H_0 a^2 L \sin\xi}{R^3}. \tag{7·10}$$

7·2. *Transverse applied field (case B)* ($\mathbf{H}_0 . \boldsymbol{\omega} = 0$, $\mathbf{H}_0 \wedge \hat{\mathbf{q}} = 0$; $\alpha \gg 1$)

The angular velocity $\boldsymbol{\omega}$ lies in a vertical plane through the centre of the rotator, $\mathbf{H}_0$ is horizontal and parallel to $\hat{\mathbf{q}}$.

We find from (5·40) and (5·41)

$$\mathbf{h}_\infty . \hat{\mathbf{r}} = -\tfrac{1}{2}H_0 a^3 L \sin\xi \frac{3}{r'^5}\{\cos\xi\, r\sin^2\theta \sin 2\lambda + 2\sin\xi(r\cos\theta - L)\sin\theta\cos\lambda\}$$
$$-\tfrac{1}{2}H_0 a^3 \frac{2\sin\theta\cos\lambda}{r'^3}, \tag{7·11}$$

and from (6·25)

$$\Psi' = \tfrac{1}{2}H_0 a^3 \sin\xi \frac{1}{r'^2}\left\{\cos\xi\left[\cos\beta - \frac{2\cos\theta}{1+\cos(\beta-\theta)}\right]\sin 2\lambda \right.$$
$$\left. + 2\sin\xi\left[-\sin\beta + \frac{2\sin\theta}{1+\cos(\beta-\theta)}\right]\cos\lambda\right\} - \tfrac{1}{2}H_0 a^3 \frac{2}{r'^2}\frac{\sin\theta\cos\lambda}{1+\cos(\beta-\theta)}. \tag{7·12}$$

As $L \to 0$, we have

$$\Psi' \to -\tfrac{1}{2}H_0 a^3 \frac{\sin\theta\cos\lambda}{r^2}, \tag{7·13}$$

i.e. the potential of a central dipole antiparallel to H_0.

As $R_C \to \infty$, $(R_C - L) \to D$, we have

$$\mathbf{h}_\infty . \hat{\mathbf{r}} \to -\tfrac{1}{2}H_0 a^3 \sin\xi \frac{3}{r'^3}\{\cos\xi\sin^2\beta\sin 2\lambda + \sin\xi\sin 2\beta\cos\lambda\}, \tag{7·14}$$

$$\Psi' \to \tfrac{1}{2}H_0 a^3 \sin\xi \frac{1}{r'^2}\left\{\cos\xi\left[\cos\beta - \frac{2}{1+\cos\beta}\right]\sin 2\lambda - 2\sin\xi\sin\beta\cos\lambda\right\}. \tag{7·15}$$

According to (4·10) and (5·42), when $\alpha \ll 1$ the same expressions multiplied by $2\alpha/15$ will describe the external induced field due to an applied field $\mathbf{H}_0$ in the direction of $\boldsymbol{\omega} \wedge \hat{\mathbf{q}}$.

7·3. *Transverse applied field (case C)* ($\mathbf{H}_0 . \boldsymbol{\omega} = 0$, $\mathbf{H}_0 \wedge \hat{\mathbf{s}} = 0$; $\alpha \gg 1$)

Both $\boldsymbol{\omega}$ and $\mathbf{H}_0$ lie in vertical planes through the centre of the rotator, $\mathbf{H}_0$ is parallel to $\hat{\mathbf{s}}$. From (5·40) and (5·41) we have

$$\mathbf{h}_\infty . \hat{\mathbf{r}} = \tfrac{1}{2} H_0 a^3 \sin\xi \frac{2}{r'^3} \left\{ \frac{3Lr}{r'^2} \sin^2\theta \cos^2\lambda - \cos\theta \right\} - \tfrac{1}{2} H_0 a^3 \cos\xi \frac{2 \sin\theta \sin\lambda}{r'^3}, \tag{7·16}$$

and by (6·25)

$$\Psi' = -\tfrac{1}{2} H_0 a^3 \sin\xi \frac{1}{r'^2} \left\{ \left[\cos\beta - \frac{2\cos\theta}{1+\cos(\beta-\theta)} \right] \cos 2\lambda + \cos\beta \right\} - \tfrac{1}{2} H_0 a^3 \cos\xi \frac{2}{r'^2} \frac{\sin\theta \sin\lambda}{1+\cos(\beta-\theta)}. \tag{7·17}$$

As $L \to 0$, we have $\quad \Psi' \to -\tfrac{1}{2} H_0 a^3 \dfrac{1}{r'^2} \{\sin\xi \cos\theta + \cos\xi \sin\theta \sin\lambda\}, \tag{7·18}$

i.e. the potential of a central dipole anti-parallel to $\mathbf{H}_0$.

For $R_C \to \infty$, $(R_C - L) \to D$, we have

$$\left.\begin{aligned} &\mathbf{h}_\infty . \hat{\mathbf{r}} \to \tfrac{1}{2} H_0 a^3 \sin\xi \frac{2}{r'^3} \{3 \sin^2\beta \cos^2\lambda - 1\}, \\ &\Psi' \to -\tfrac{1}{2} H_0 a^3 \sin\xi \frac{1}{r'^2} \left\{ \left[\cos\beta - \frac{2}{1+\cos\beta} \right] \cos 2\lambda + \cos\beta \right\}. \end{aligned}\right\} \tag{7·19}$$

According to (4·10) and (5·42), when $\alpha \ll 1$ the same expressions multiplied by $2\alpha/15$ describe the induced field due to a field $\mathbf{H}_0$ of the same magnitude but in the direction $\hat{\mathbf{q}}$.

7·4. *Effect of the reflected current*

In this subsection we discuss the induction effect of the current system reflected at the boundary of the conducting medium. We consider the two extreme cases of a rotating sphere in a concentric shell and near the plane boundary of a conducting half space.

Concentric spherical shell

When a spherical rotator is surrounded by a concentric spherical conducting shell, we have the limiting cases $L \to 0$ of §§ 7·1, 7·2 and 7·3. In the axially symmetric case A, we have $\mathbf{h} = 0$ outside the shell (7·3), in agreement with the theorem of § 6·1. In the cases of $\mathbf{H}_0$ perpendicular to the axis of rotation, we have, (7·13) and (7·18),

$$\mathbf{h} = -\boldsymbol{\nabla} [\tfrac{1}{2} a^3 \mathbf{H}_0 . \boldsymbol{\nabla} (1/r)], \tag{7·20}$$

where r is the distance from the common centre of the spheres. Equation (7·20) is identical with the result (5·34) for an isolated sphere. It is shown rigorously by Bullard (1949*b*) that the field due to a rotating sphere in a concentric conducting shell is independent of the shell in the region outside the shell. Thus in this case the approximate method used leads to the exact result.

Half-space, general formulae

For the case of a conducting half-space with a plane boundary, the reflected current system will give rise to a field $\mathbf{h}_{10}$ at the rotator; this may be taken as an additional applied field and the procedure repeated. In this way we can write for the inducing field at the rotator

$$\mathbf{H}_{\text{inducing}} = \mathbf{H}_0 + \mathbf{h}_{10} + \mathbf{h}_{20} + \ldots, \tag{7·21}$$

where $\mathbf{h}_{10}$, $\mathbf{h}_{20}$ are the fields at the rotator due to reflected current systems in successive approximations. Correspondingly, we may write for the external induced field

$$\mathbf{h} = \mathbf{h}_1 + \mathbf{h}_2 + \ldots, \tag{7·22}$$

where $\mathbf{h}_1$ is the induced field due to $\mathbf{H}_0$, $\mathbf{h}_2$ that due to $\mathbf{h}_{10}$, etc. We shall consider only the averages $(\mathbf{h}_{10})_{\text{av.}}$, $(\mathbf{h}_{20})_{\text{av.}}$, ... over the rotator. According to (6·7) we need to calculate only $(\mathbf{h}_\infty)_{\text{av.}}$, $(\mathbf{h}_1)_{\text{av.}}$, ... over the image of the rotator outside the conductor. This calculation is simplified by the fact that $\nabla^2\mathbf{h}_\infty = \nabla^2\mathbf{h}_1 = \nabla^2\mathbf{h}_2 \ldots = 0$ over the image, so that, by a trivial extension of a well-known result of potential theory, we have, for a spherical rotator,

$$(\mathbf{h}_\infty)_{\text{av.}} = \mathbf{h}_\infty(Q'), \quad (\mathbf{h}_1)_{\text{av.}} = \mathbf{h}_1(Q'), \ldots, \tag{7·23}$$

where Q' is the centre of the image sphere. According to (6·7) and (7·23) we have

$$\left.\begin{aligned} (\mathbf{h}_{10})_{\text{av.}} &= \mathbf{h}_1(Q') - \mathbf{h}_\infty(Q', \mathbf{H}_0), \\ (\mathbf{h}_{20})_{\text{av.}} &= \mathbf{h}_2(Q') - \mathbf{h}_\infty(Q', (\mathbf{h}_{10})_{\text{av.}}), \\ (\mathbf{h}_{30})_{\text{av.}} &= \mathbf{h}_3(Q') - \mathbf{h}_\infty(Q', (\mathbf{h}_{20})_{\text{av.}}), \\ &\text{etc.}, \end{aligned}\right\} \tag{7·24}$$

where $\mathbf{h}_\infty(Q', \mathbf{H}_0)$, $\mathbf{h}\infty(Q', (\mathbf{h}_{10})_{\text{av.}})$, ... are the induced fields at Q' due to uniform applied fields $\mathbf{H}_0$, $(\mathbf{h}_{10})_{\text{av.}}$, ... at the rotator for conducting surroundings of infinite extent.

Spherical rotator near plane boundary

We now calculate $(\mathbf{h}_{10})_{\text{av.}}$ for the three cases A, B, C of §§ 7·1, 7·2 and 7·3 in the high-velocity approximation $\alpha \gg 1$, and then combine the results to investigate the convergence of the series (7·21) and (7·22).

For case A we have from (3·22), (7·5) and (7·24),

$$\begin{aligned} (\mathbf{h}_{10})_{\text{av.}} &= \mathbf{h}_1(Q') - \mathbf{h}_\infty(Q', \mathbf{H}_0) \\ &= (H_0\alpha/15)\sin 2\xi\,(a/2D)^3\,\hat{\mathbf{q}} - (H_0\alpha/5)\sin 2\xi\,(a/2D)^3\,\hat{\mathbf{q}} \\ &= -(2H_0\alpha/15)\sin 2\xi\,(a/2D)^3\,\hat{\mathbf{q}}. \end{aligned} \tag{7·25}$$

This reflected field is anti-parallel to the applied field of case B.

(For the single-ended cylinder, from (3·18) and (7·9) we have similarly

$$\begin{aligned} (\mathbf{h}_{10})_{\text{av.}} &= \mathbf{h}_1(Q') - \mathbf{h}_\infty(Q', \mathbf{H}_0) \\ &= (H_0\alpha/16)\sin\xi\,(a/2D)^2\,\hat{\mathbf{q}} - (H_0\alpha/8)\sin\xi\,(a/2D)^2\,\hat{\mathbf{q}} \\ &= -(H_0\alpha/16)\sin\xi\,(a/2D)^2\,\hat{\mathbf{q}}. \end{aligned} \tag{7·26}$$

This reflected field is also anti-parallel to the inducing field of case B.)

For case B, we have from (5·40), (5·41), (5·42) and (7·15)

$$\begin{aligned}(\mathbf{h}_{10})_{\text{av.}} &= \mathbf{h}_1(Q') - \mathbf{h}_\infty(Q', \mathbf{H}_0) \\ &= H_0 \sin^2\xi\,(a/2D)^3\,\hat{\mathbf{q}} - H_0(1-3\sin^2\xi)\,(a/2D)^3\,\hat{\mathbf{q}} \\ &= H_0 \cos 2\xi\,(a/2D)^3\,\hat{\mathbf{q}}. \end{aligned} \tag{7·27}$$

This field is parallel to the applied field $\mathbf{H}_0$, i.e. again case B.

For case C we have from (5·40), (5·41), (5·42) and (7·19)

$$\begin{aligned}(\mathbf{h}_{10})_{\text{av.}} &= \mathbf{h}_1(Q') - \mathbf{h}_\infty(Q', \mathbf{H}_0) \\ &= -H_0 \sin\xi\,(a/2D)^3\,\hat{\mathbf{r}} + H_0(a/2D)^3\,\hat{\mathbf{s}} \\ &= H_0 \cos\xi\,(a/2D)^3\,[\cos\xi\,\hat{\mathbf{s}} - \sin\xi\,\hat{\boldsymbol{\omega}}]. \end{aligned} \tag{7·28}$$

This field contains a component parallel to the applied $\mathbf{H}_0$ (case C), and a component antiparallel to $\boldsymbol{\omega}$ (case A).

For the case B the fields $(\mathbf{h}_{10})_{\text{av.}}$, $(\mathbf{h}_{20})_{\text{av.}}$, ... are all of the same type as $\mathbf{H}_0$, so that the total external induced field must be

$$\mathbf{h}_B = \mathbf{h}_{1B} \sum_{n=0}^{\infty} \left[\cos 2\xi \left(\frac{a}{2D}\right)^3\right]^n = \mathbf{h}_{1B} \Big/ \left[1 - \cos 2\xi \left(\frac{a}{2D}\right)^3\right], \tag{7·29}$$

where $\mathbf{h}_{1B}$ denotes the first-order external field for case B given by (7·15).

For the case A the additional inducing field $\mathbf{h}_{10}$, and hence all $\mathbf{h}_{n0}$ $(n>0)$, will be of type B (with the sign reversed), so that the total external induced field will be

$$\mathbf{h}_A = \mathbf{h}_{1A} - \frac{2\alpha}{15}\mathbf{h}_{1B} \frac{\sin 2\xi \left(\frac{a}{2D}\right)^3}{1 - \cos 2\xi \left(\frac{a}{2D}\right)^3}, \tag{7·30}$$

where $\mathbf{h}_{1A}$ is the first-order external field for case A given by (7·5) and $\mathbf{h}_{1B}$ has the meaning given above. It is important to note that, according to (7·5), (7·15) and (7·19), $\mathbf{h}_{1A}$, $(2\alpha/15)\,\mathbf{h}_{1B}$ and $(2\alpha/15)\,\mathbf{h}_{1C}$ are of the same order of magnitude for $\alpha \gg 1$.

The case C is more complicated. The type C field due to the reflected currents will always generate a type C and a type A field at the rotator in the next approximation. The type A part, and all its further approximations, can be summed as in (7·30). The resulting total external field is

$$\mathbf{h}_C = \mathbf{h}_{1C} \frac{1}{1 - \cos^2\xi \left(\frac{a}{2D}\right)^3} - \frac{\frac{1}{2}\sin 2\xi \left(\frac{a}{2D}\right)^3}{1 - \cos^2\xi \left(\frac{a}{2D}\right)^3} \left\{\mathbf{h}_{1A} - \frac{2\alpha}{15}\mathbf{h}_{1B} \frac{\sin 2\xi \left(\frac{a}{2D}\right)^3}{1 - \cos 2\xi \left(\frac{a}{2D}\right)^3}\right\}, \tag{7·31}$$

where $\mathbf{h}_{1C}$ is the first-order field calculated by (7·19), while $\mathbf{h}_{1A}$, $\mathbf{h}_{1B}$ are defined above. In this case the relative magnitude of the second term increases indefinitely with α.

The argument leading to (7·29), (7·30) and (7·31) shows that the series (7·22) converges in the approximation of keeping only the average reflected field over the rotator at each stage.

If the rotator is spinning slowly ($\alpha \ll 1$), the above analysis will be somewhat different, but the convergence will be more rapid since there will be an extra factor α associated with cases B and C in each approximation.

Discussion

We have seen above that in the limiting case of a spherical rotator at the centre of a spherical conductor the approximate results (7·3), (7·13) and (7·18) obtained by neglecting the reflected currents are in fact exact. It is therefore plausible that the estimates (7·29), (7·30) and (7·31) of the effect of the currents reflected by a plane boundary (the other limiting case) will give the maximum error for any position of the rotator in a spherical conductor.

Since $D \geqslant a$ and $|\cos 2\xi| \leqslant 1$, the estimates (7·29) and (7·30) show that the error in the induced fields derived from (7·2) and (7·12) of cases A and B is less than about 10%, and falls off rapidly as the distance D from the boundary of the conductor is increased. The error in case C will, however, depend on the value of α. The first term of (7·31) differs from $\mathbf{h}_{1C}$ by a factor differing from unity by less than $\frac{1}{8}$, but the ratio of the second term to the first term is of order of magnitude $\frac{1}{2}(2\alpha/15)\,(a/2D)^3$, so that the result (7·19) will break down when $\alpha \ll 15(2D/a)^3\,(\geqslant 120)$ is not satisfied. For $1 \ll \alpha \lesssim 120$ the error in (7·19) is less than 10% and falls off rapidly as D is increased, but for $\alpha \gtrsim 120$ there is the possibility that the reflected currents will be so large as to make (7·19) invalid. (The physical reason for this situation is that in this case the reflected currents produce an axial field at the rotator. The induced field given by this axial field increases without limit as α is increased, while the other induced fields tend to a finite limit.)

Thus, apart from the one exceptional case, we may assume that all the results given in §§ 7·1, 7·2 and 7·3 are correct to within about 10%.

7·5. *Charts of induced field*

It is generally believed that inside the earth there is a liquid conducting core of radius $R_C = 3{\cdot}5 \times 10^3$ km and with a conductivity $\sigma \sim 3 \times 10^{-6}$ e.m.u.; this core is surrounded by a rigid mantle of outside radius $R_E = 6{\cdot}4 \times 10^3$ km and a conductivity not greater than 10^{-8} e.m.u. (see § 8). We use the results of §§ 7·1, 7·2 and 7·3 to give the induced magnetic field to be expected at the surface from an eddy in the core.

We represent the eddy by a rigid sphere of radius a rotating at constant angular velocity $\boldsymbol{\omega}$ in a rigid spherical conducting shell of radius R_C and in a uniform applied field $\mathbf{H}_0$. Since the field equations are linear, we may consider separately the effect due to various directions of $\mathbf{H}_0$ and $\boldsymbol{\omega}$. Figures 23 to 29 show the induced field $\mathbf{h}$ at the earth's surface ($r = R_E$) due to a rotator whose centre is at a distance $L = 0{\cdot}4R_E$ from the centre of the earth. These charts have been computed from (7·1), (7·2), (7·11), (7·12), (7·16) and (7·17). In this subsection we discuss the field patterns shown on these charts, and try to give the physical reasons for the patterns.

The main features of the patterns are their very large extent (over a whole hemisphere) and the well-defined distinct source centres composing them. The spread of the patterns will vary somewhat with the depth of the rotator centre, but table 1 shows that this variation is not great. This table gives the angular distance of the points of maximum vertical

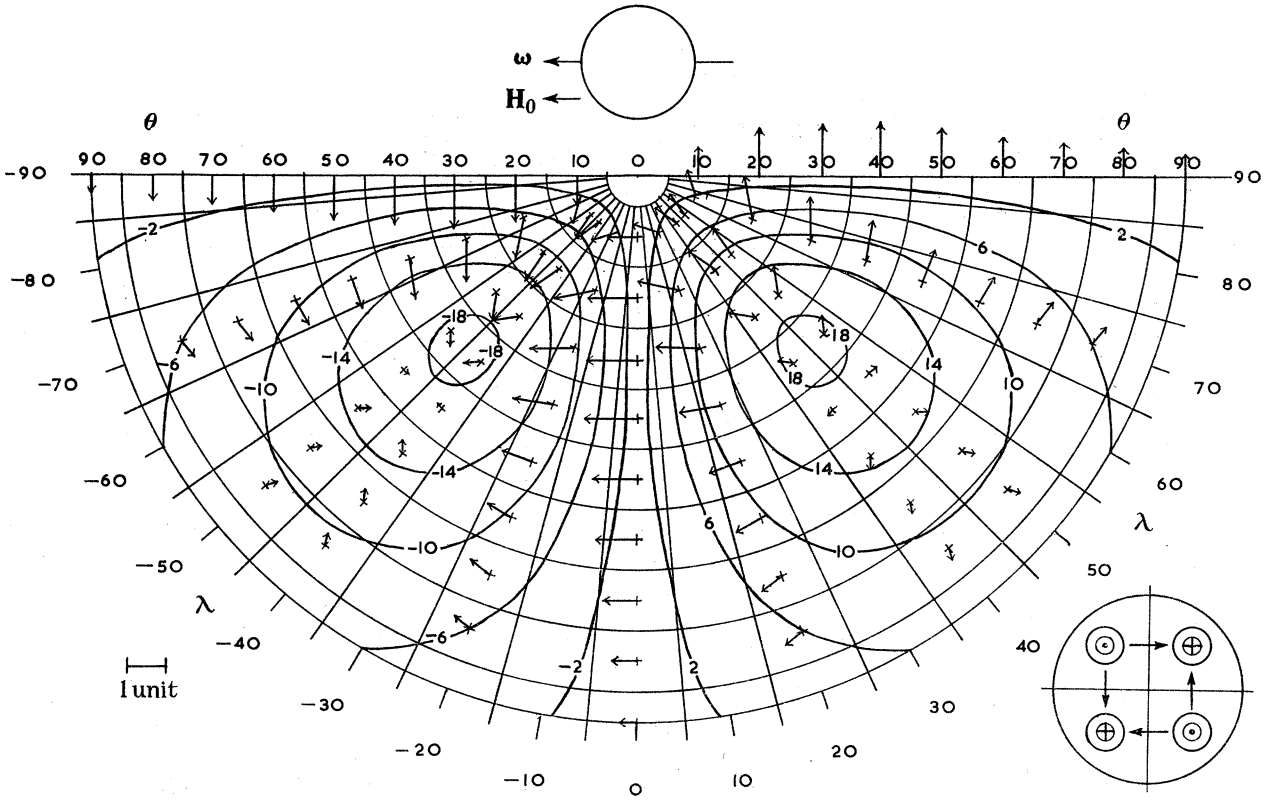

FIGURE 23. Case A, $\xi = \frac{1}{2}\pi$ ($\mathbf{H}_0$ parallel to $\boldsymbol{\omega}$, both horizontal).

Units: vertical $0{\cdot}008\alpha H_0(a/R_E)^3$,

horizontal $0{\cdot}08\alpha H_0(a/R_E)^3$.

FIGURES 23 TO 29. Charts of magnetic fields on the surface of the earth.

Figures 23 to 29 show the magnetic fields on the surface of the earth due to a spherical eddy rotating as a rigid body in the core of the earth, assumed to be rigid. The contours and arrows respectively show the behaviour of the vertical and horizontal field components. (We use the convention that the positive direction of the vertical component is upwards.) Each arrow gives the magnitude and direction of the horizontal component at the point at the arrow foot. The centre of the eddy is taken to be at a distance $L = 0{\cdot}4R_E$ from the centre of the earth, and the centre of each chart is directly above the eddy centre. The charts are computed from the formulae given in §§ 7·1, 7·2, 7·3. When the inducing field $\mathbf{H}_0$ is perpendicular to the eddy axis, the high-velocity approximation $\alpha \gg 1$ is used. The orientation of the eddy and $\mathbf{H}_0$, as seen by an observer looking downwards from the earth's surface, is indicated in each case by the sketch above the chart. Since the field patterns all show some degree of symmetry, only the region $-\frac{1}{2}\pi < \lambda < \frac{1}{2}\pi$ is shown; the schematic diagram to the lower right of each chart indicates how the chart is to be completed. The units in which the field is measured are given below each chart, together with a line showing the length of unit vector of horizontal field. The angular distance of any point on the surface of the earth from the point vertically above the eddy centre is measured by the angle θ. In the projection used, the radial distance ρ of a point from the centre of the chart is proportional to the angle θ. This projection is therefore intermediate between an equal area projection (where $\rho \propto \sin \frac{1}{2}\theta$) and a conformal projection (where $\rho \propto \tan \frac{1}{2}\theta$). Correction factors have been used so that, if the charts were made elastic and stretched over the surface of a sphere, the arrows would take up their correct directions; the arrows are however drawn to a constant scale on each chart.

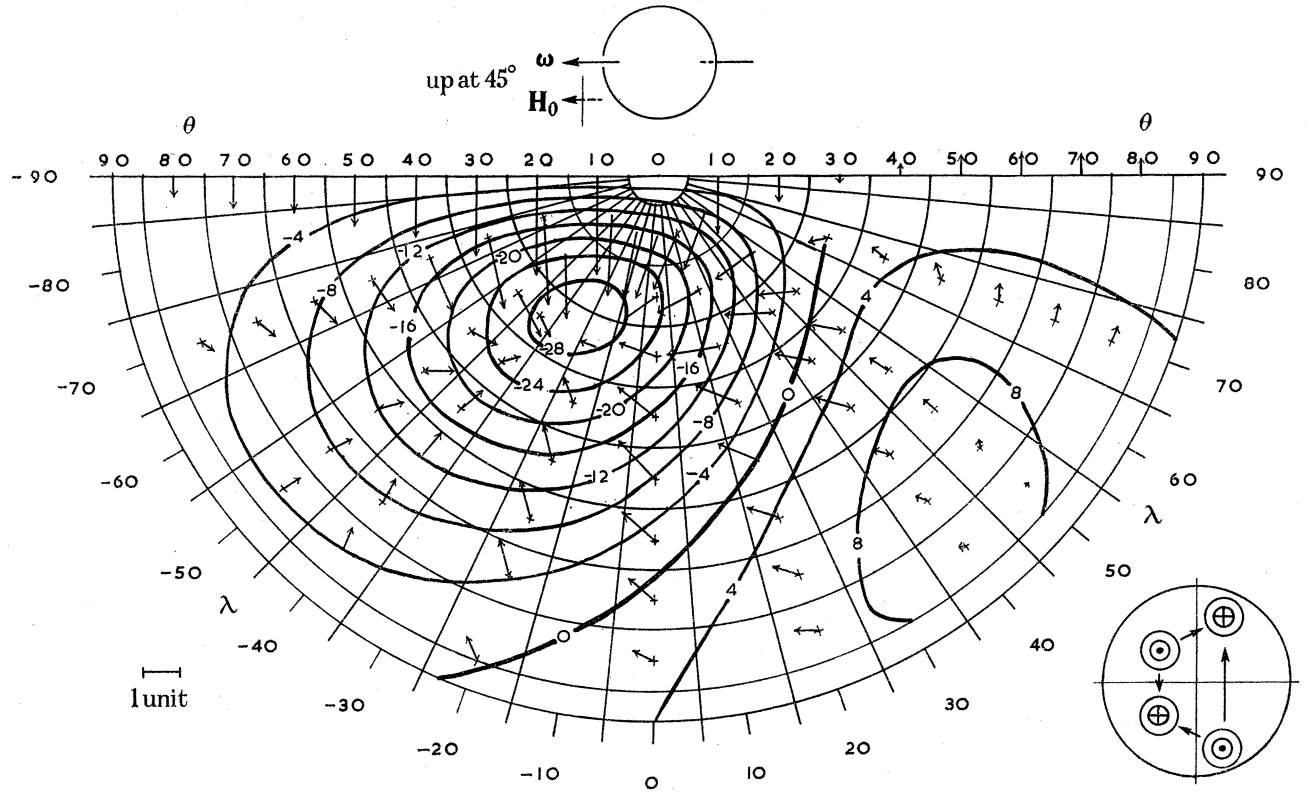

FIGURE 24. Case A, $\xi = \frac{1}{4}\pi$ ($\mathbf{H}_0$ parallel to $\boldsymbol{\omega}$, both at 45° to the horizontal).

Units: vertical $0{\cdot}0057\alpha H_0(a/R_E)^3$,

horizontal $0{\cdot}057\alpha H_0(a/R_E)^3$.

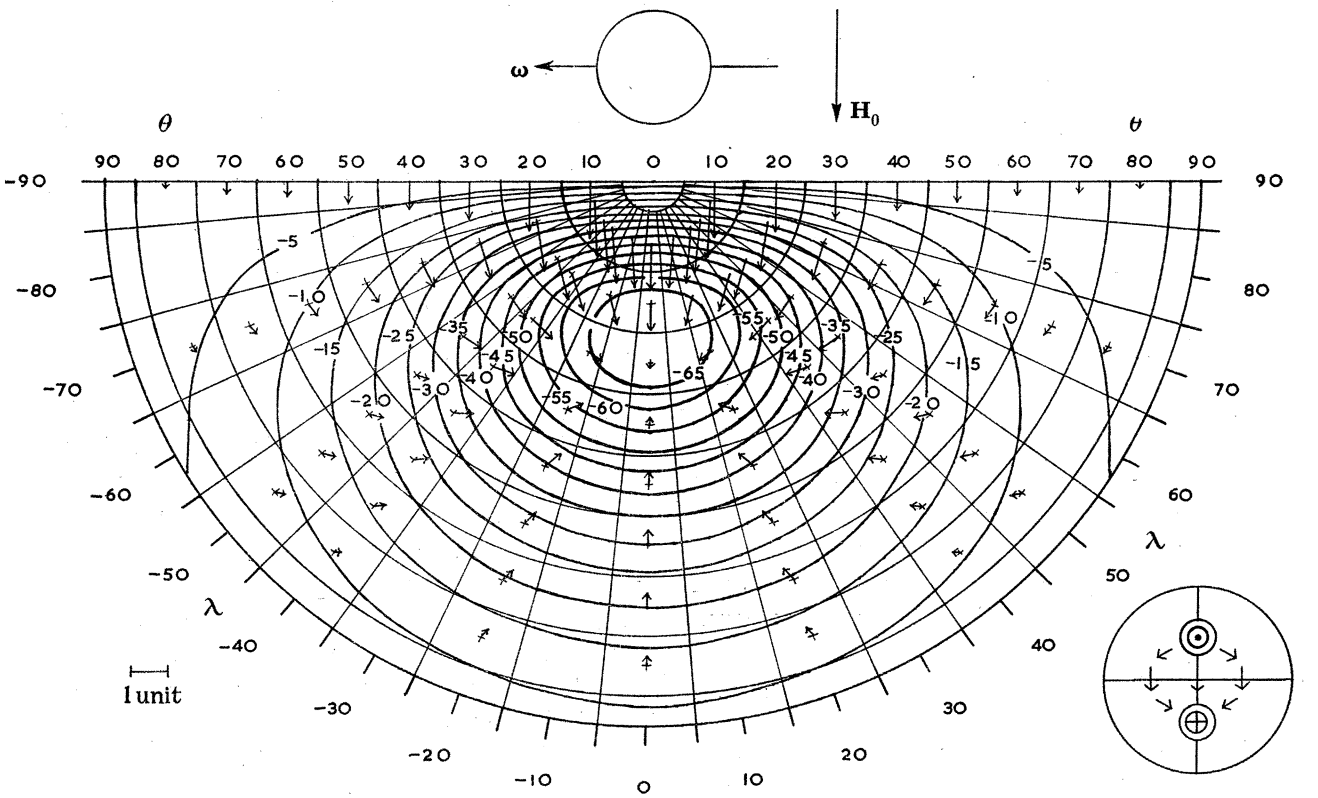

FIGURE 25. Case B, $\xi = \frac{1}{2}\pi$ ($\mathbf{H}_0$ perpendicular to $\boldsymbol{\omega}$; $\mathbf{H}_0$ horizontal, $\boldsymbol{\omega}$ horizontal).

Units: vertical $0{\cdot}05H_0(a/R_E)^3$,

horizontal $2H_0(a/R_E)^3$.

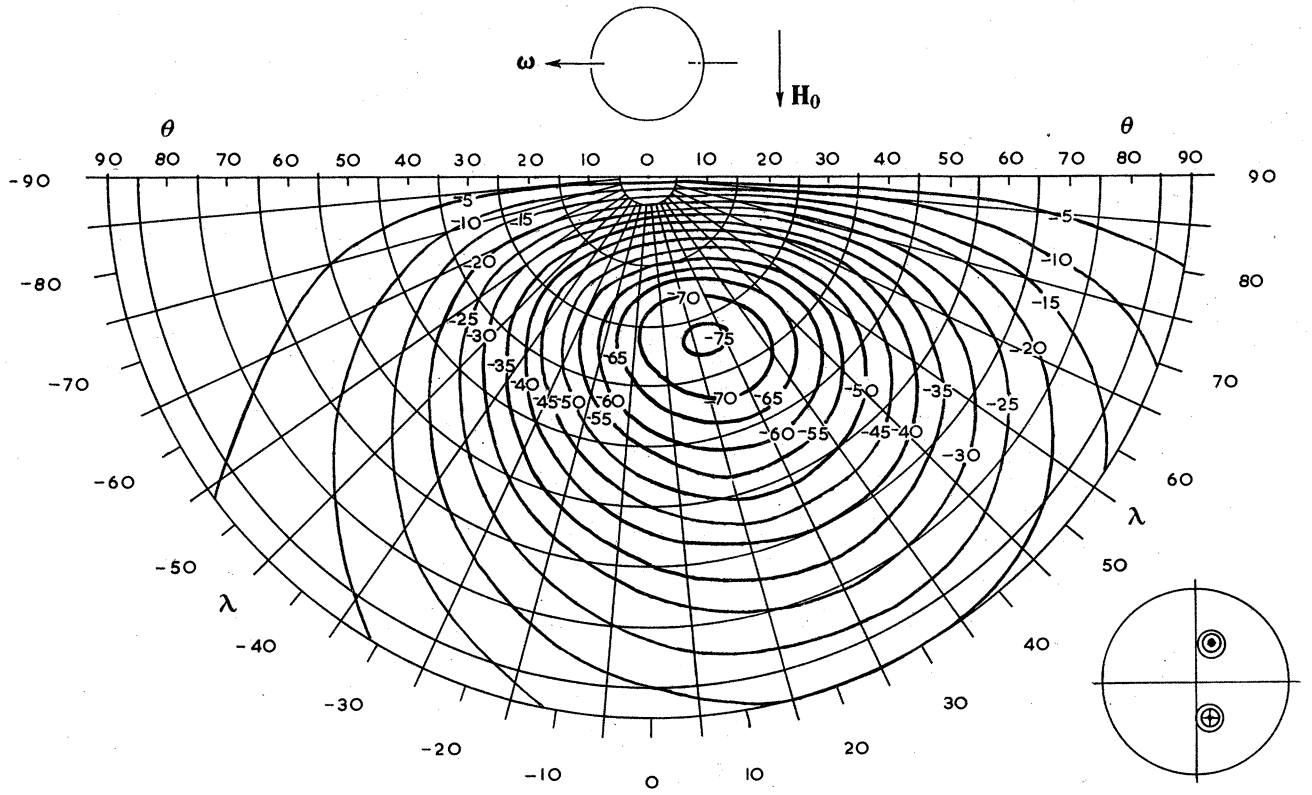

FIGURE 26. Case B, $\xi = \frac{1}{4}\pi$ ($\mathbf{H}_0$ perpendicular to $\boldsymbol{\omega}$; $\mathbf{H}_0$ horizontal, $\boldsymbol{\omega}$ at 45° to the horizontal).
Unit: vertical $0{\cdot}035 H_0(a/R_E)^3$.

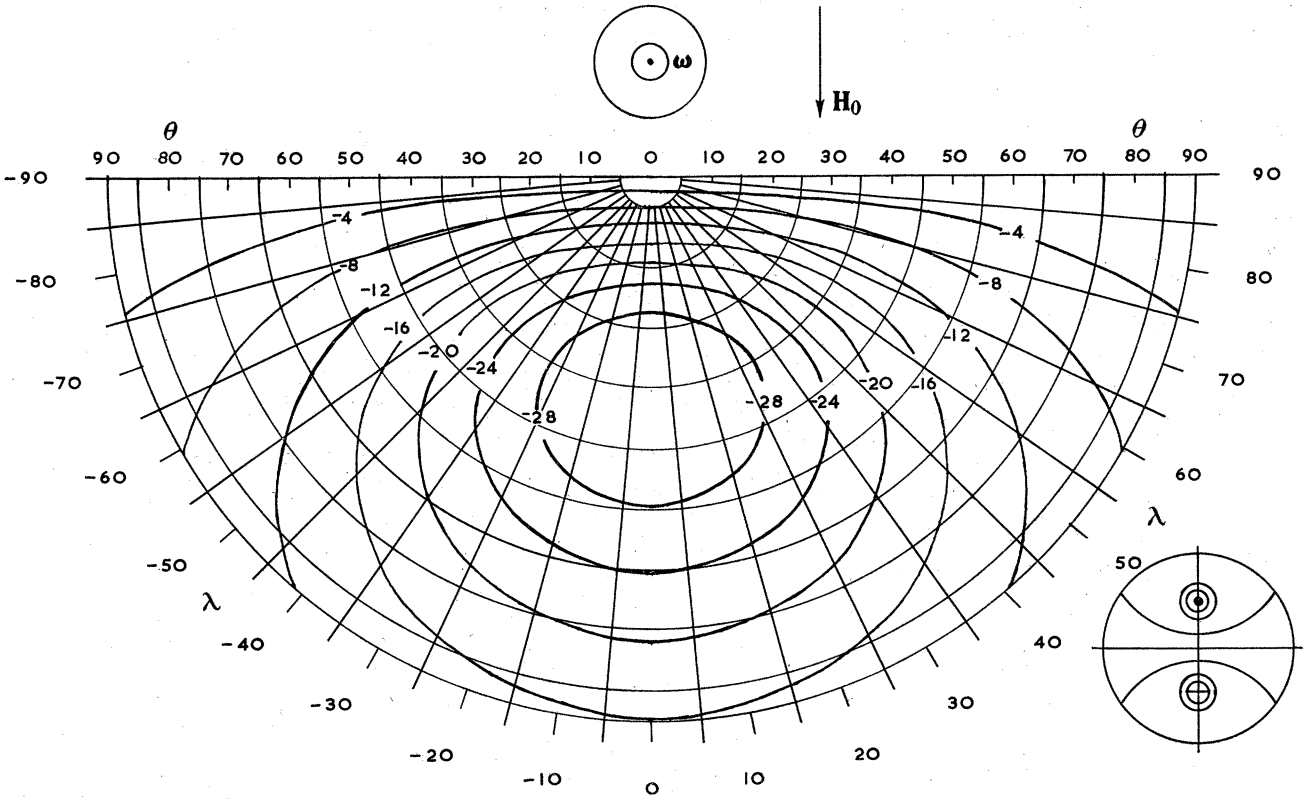

FIGURE 27. Cases B and C; $\xi = 0$ ($\mathbf{H}_0$ perpendicular to $\boldsymbol{\omega}$; $\mathbf{H}_0$ horizontal, $\boldsymbol{\omega}$ vertical).
Unit: vertical $0{\cdot}05 H_0(a/R_E)^3$.

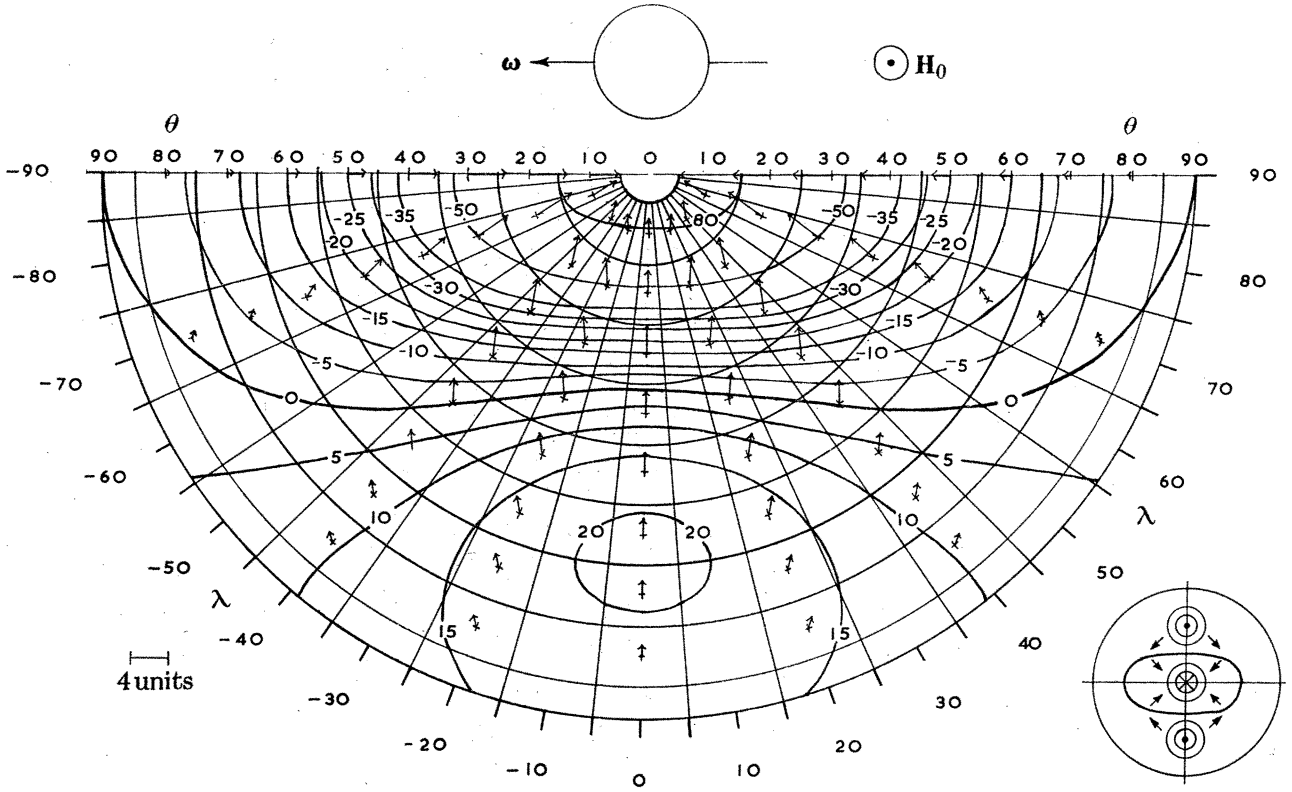

FIGURE 28.* Case C, $\xi = \frac{1}{2}\pi$ ($\mathbf{H}_0$ perpendicular to $\boldsymbol{\omega}$; $\mathbf{H}_0$ vertical, $\boldsymbol{\omega}$ horizontal).
Unit: vertical $0{\cdot}05\ H_0(a/R_E)^3$.

* *Note added in proof.* An error has been made in the computation of the horizontal field. However the vectors drawn do provide a schematic representation of the field. The contours of the vertical field are correct.

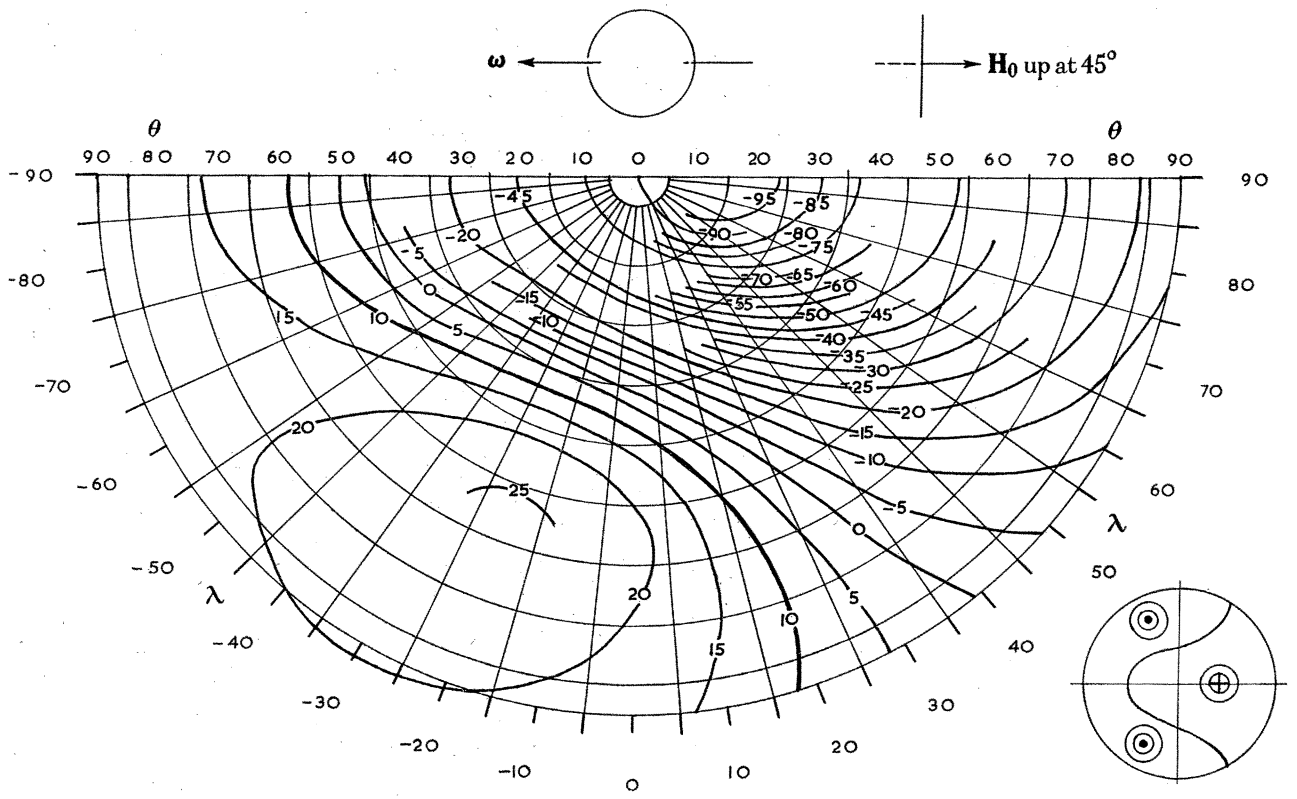

FIGURE 29. Case C, $\xi = \frac{1}{2}\pi$ ($\mathbf{H}_0$ perpendicular to $\boldsymbol{\omega}$, both at 45° to the horizontal).
Unit: vertical $0{\cdot}035\ H_0(a/R_E)^3$.

component of **h** from a point vertically above the rotator centre for a rotator with horizontal axis in an axially symmetric field $\mathbf{H}_0$ (case A, $\xi = \frac{1}{2}\pi$, figure 23). The last column in table 1 gives $(LR_E \sin^2\theta/r'^5)_{\text{max.}}$, which determines the dependence of $(\mathbf{h}.\hat{\mathbf{r}})_{\text{max.}}$ on L for case A (§ 7·1). The variation with L of spread and magnitude of the induced field is similar for cases B and C.

TABLE 1

L is the distance of the rotator centre from the centre of the earth. $\theta_{\text{max.}}$ is the angular distance of the maxima of $\mathbf{h}.\hat{\mathbf{r}}$ from the centre of the pattern. (Case A, $\xi = \frac{1}{2}\pi$.)

L	$\theta_{\text{max.}}$	$\left(\frac{LR_E \sin^2\theta}{r'^5}\right)_{\text{max.}}$
$0{\cdot}0R_E$	—	$0{\cdot}00R_E^{-3}$
0·2	62·6°	0·23
0·3	50·2°	0·42
0·4	40·6°	0·76
0·5	32·0°	1·40

The field pattern of figures 23 and 24 ($\mathbf{H}_0$ parallel to $\boldsymbol{\omega}$) can be understood from the current system of the short cylinder or sphere in infinite conducting surroundings (figure 16). The current flow is over two sets of toroidal surfaces centred on the axis of rotation. In figure 23 we see the four ends of the two (now incomplete) systems of toroids facing the boundary, so that the external field appears to emerge from four distinct sources of alternating sign spaced at 90° in λ. In figure 24 (case A, $\xi = 45°$) the whole current system has been tilted through 45° with respect to the boundary. For $\xi = 0°$ the symmetry theorem of § 6·1 predicts that there will be no external induced field.

The patterns and magnitudes of the fields shown in figures 25 to 29 ($\mathbf{H}_0$ perpendicular to $\boldsymbol{\omega}$) can also be interpreted in terms of a simple physical model. In an infinite conducting medium, the electric field and current flow outside a rotator in a transverse inducing field resemble those of a quadrupole at the centre of the rotator, the plane of the quadrupole being perpendicular to $\mathbf{H}_0$ for $\alpha \gg 1$. (Figure 10 shows the situation for $\alpha \ll 1$.) Thus there are four external current circuits, and another in the rotator. It is convenient to call the two external circuits along the axis of rotation end loops, and the other two side loops. These five loops can be considered to possess separate dipole moments, the end two being in the same direction as the central one, and the side two being in the opposite direction. We shall now assume that all these moments are equal to that of an isolated rotator, and that when the rotator is near a boundary of the conducting surround the moment of any current circuit which would try to cross the boundary is reduced accordingly.

In figure 28 we have a plan view of the five current loops. In this case the plane of the loops is perpendicular to the vertical at the origin, and the presence of all five loops is clearly shown. The four loops outside the rotator are all equally modified by the boundary, and the resultant field has the same general magnitude as the field of an isolated rotator. When the centre of the rotator is at the centre of the core, the moments of the external loops cancel and the field outside the core is exactly that of an isolated rotator (7·20).

In figures 25 to 27 the current loop system is in the vertical plane through the origin. In figure 25 the core boundary prevents the formation of one side loop, with only slight modification of the end loops, and the result is a net moment about twice that of an isolated

PHILOSOPHICAL TRANSACTIONS OF THE ROYAL SOCIETY A MATHEMATICAL, PHYSICAL & ENGINEERING SCIENCES

rotator. In figure 27 it is an end loop that has been cut off. For a plane boundary the other four would exactly cancel and there would be no external field, but with a spherical boundary the two side loops are somewhat reduced. The result is a small net dipole moment about one third that of an isolated rotator. Figure 26 is an intermediate case, both one end and one side loop being partially cut off, the net moment being about equal to that of an isolated rotator.

The case of figure 29 is intermediate between those of figures 27 and 28. The plane of the current loops is at 45° to the vertical at the origin, and most of the uppermost end loop is cut off. The two side loops and the combined field of the central and lower end loops are clearly visible.

The charts of figures 25 to 29 are given for the high-velocity approximation $\alpha \gg 1$. The same charts, with the field values multiplied by $2\alpha/15$, give the induced fields for the low-velocity approximation $\alpha \ll 1$ for applied fields perpendicular to those indicated (see §§ 7·2 and 7·3). For intermediate values of α a rough picture of the surface induced field can be obtained by using the five loop model. The magnitude and direction of the central loop dipole moment would be taken as those produced by an isolated rotator, which are given by (2·12) and in figure 9.

7·6. *Discussion*

All the results derived in §§ 7·1, 7·2 and 7·3 are approximate in that the induction effect associated with the magnetic field of the current system reflected by the boundary was neglected. However, it was shown in § 7·4 that the errors involved in this approximation are small, and none of the results discussed below will be appreciably different from those given by an exact solution.

The external induced fields derived in this section and given in the charts of § 7·5 are for spherical rotators, but the fields are not likely to be very different for other shapes of rotators. For all the squat rotator shapes considered in §§ 3, 4 and 5 (axial $\mathbf{H}_0$; transverse $\mathbf{H}_0$, $\alpha \ll 1$; transverse $\mathbf{H}_0$, $\alpha \gg 1$), the induced field h_∞ is proportional to the volume of the rotator, and the constants of proportionality are very little different for spheres, cylinders, or prolate spheroids (cf. (3·21) and (3·22), (4·10) and (4·12), (5·42) and (5·43)). Moreover, the results quoted show that the leading term in an expansion of $\mathbf{h}_\infty$ in powers of $1/r$ always has the same form as for a spherical rotator. Thus it is reasonable to assume that, for all values of α and directions of $\mathbf{H}_0$, little error will be made by replacing any axially symmetric squat rotator by a sphere of the same volume.

An interesting and somewhat unexpected feature of the results of §§ 7·1, 7·2 and 7·3, for both spherical and plane boundaries of the conducting medium, is their lack of dependence on the position of this boundary. This is shown by the absence of D, the depth of the rotator beneath the boundary, in these results. Thus, at any given point outside the conductor, the induced magnetic field is unchanged by any change in radius of a spherical boundary or any normal displacement of a plane boundary. (This result does not hold if there is any time variation; see §§ 6·5 and 6·6.)

Axial applied field

The results of § 7·1 bring out the important fact that for axial $\mathbf{H}_0$ and an asymmetrical boundary the induced field outside the conductor increases without limit as the angular

velocity is increased. The experimental results given in § 2·6 confirm this result, and they also confirm the absence of external induced field with a symmetrical boundary.

Transverse applied field

The expressions (7·12) and (7·17) give the potential of the external induced field for the high-velocity approximation $\alpha \gg 1$. A comparison of (4·10) and (5·42) shows that the same expressions, multiplied by $2\alpha/15$, give the induced fields for the low-velocity approximation $\alpha \ll 1$ for applied fields perpendicular to the ones given. For intermediate values of α solutions could be obtained by applying the method of § 6 to the solutions for infinite conducting medium given by Bullard. (Bullard 1949*b*, pp. 422–3; put $n = m = 1, a \to \infty$.) If only a rough picture of the surface field were required it would be much simpler, however, to use the five-loop model as described in § 7·5.

With a rotator in a surrounding conductor, as with an isolated rotator, the field everywhere tends to a finite limit as the angular velocity is increased, though the magnitudes in the two cases are somewhat different.

In the most favourable orientation the magnitude of the external induced field is increased by a factor of two by the current outside the rotator, and in the least favourable case it is reduced to one-third of its magnitude for an isolated rotator. Thus for the purpose of the order of magnitude calculations of § 8 it is sufficiently accurate to use the isolated rotator induced fields. The variation of field magnitude with velocity will also be similar to that of an isolated rotator.

7·7. *Summary of results of part D*

We have calculated the induced magnetic field due to a rigid conducting sphere rotating at constant angular velocity in a uniform applied magnetic field $\mathbf{H}_0$, and surrounded by, and in perfect electrical contact with, a rigid conducting shell. The results form an extension of those of Bullard (1949*b*) which were for a rotating sphere either isolated or surrounded by a concentric spherical shell. The spread of the current from the rotating sphere to the shell, and the fact that the rotator and shell are not concentric, profoundly affect the induced fields. In particular, there is an induced field outside the shell even when the applied field has rotational symmetry about the axis of rotation, and this induced field increases without limit with the angular velocity.

For an axial applied field, the single expression (7·2) gives the induced field outside the conductor for all orientations and angular velocities of the rotator. For transverse applied field, solutions are given only for two simple geometrical configurations, (7·12) and (7·17), and for the limit $\alpha \gg 1$. The induced fields for all other configurations can be obtained by a suitable linear combination of these two.

Some typical patterns are drawn in figures 23 to 29 of the induced field on a particular spherical surface outside and concentric with the conducting spherical shell containing the rotator. The rotator is not concentric with its shell. The dimensions are chosen to represent the induced field at the surface of the earth due to an eddy in the core.

PART E. THE EDDY HYPOTHESIS

After the preparatory work of the last three parts, we can now discuss the eddy hypothesis in more detail. We shall start by summarizing the essential facts which enter into the

argument, and stating the values of the relevant physical parameters. After that, in § 8, we show that an eddy spinning in a magnetic field of given magnitude must have a radius exceeding a certain minimum if it is to account for the observed magnitude of a focus of the non-dipole field (we shall need this result when we come to consider the implications of the electromagnetic skin effect for the eddy hypothesis). The application of our results to the eddy hypothesis is made in § 9, where we summarize the paper and draw our conclusions. Throughout the discussion we shall assume the applied magnetic field to be given, and shall not inquire into its origin.

The magnetic field at the earth's surface

The geomagnetic field at the surface of the earth is of order of magnitude 0·3 to 0·6 G and is predominantly of internal origin and of dipole form. The non-dipole component is of order of magnitude 0·1 to 0·15 G (Vestine, Laporte, Lange & Scott 1947), and is concentrated into about ten so-called 'foci' of roughly continental extent. There is a secular variation amounting to about 1 to $1{\cdot}5\times10^{-3}$ G/year. It is mainly due to the variation of the non-dipole field and shows the same sort of regional concentration. Long-period observations show that the geomagnetic field has a continuous frequency spectrum extending from periods of less than a hundred to periods of a few thousand years (Hughes & Moore, reported by Runcorn 1955). The magnitude of the corresponding secular variation (i.e. $\mathrm{d}\mathbf{H}/\mathrm{d}t$) has a maximum at about 200 years. The discussion of the origin of the secular variation is complicated by the fact that the whole dipole field drifts westward by on the average about 0·2° per year (Bullard, Freedman, Gellman & Nixon 1950) with respect to the earth's mantle. Therefore a part of the secular variation at a given point is due to the drift of the non-dipole field. But the major part of the secular variation would be observed also in a frame of reference drifting at the westward drift velocity with respect to the earth's mantle; that this is so can be seen from the charts given by Vestine *et al.* (1947), where the individual foci of the non-dipole can be followed over the first half of this century and are clearly seen to vary in magnitude during this period.

The magnetic field in the earth's core

It turns out that this is the most important parameter in the discussion of the eddy mechanism. If one extrapolates the dipole field downwards from the earth's surface, one gets a magnitude of about 4 G at the surface of the core. Within the core there may well be much larger toroidal magnetic fields which do not penetrate to any great extent into the mantle. From their dynamo theory, Bullard & Gellman (1954) estimate a maximum toroidal field of about 400 G inside the core; this field would be very small at the core surface. The explanation of the westward drift given by Bullard *et al.* (1950) leads to a maximum toroidal field inside the core of 150 G. We shall consider fields up to about 500 G.

Other parameters

The only direct estimate of the velocities of motions in the earth's core comes from the westward drift and implies relative velocities of 0·02 to 0·06 cm s^{-1} between the mantle and upper part of the core (Bullard *et al.* 1950). Bullard & Gellman (1954) estimate the maximum equilibrium velocity in a self-exciting dynamo to be 0·01 to 0·04 cm s^{-1}.

The radius of the earth is $R_E = 6400$ km, and that of the core is $R_C = 3500$ km. The density of the core material will be taken to be $\rho = 10\,\mathrm{g\,cm^{-3}}$ (Bullen 1947), the viscosity $\eta = 10^{-2}$ c.g.s. (after Bullard 1949 *a*).

We will take the electrical conductivity of the core $\sigma = 3\times 10^{-6}$ e.m.u. after Bullard (1949 *a*). The conductivity of the lower part of the mantle is probably 10^{-9} to 10^{-7} e.m.u. (Runcorn 1955); therefore for our purposes the mantle may be treated as an insulator. We assume a permeability and dielectric constant of unity throughout.

8. The minimum radius of an eddy

8·1. *Magnitude of the induced field*

We start by collecting a number of formulae for the magnitude of the induced field due to induction in eddies. We approximate each eddy by a rigid conductor rotating at constant angular velocity, and treat the rest of the core as a rigid stationary conductor. We consider only spherical and long thin cylindrical eddies. (We saw in § 7·6 that a spherical rotator is a good approximation for any squat rotator of the same volume.) The applied field $\mathbf{H}_0$ is assumed to be uniform throughout the eddy. Time variation is neglected.

Consider a spherical eddy spinning about a horizontal axis in the earth's core ($\xi = \frac{1}{2}\pi$ in the notation of § 7). If $\mathbf{H}_0$ is parallel to the axis of rotation we have (§ 7·1)

$$(h_r)_{\max.} = \tfrac{1}{5}LR_E\left(\frac{\sin^2\theta\sin 2\lambda}{r'^5}\right)_{\max.} H_0 a^3\alpha$$

$$= 0{\cdot}96R_E^{-3}\sigma v a^4 H_0, \qquad (8{\cdot}1)$$

where $(h_r)_{\max.}$ is the maximum radial (vertical) component of the induced field $\mathbf{h}$ at the earth's surface, v is the peripheral velocity of the eddy, σ its conductivity and a is its radius. We have taken L, the distance of the centre of the eddy from the centre of the core, to be $0{\cdot}4R_E$. Variation of L would change the result (8·1), but (see table 1), unless the centre of the sphere is very close to the centre of the earth, (8·1) is correct to within a factor two. Again, even if the axis is inclined to the horizontal, (8·1) gives the right order of magnitude unless $\xi \simeq 0$ (axis vertical), when $\mathbf{h}$ is very small.

For one end of a cylinder of radius a in a magnetic field $\mathbf{H}_0$ parallel to the axis, we have from (7·10)

$$(h_r)_{\max.} = 0{\cdot}2\frac{L\sin\xi}{R_E^3} H_0 a^2\alpha$$

$$\simeq 0{\cdot}5R_E^{-2}\sigma v a^3 H_0, \qquad (8{\cdot}2)$$

unless $\xi \simeq 0$. The estimate (8·2) would be useful if there were a long cylindrical eddy of which one end is near the core surface, the effect of the other end being screened from an external observer by the skin effect.

If $\mathbf{H}_0$ at the sphere is perpendicular to the axis of rotation, we can estimate the order of magnitude of $\mathbf{h}$ at the earth's surface by treating the sphere as an isolated rotator (§ 7·6). We find, for $\alpha = 2\pi\sigma a v \gg 1$,

$$h_{\max.} \sim \tfrac{1}{2}H_0 a^3/r'^3, \qquad (8{\cdot}3)$$

where r' is the distance from the centre of the sphere to the surface of the earth. For $\alpha \ll 1$ we have

$$h_{\max.} \sim (2\alpha/15)\, \tfrac{1}{2} H_0 a^3/r'^3. \qquad (8{\cdot}4)$$

As we have seen in § 8·4, formula (8·3) can become invalid for large α because the currents reflected from the core boundary can sometimes produce a magnetic field parallel to the rotator axis. We can, however, ignore this possibility in a discussion of the order of magnitude of the induced field, because the field due to the reflected currents does not exceed $\frac{1}{8} H_0$; therefore a bigger axial inducing field is obtained simply by alining the axis of rotation with $\mathbf{H}_0$.

A long thin cylindrical eddy with a transverse $\mathbf{H}_0$ can also be approximated by the similar isolated rotator. If $\alpha \gg 1$ this behaves as a line of dipoles of line density $\frac{1}{2} H_0 a^2$ per unit length. (For $\alpha \ll 1$ the induced moment is smaller than this.) The induced field on the surface of the earth above the centre of an eddy of length $2u$ is then

$$h_{\max.} \simeq \frac{H_0 a^2 u}{r'^2 (r'^2 + u^2)^{\frac{1}{2}}}$$

for a horizontal eddy. (The field for a vertical eddy is less than this.) In the core, at the most $u \sim r'$, so this case is not appreciably different from that of a squat eddy in transverse $\mathbf{H}_0$, and will not be discussed further.

A comparison of (8·1) and (8·3) shows that for a given size of squat eddy an axial $\mathbf{H}_0$ will lead to a greater $h_{\max.}$ than would a transverse $\mathbf{H}_0$ if $\alpha \gtrsim 15$ ($r' \simeq (3{\cdot}5/6{\cdot}4)\, R_E$). For given velocity the long thin eddy in an axial $\mathbf{H}_0$ produces greater induced fields than the squat eddy for all feasible values of radius a.

We see from (8·3) that for a given transverse $\mathbf{H}_0$ there is an upper limit to the induced field that can be produced from an eddy of given radius. Conversely, to produce a given magnitude of induced field from a given transverse $\mathbf{H}_0$ there is a lower limit to the eddy radius. From (8·1) we see that for axial $\mathbf{H}_0$ there are no similar limits; the magnitude of the induced field increases indefinitely as the velocity is increased.

8·2. *Power consumption*

We now discuss the power consumption of the eddies. We show that if the available power is limited, then a given induced field can be produced only if the eddy size exceeds a certain minimum for *axial* as well as transverse $\mathbf{H}_0$. We determine this minimum size by comparing the power consumption of an eddy with that of the core as a whole.

The energy losses will be due to Joule heating and viscous friction. It has been shown by Bullard (1948) that the forces due to viscous friction in laminar flow are small compared with the electromagnetic forces, so that the former may be neglected. However, the Reynolds number $(av\rho/\eta)$ of the eddy motions is likely to be large, $av\rho/\eta = 3 \times 10^8$ for $\alpha = 5$. Therefore turbulence must be taken into account.

We now estimate the power consumption due to turbulence. We neglect the effect of the magnetic field on the turbulence, but since electromagnetic induction tends to inhibit turbulence our result for the turbulent power consumption will probably be an upper limit. It has been suggested by H. B. Squire* that the effect of turbulence on a vortex in air can be

* Private communication. The use of this comparison for the estimate of the effects of turbulence was suggested to us by Professor M. J. Lighthill, F.R.S.

represented by a 'turbulent kinematic viscosity' ν_T of the form $\nu_T = bK$, where K is the circulation $\oint \mathbf{v}.d\mathbf{s}$ around a closed loop moving with the eddy, and b is a non-dimensional constant. (By Kelvin's theorem, K is a constant of the motion when the Reynolds number is large.) Professor Squire informs us that according to wind-tunnel and flight-test experiments the value of b is probably within a factor 5 of 5×10^{-4}. For an eddy of radius a, we have $K\sim2\pi av$, where v is a typical macroscopic (non-turbulent) velocity. We estimate the power loss as for viscous dissipation in laminar flow, where the power loss per unit mass is $\nu[(\nabla v_x)^2+(\nabla v_y)^2+(\nabla v_z)^2]$ for an incompressible fluid (ν is the kinematic viscosity; v_x, v_y, v_z are the Cartesian components of velocity). For an eddy, the mean turbulent power loss per unit mass is therefore of the order of magnitude

$$b2\pi av(v/a)^2\sim3\times10^{-3}v^3/a. \tag{8·5}$$

(For laminar flow the power loss per unit mass would be $\sim(\eta/\rho)\,(v/a)^3$. For $a=50$ km, $v=10^{-1}$ cm s^{-1}, this is only 3×10^{-6} of that given by (8·5).)

Eddy

The power dissipation by Joule heating in an eddy can be estimated as follows. The electromagnetic couples acting on a spherical rotator in a conducting medium of infinite extent, and in a uniform applied magnetic field $\mathbf{H}_0$, are (Bullard 1949*b*)

$$(\mathbf{H}_0\wedge\boldsymbol{\omega}=0)\quad \Gamma_{\parallel}=\tfrac{4}{75}H_0^2a^3\alpha, \tag{8·6}$$

$$(\mathbf{H}_0.\boldsymbol{\omega}=0)\quad \Gamma_{\perp}=\tfrac{8}{75}H_0^2a^3\alpha \quad \text{for } \alpha\ll1, \tag{8·7}$$

$$=1{\cdot}2H_0^2a^3\alpha^{-\frac{1}{2}} \quad \text{for } \alpha\gg1. \tag{8·8}$$

The corresponding power consumptions $\epsilon_{J\parallel}$ and $\epsilon_{J\perp}$ are

$$(\mathbf{H}_0\wedge\boldsymbol{\omega}=0)\quad \epsilon_{J\parallel}=\Gamma_{\parallel}\omega=0{\cdot}34H_0^2a^3v^2\sigma; \tag{8·9}$$

$$(\mathbf{H}_0.\boldsymbol{\omega}=0)\quad \epsilon_{J\perp}=\Gamma_{\perp}\omega=0{\cdot}68H_0^2a^3v^2\sigma \quad \text{for } \alpha\ll1, \tag{8·10}$$

$$=0{\cdot}48H_0^2(a^3v/\sigma)^{\frac{1}{2}} \text{ for } \alpha\gg1. \tag{8·11}$$

For one end of a long cylinder in axial $\mathbf{H}_0$ we have from (3·26)

$$\Gamma_{\parallel\text{cyl.}}\simeq\tfrac{1}{8}H_0^2a^3\alpha, \tag{8·12}$$

and the power consumption is

$$\epsilon_{J\parallel\text{cyl.}}=\Gamma_{\parallel\text{cyl.}}\omega\simeq0{\cdot}79H_0^2a^3v^2\sigma. \tag{8·13}$$

This is very similar to that for a squat eddy in axial $\mathbf{H}_0$.

To estimate the effect of turbulence, we take the typical velocity to be the peripheral velocity v. The energy dissipation ϵ_T from turbulence is then

$$\epsilon_T\sim b(4\pi a^3/3)\,\rho(v^3/a)\sim2\times10^{-2}v^3a^2. \tag{8·14}$$

If we put $\sigma=3\times10^{-6}$ e.m.u. in (8·9), (8·10) and (8·11), and compare the results with (8·14), then we see that for our purposes (say 1000 km$>a>$10 km, $v<0{\cdot}1$ cm s^{-1}, $H_0>4$ G) the turbulent power loss is negligible as compared with Joule heating.

Core

We estimate the power dissipation κ_J by Joule heating in the whole core by assuming the mean magnetic field $\mathbf{H}_C$ in the core to be entirely due to electric currents. Then we have

$$\kappa_J = \int_{\text{core}} \mathrm{d}V\,\mathbf{J}.\mathbf{E} = \frac{1}{16\pi^2\sigma}\int_{\text{core}} \mathrm{d}V\,(\boldsymbol{\nabla}\wedge\mathbf{H})^2$$
$$\sim \frac{1}{16\pi^2\sigma}\left(\frac{2\pi}{2R_C}H_C\right)^2 \tfrac{4}{3}\pi R_C^3 \simeq 3\times 10^{13} H_C^2. \tag{8·15}$$

(Bullard (1949*a*) and Elsasser (1950) obtain similar values by different methods.)

To estimate the turbulent power loss κ_T for the whole core, we assume that there is a number of fairly large vortices (due, perhaps, to convection) with a radius of $\sim\frac{1}{2}R_C$, which lose some of their energy by turbulence. We have then from (8·5)

$$\kappa_T \sim \tfrac{4}{3}\pi R_C^3 \rho\, 3\times 10^{-3}\left(\frac{v_C^3}{\frac{1}{2}R_C}\right)$$
$$\simeq 3\times 10^{16} v_C^3, \tag{8·16}$$

where v_C is a typical core velocity.

The ratio κ_J/κ_T is, from (8·15) and (8·16),

$$\frac{\kappa_J}{\kappa_T} \sim 10^{-3}\frac{H_C^2}{v_C^3}. \tag{8·17}$$

Putting $v_C = 0{\cdot}1\ \mathrm{cm\,s^{-1}}$, we have $\kappa_J/\kappa_T \sim H_C^2$. Hence if we have $H_C \gtrsim 4\ \mathrm{G}$, then $\kappa_J \gg \kappa_T$, i.e. for the whole core the energy dissipation by turbulence is much less than that by Joule heating.

In the following discussion we neglect turbulent power dissipation, and omit the subscript J from ϵ and κ.

Minimum radius

We now show that the formulae derived above imply that, if the power consumption is limited, then the eddy radius must exceed a minimum value if h and H_0 are fixed. We set a limit on the eddy power consumption by assuming that a single eddy does not consume more power than the mechanism responsible for producing the main field throughout the core.

For a squat eddy in axial $\mathbf{H}_0$ it follows from (8·9) and (8·15) that

$$\left(\frac{\epsilon}{\kappa}\right)_{\parallel} \simeq 1{\cdot}3a^3(\sigma v)^2\frac{1}{R_C}\left(\frac{H_0}{H_C}\right)^2. \tag{8·18}$$

For one end of a long cylinder in axial $\mathbf{H}_0$ we have from (8·13) and (8·15)

$$\left(\frac{\epsilon}{\kappa}\right)_{\text{cyl.}\parallel} \simeq 3{\cdot}0a^3(\sigma v)^2\frac{1}{R_C}\left(\frac{H_0}{H_C}\right)^2. \tag{8·19}$$

In § 8·1 we gave formulae for the induced field $\mathbf{h}$ obtainable by the various eddy mechanisms from an axial applied field $\mathbf{H}_0$. If we combine these equations with those for power consumption given above, and assume that

$$\left(\frac{\epsilon}{\kappa}\right) \leqslant \xi < 1, \tag{8·20}$$

we find that the factor (σv) can be eliminated, and we obtain the following inequalities:

squat rotator
$$a \geqslant 1{\cdot}2\xi^{-\frac{1}{5}} R_E \left(\frac{h}{H_C}\right)^{\frac{2}{5}}; \tag{8·21}$$

one end of a long cylinder
$$a \geqslant 2{\cdot}0\xi^{-\frac{1}{3}} R_E \left(\frac{h}{H_C}\right)^{\frac{2}{3}}. \tag{8·22}$$

For transverse $\mathbf{H}_0$, because of the saturation at high velocities, we can obtain a limit for a from (8·3). This gives
$$a \gtrsim 0{\cdot}69 R_E \left(\frac{h}{H_0}\right)^{\frac{1}{3}}. \tag{8·23}$$

(The power limitation only gives an upper limit to the velocity and does not affect the inequality for a.)

It is important to note that in (8·21) and (8·22) it is the average field H_C throughout the *core* which appears; in (8·23) it is the average field H_0 throughout the *eddy*.

The dependence of (8·21) and (8·22) upon ξ, the assumed maximum value of the ratio between eddy power and core power, is very weak. In the following discussion we will assume $\xi \simeq 1$. It is important to note that the equations (8·21), (8·22) and (8·23) for the minimum values of eddy radii do not depend on any property of the core material, e.g. conductivity or viscosity, which is subject to large error.

9. Summary and conclusion

In this paper we set out to investigate the eddy hypothesis as a possible explanation of the non-dipole part and the secular variation of the earth's magnetic field. We have considered a model in which a rigid conductor with a sharp boundary (the eddy) rotates steadily within a rigid stationary conductor (the earth's core) with which it is in electrical contact. The eddy lies in a constant magnetic field which can, but need not be, uniform. (We have also gone some way to look into the effects of an angular velocity varying with time, and of diffuse rather than sharp boundaries of the rotators.) We have made an experiment with a scale model (part B), and a theoretical investigation in which we discussed first an eddy within a surrounding conductor of infinite extent (part C), and then within a finite conductor (part D). The theoretical work led up to a set of charts (§ 7) giving the induced magnetic field at the earth's surface predicted by the model for an eddy near the surface of the earth's core. (These charts have already been discussed at the end of § 7.)

With an understanding of induction in an eddy in a finite shell, we can now try to see whether the eddy hypothesis can account for the magnitude and pattern of the non-dipole field and the secular variation. We cannot of course make any attempt to account for the origin of time dependence manifested in the secular variation because there is no detailed dynamical theory of the eddy motions available. All we can do here is to use the observed time variation to impose limitations on the theory.

We saw in the preceding section that if the eddy hypothesis is to account for the magnitude of the non-dipole field, then for a given mean value of the magnetic field in the earth's core (for the case of axial induction) or mean value of the applied magnetic field over the eddy (for transverse induction), there is a minimum value for the eddy radius which decreases as the specified magnetic field increases. Some typical lower limits on the radius are given in

PHILOSOPHICAL TRANSACTIONS OF THE ROYAL SOCIETY A MATHEMATICAL, PHYSICAL & ENGINEERING SCIENCES

table 2 on the assumption that the eddies are to give an induced field of 0·1 G at the earth's surface, i.e. the magnitude of a typical non-dipole field focus. (We saw in § 7·6 that a spherical eddy is a good approximation for any squat eddy. The results quoted for one end of a long cylinder would apply to axial induction in a long cylinder when the effect of one end is hidden by the skin effect.) Since the radius of the earth's core is 3500 km, the figures in table 2 show that if the only limit on the size of an eddy is set by that of the core, then the eddy hypothesis can account for the observed magnitude of the non-dipole field even if the main field in the core is no bigger than 4 G, the value one gets by extrapolating the dipole field from the earth's surface to the surface of the core. If the main field in the core is as large as the 400 G estimated by Bullard & Gellman (1954) from the dynamo theory, then an eddy radius of at most a few hundred kilometres would be sufficient, provided, of course, that the velocity is large enough.

TABLE 2

$\mathbf{H}_C$ (mean field throughout the core, for axial induction)	eddy radius a (km)		
$\mathbf{H}_0$ (mean field over the eddy for transverse induction) (G)	spherical eddy		one end of a long cylinder
	transverse $\mathbf{H}_0$	axial $\mathbf{H}_0$	axial $\mathbf{H}_0$
4	1290	1700	1100
20	760	930	380
100	440	490	130
500	260	260	44

However, if the core outside the eddy behaves like a rigid body, as we have assumed in constructing our modification of Bullard's eddy model, and if also there is time-dependence, then our results are only valid for an eddy smaller than a skin depth. The argument of § 4·4 and the remarks following equations (6·42) and (6·55) permit us to treat as steady a rotator lying within a skin depth from the core surface. In any case the induced field from an eddy will be attenuated by the skin effect. Therefore we shall assume that an eddy capable of accounting for the secular variation must lie within a skin depth from the surface of the core, the relevant period being taken from the observed behaviour of the secular variation. Periods of 200 years certainly appear in the Fourier spectrum of the secular variation; taking $\sigma = 3 \times 10^{-6}$ e.m.u., we get a skin depth $d = (\tau/4\pi^2\sigma)^{\frac{1}{2}} = 70$ km, and with it an upper limit for the acceptable radius. We see from table 2 that a sphere will not do: unless the main field in the core of the earth is to be unreasonably large, it is impossible to squeeze into a skin depth a spherical eddy capable of giving a sufficiently large induced field; for transverse induction the reason is the high-velocity saturation effect, and for axial induction it is that too much power would be required. The only mechanism that does pass the skin-depth test for a reasonable magnitude of the main field is the single-ended cylinder in a main field parallel to its axis. (There would have to be a finite cylinder with one end near the surface of the core, the induced field of the other end being screened from observation by the skin effect. This mechanism is much more efficient than a squat eddy because in the latter the magnetic fields due to the current systems emerging from the two ends interfere destructively.) But we see from (8·2) that if a single-ended cylinder is to provide an induced field with a maximum value of 0·1 G at the earth's surface, then for $\sigma = 3 \times 10^{-6}$ e.m.u. and

a radius $a = 44$ km, we must have $vH_0 = 300\,\mathrm{G\,cm\,s^{-1}}$, where v is the peripheral velocity, and H_0 the main field at the end of the cylinder, i.e. at the core surface. Thus if H_0 had its dipole field value of 4 G, we would need the altogether unreasonably high velocity of $80\,\mathrm{cm\,s^{-1}}$. Even with $H_0 = 500$ G we need $0{\cdot}7\,\mathrm{cm\,s^{-1}}$, still unreasonably high.

It therefore appears that if the skin-depth mechanism operates, then the eddy hypothesis must fail. This is the conclusion from Bullard's original discussion (Bullard 1948), on the basis of the model of the isolated eddy, and we see that our attempt to construct a more realistic model of an eddy has met with no more success.

It remains to see whether there is any possible way out of the difficulty by constructing a yet more realistic model. We have treated an eddy rotating in a rigid core of the earth. The obvious thing to do is to take into account the motion of the core material outside the eddy under the influence of the electromagnetic forces. Although a more detailed investigation would be required for a proper understanding, there is no reason for believing that the skin-depth mechanism operates in a fluid conductor in the same way as it does in a rigid one. The basis of the skin-depth mechanism in the theory of the eddy hypothesis is that currents are induced by the variable magnetic field spreading out from an eddy starting up, and these currents themselves have a magnetic field which cancels that spreading from the eddy. In a fluid conductor, the electromagnetic forces will move the fluid in such a way as to reduce the induced currents, and therefore so as to facilitate the spread of the magnetic field. Roberts (1955) has demonstrated how effective this mechanism can be; for example, in a uniform magnetic field $H_0 = 4$ G, with a matter density of $10\,\mathrm{g\,cm^{-3}}$, a period of 200 years, and $\sigma = 3 \times 10^{-6}$ e.m.u., there exists a plane magneto-hydrodynamic wave whose amplitude falls by a factor e in a distance of 4×10^7 km. There is therefore no reason why the large radii which the eddy model requires should be ruled out by the skin effect.

The assumption of a sharp eddy boundary which we have made is also unrealistic. As we have seen at the end of § 5, it is possible with a rotator with a diffuse boundary in an applied magnetic field perpendicular to the axis of rotation to produce induced fields much larger than those possible for a sharp boundary. A magneto-hydrodynamic wave would seem to offer a means of transporting them away from the eddy.

Because the only way in which the eddy hypothesis can work involves fluid motion of the material around an eddy, and because such motions would necessarily lead to distortion of the induced magnetic field, we have not attempted any detailed comparison of our computed charts with the observed geomagnetic non-dipole field. Nevertheless, it would be surprising if the fluid motion destroyed such qualitative properties of the induced magnetic field as its wide angular spread at the earth's surface and the fact that the induced field from a single eddy can have as many as four separate foci of vertical field. The separation of these foci is of the same order as that observed (according to table 1 the angular spacing of the foci can be of the order of 80°). The large spread of the patterns disposes of one apparent difficulty in the way of the eddy hypothesis. This is that the main toroidal field within the core is probably small near the equator, whereas foci of non-dipole field near the equator nevertheless exist (Lowes & Runcorn 1951; Bullard & Gellmann 1954). The large angular spread of the field due to a single eddy implies that non-dipole foci at the equator can arise from eddies in higher latitudes, so that the presence of foci of the non-dipole field at the equator does not require the presence of eddies at the equator.

PHILOSOPHICAL TRANSACTIONS OF THE ROYAL SOCIETY A MATHEMATICAL, PHYSICAL & ENGINEERING SCIENCES

We wish to express our thanks to Professor P. M. S. Blackett, F.R.S., who suggested the problem, for his interest and encouragement and for placing the facilities of the Manchester University Physical Laboratories at our disposal. We are grateful to Dr H. J. J. Braddick for his assistance in designing the experimental apparatus, and to Professor M. J. Lighthill, F.R.S., for a very informative discussion on the subject of turbulence. To Professor S. K. Runcorn, Sir Edward Bullard, F.R.S., and many colleagues, we are indebted for much helpful discussion and criticism.

Professor H. B. Squire has very kindly given us permission to quote from his work prior to publication.

Much of the work was done while both of us were in receipt of maintenance grants from the Department of Scientific and Industrial Research.

References

Blatt, J. M. & Weisskopf, V. F. 1952 *Theoretical nuclear physics*. New York: John Wiley and Sons.
Brewer, A. W., Squires, J. & Ross, H. McG. 1951 *J. Elliot Bros* (*Lond.*), **1**, 38.
Bullard, E. C. 1948 *Mon. Not. R. Astr. Soc. Geophys. Suppl.* **5**, 248–257.
Bullard, E. C. 1949*a* *Proc. Roy. Soc.* A, **197**, 433–453.
Bullard, E. C. 1949*b* *Proc. Roy. Soc.* A, **199**, 413–443.
Bullard, E. C., Freedman, C., Gellman, H. & Nixon, J. 1950 *Phil. Trans* A, **243**, 67–92.
Bullard, E. C. & Gellman, H. 1954 *Phil. Trans.* A, **247**, 213–278.
Bullen, K. E. 1947 *An introduction to the theory of seismology*. Cambridge University Press.
Chapman, S. & Bartels, J. 1940 *Geomagnetism*. Oxford University Press.
Dungey, J. W. 1950 *Proc. Camb. Phil. Soc.* **46**, 651–654.
Elsasser, W. M. 1946*a* *Phys. Rev.* **69**, 106–116.
Elsasser, W. M. 1946*b* *Phys. Rev.* **70**, 202–212.
Elsasser, W. M. 1950 *Rev. Mod. Phys.* **22**, 1–35.
Gans, R. 1921 *Arch. Elektrotech.* **9**, 413–426.
Hansen, W. W. 1935 *Phys. Rev.* **47**, 139–143.
Inglis, D. R. 1955 *Rev. Mod. Phys.* **27**, 212–248.
Jeffreys, H. & Jeffreys, B. S. 1950 *Methods of mathematical physics*. Cambridge University Press.
Lamb, H. 1881 *Proc. Lond. Math. Soc.* **13**, 51–66.
Lowes, F. J. & Runcorn, S. K. 1951 *Phil. Trans* A, **243**, 525–546.
MacDonald, H. M. 1934 *Electromagnetism*. London: G. Bell and Sons.
Roberts, P. H. 1955 *Astrophys J.* **122**, 315–326.
Runcorn, S. K. 1955 *Trans. Amer. Geophys. Un.* **36**, 191–198.
Stratton, J. A. 1941 *Electromagnetic theory*. New York: McGraw Hill.
Thomson, J. J. 1893 *Notes on recent researches in electricity and magnetism*. Oxford: Clarendon Press.
Valentiner, S. 1927 *Handbuch der Physik*, **15**, 360.
Vestine, E. H., Laporte, L., Lange, I. & Scott, W. E. 1947 *Publ. Carneg. Instn*, no. 580.

PHILOSOPHICAL TRANSACTIONS OF THE ROYAL SOCIETY A MATHEMATICAL, PHYSICAL & ENGINEERING SCIENCES

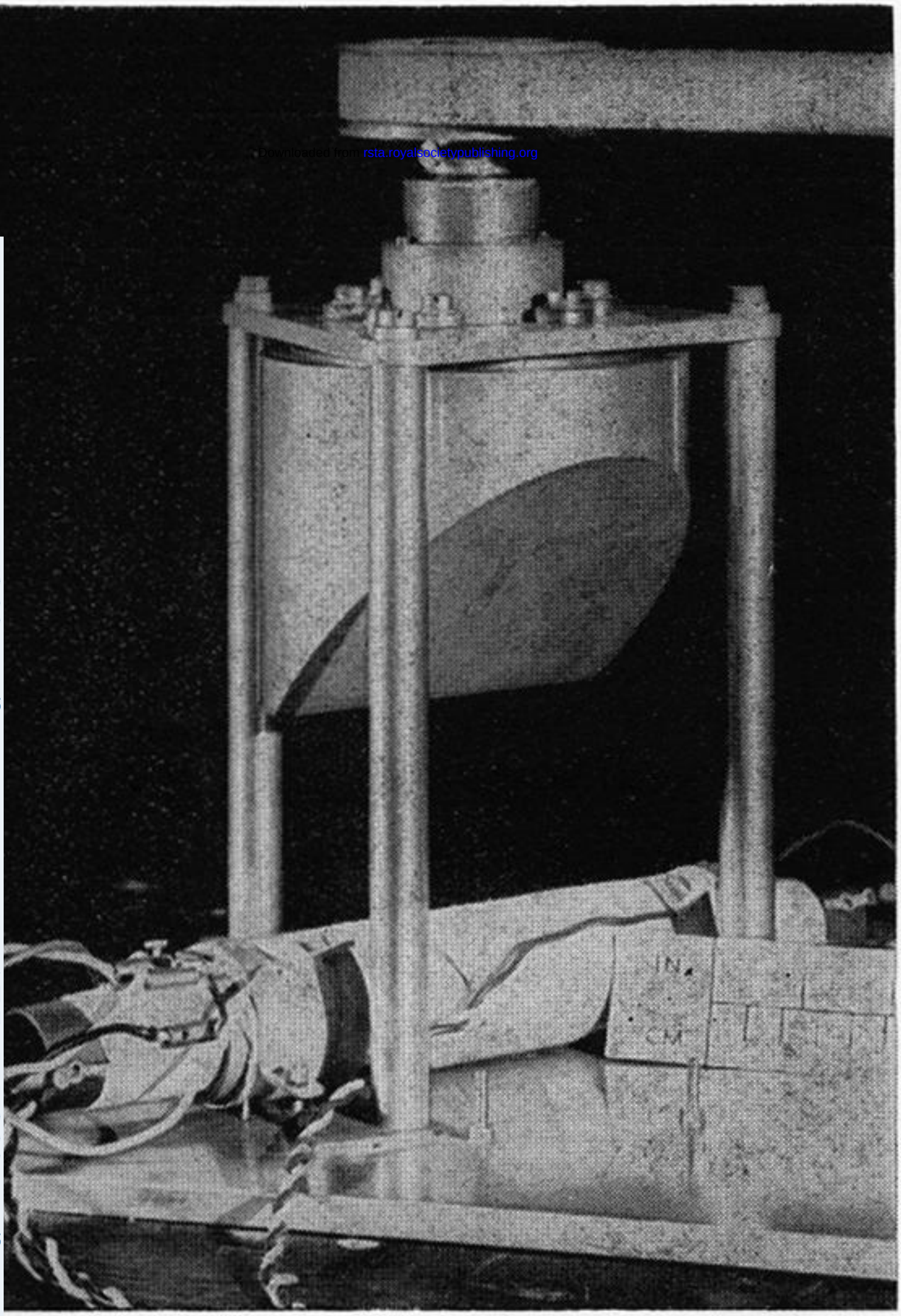

FIGURE 2. Fluxgate and rotor assembly.

PHILOSOPHICAL TRANSACTIONS OF THE ROYAL SOCIETY A MATHEMATICAL, PHYSICAL & ENGINEERING SCIENCES

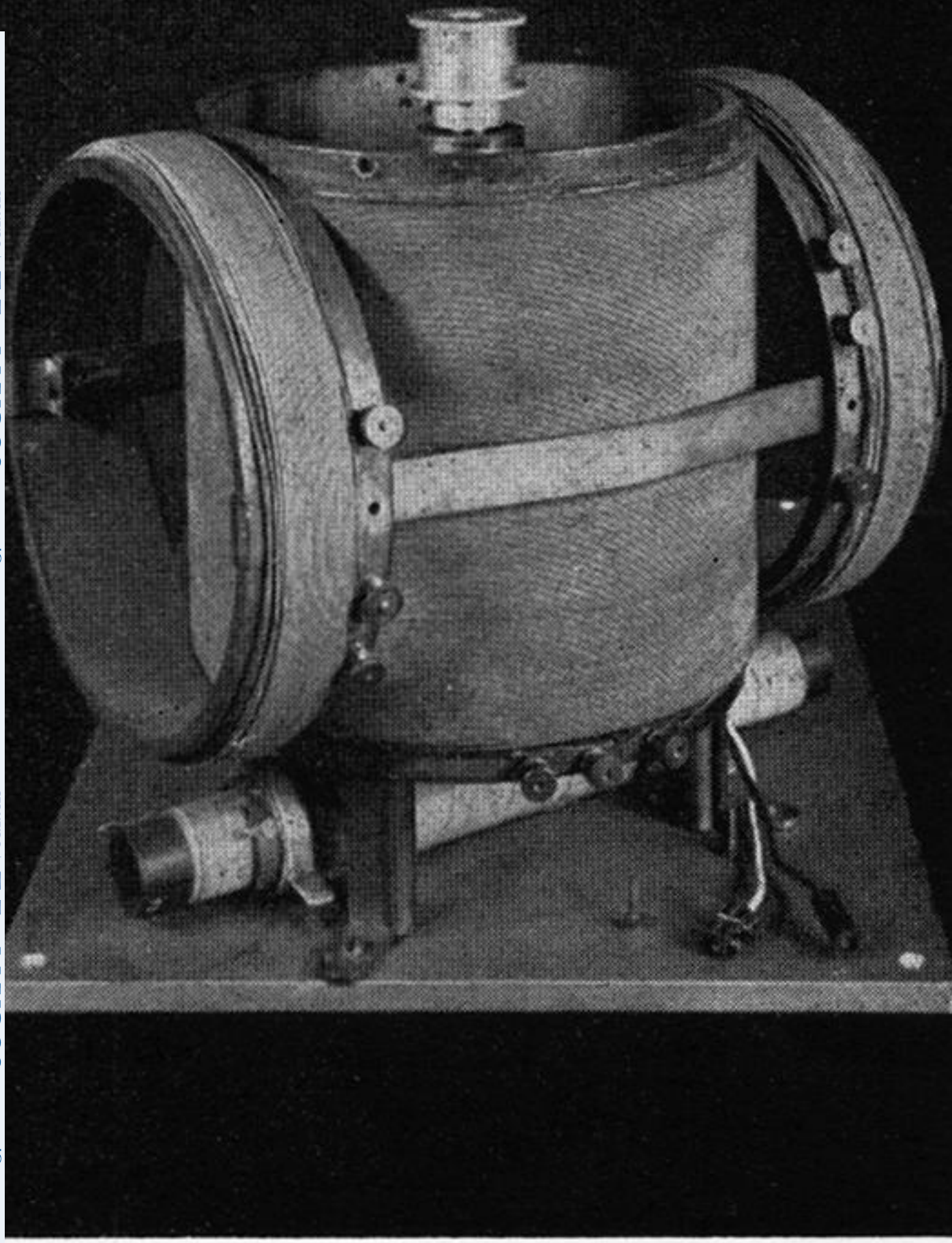

FIGURE 3. Inducing field coil assembly.

PHILOSOPHICAL TRANSACTIONS OF THE ROYAL SOCIETY A MATHEMATICAL, PHYSICAL & ENGINEERING SCIENCES